Using a Transport Model for Source-Dependent Lidar Ratios of Dust

Greg Schuster, NASA LaRC; Dongchul Kim, NASA GSFC, USRA;
Zhaoyan Liu, NASA LaRC; Mian Chin, NASA GSFC; Kerstin Schepanski, TROPOS.

Motivation

- CALIPSO/CALIOP extinction retrievals require an extinction-to-backscatter ratio assumption (i.e., a lidar ratio assumption).
- Presently, CALIOP uses a single lidar ratio for dust (45 sr).
- However, the lidar ratio of dust is sensitive to mineralogy.
- Dust single-scatter albedo
- Dust aerosol optical depth (AOD)

"Pure" Dust Indicates Regional Variability of the Real Refractive Index (according to AERONET)

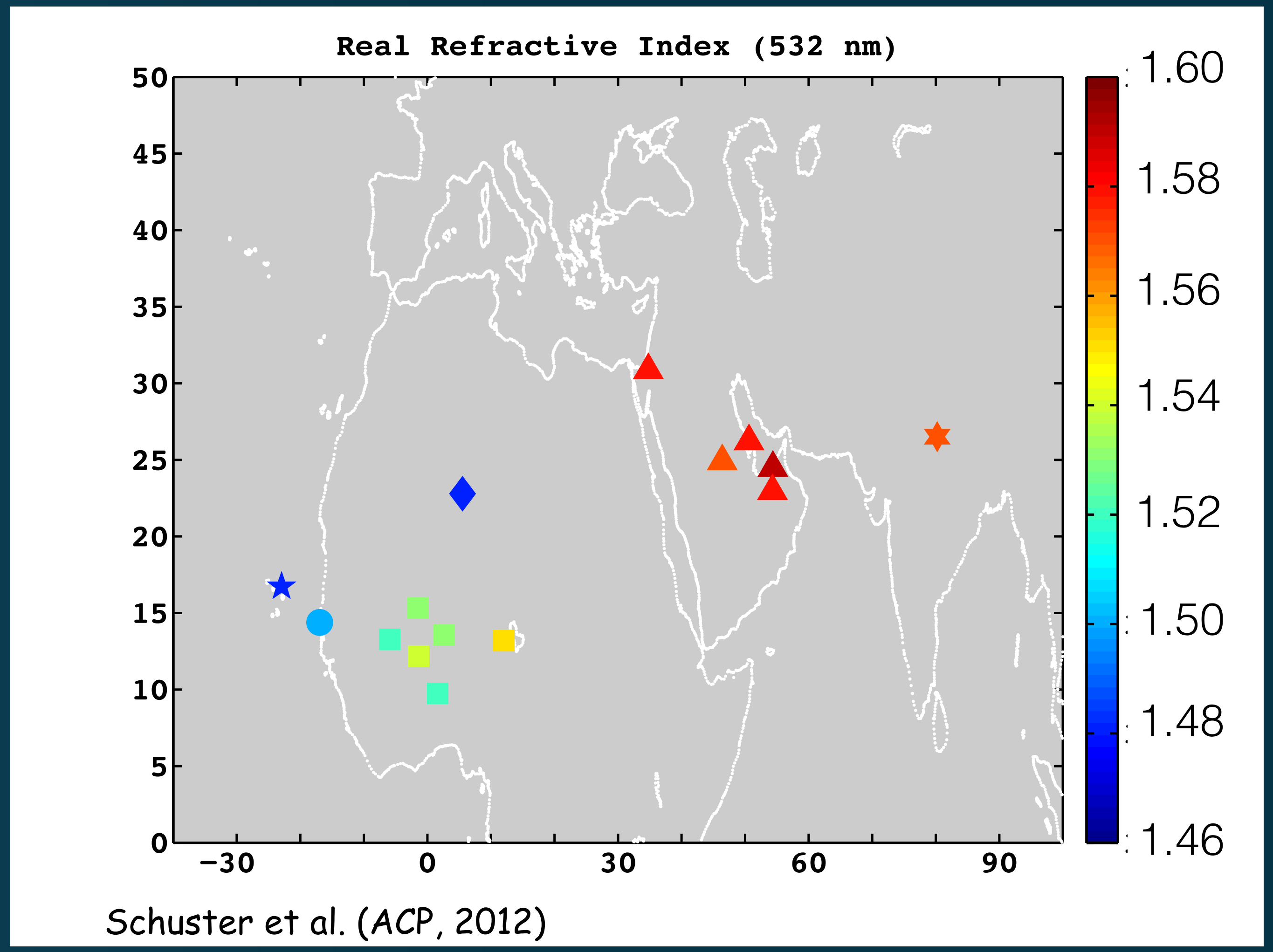

"Pure" Dust: dp > 0.2, fvf < 0.05

"Pure" Dust Indicates Regional Variability of the Real Refractive Index (according to AERONET)

AERONET provides single-scatter albedo and phase function, so lidar ratio is:

$$S_a = \frac{4\pi}{\omega_\circ P_{11}(180)}$$

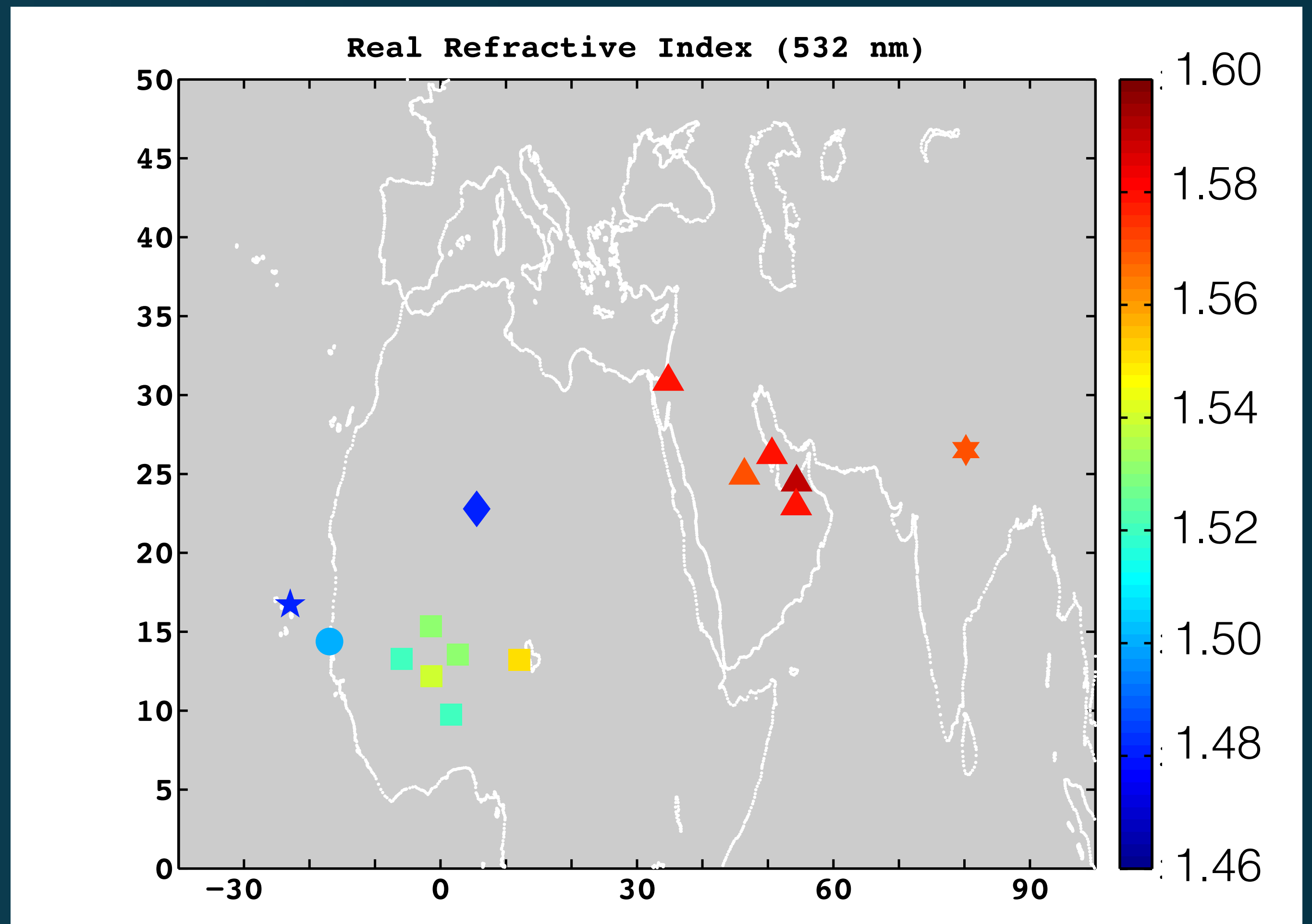

Schuster et al. (*ACP*, 2012)

"Pure" Dust: dp > 0.2, fvf < 0.05

"Pure" Dust Indicates Regional Variability of the Real Refractive Index (according to AERONET)

AERONET provides single-scatter albedo and phase function, so lidar ratio is:

$$S_a = \frac{4\pi}{\omega_\circ P_{11}(180)}$$

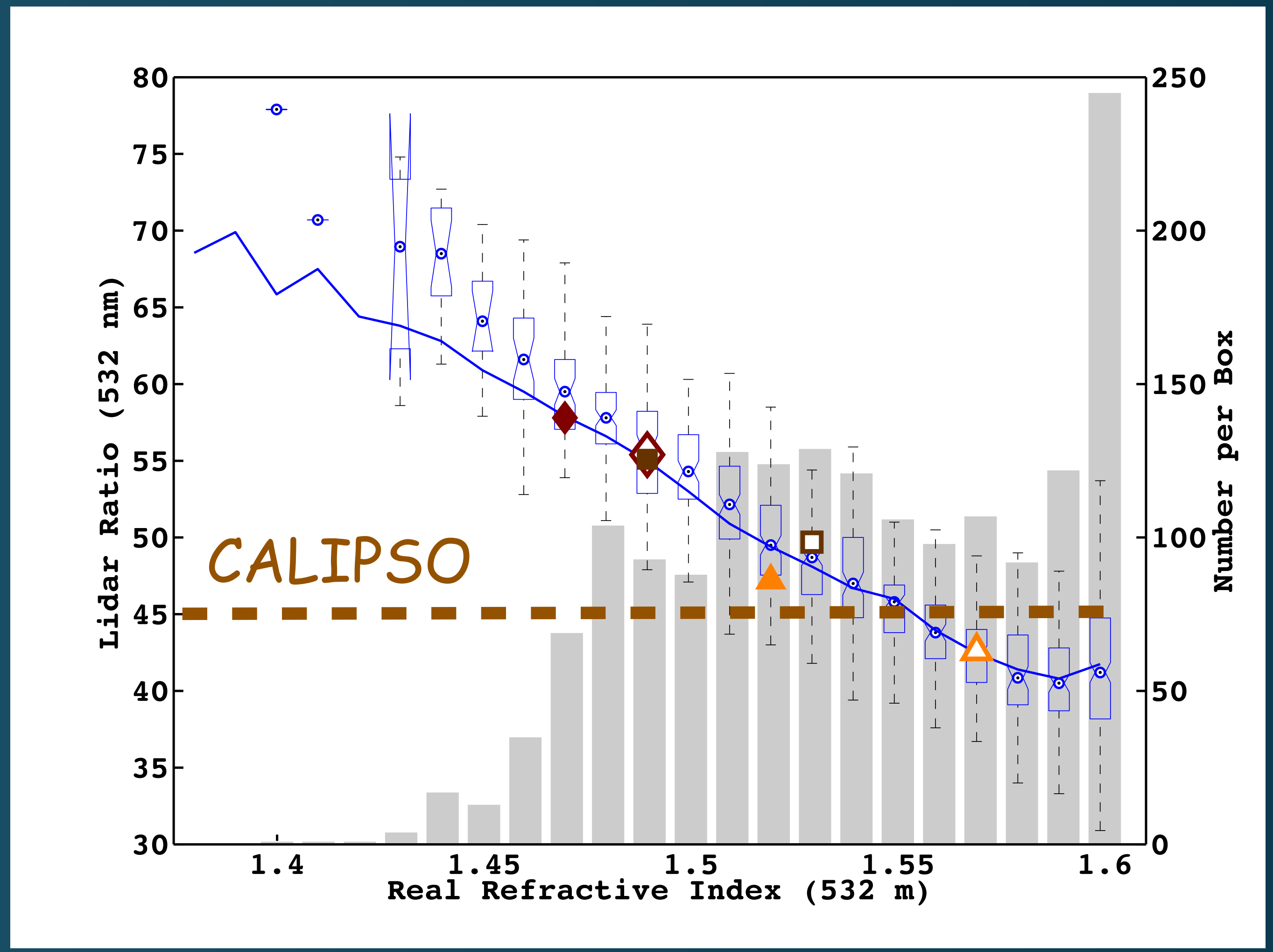

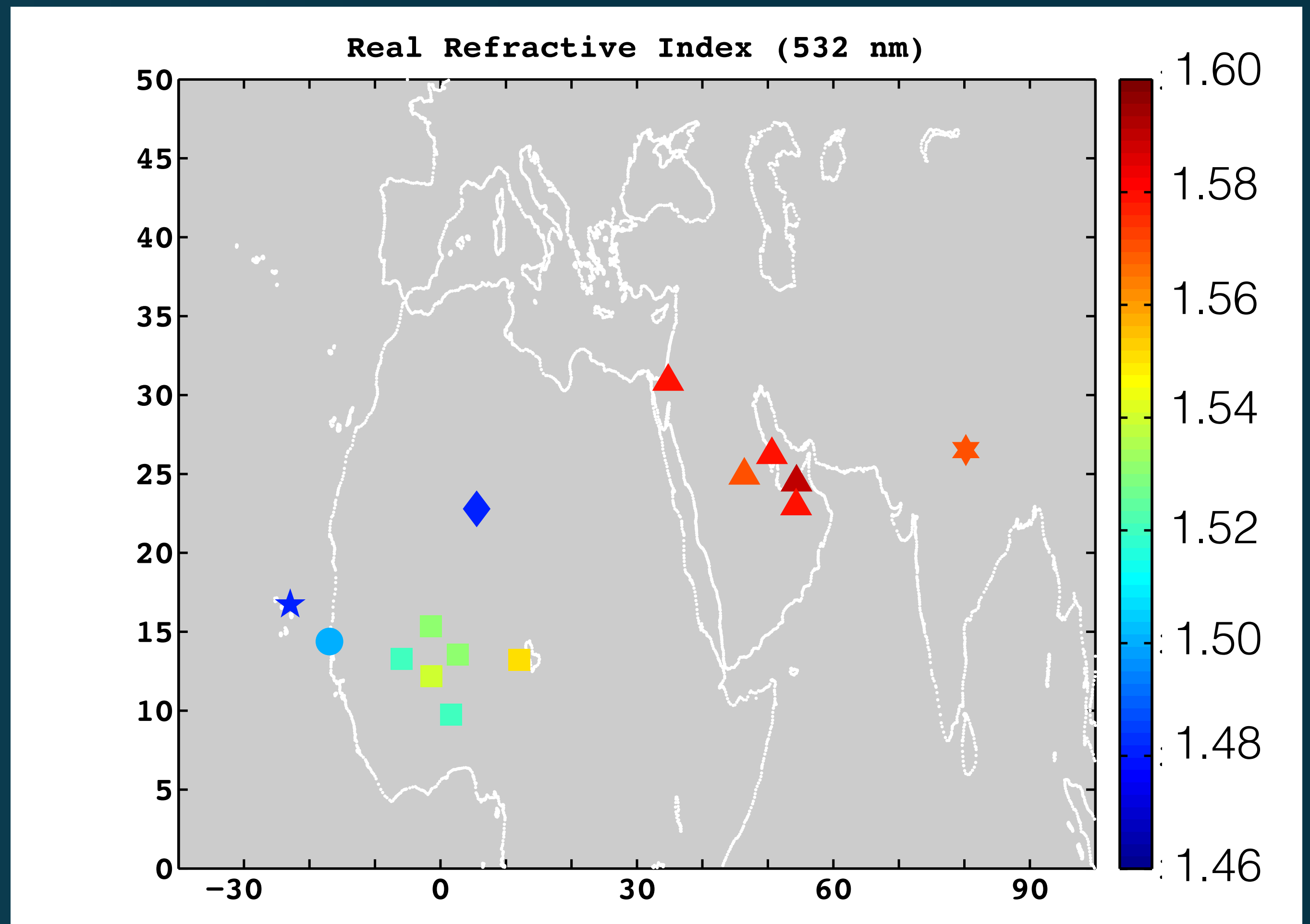

Schuster et al. (*ACP*, 2012)

Correlation	"Pure" Dust	Dust
North Africa	-0.85	-0.79
Middle East	-0.68	-0.81

"Pure" Dust: dp > 0.2, fvf < 0.05

Dust: dp > 0.2

How can we Link Measurements to Potential Source Areas?

- Backtrajectories can not quantify the proportion of dust originating from different Potential Source Areas (PSAs).

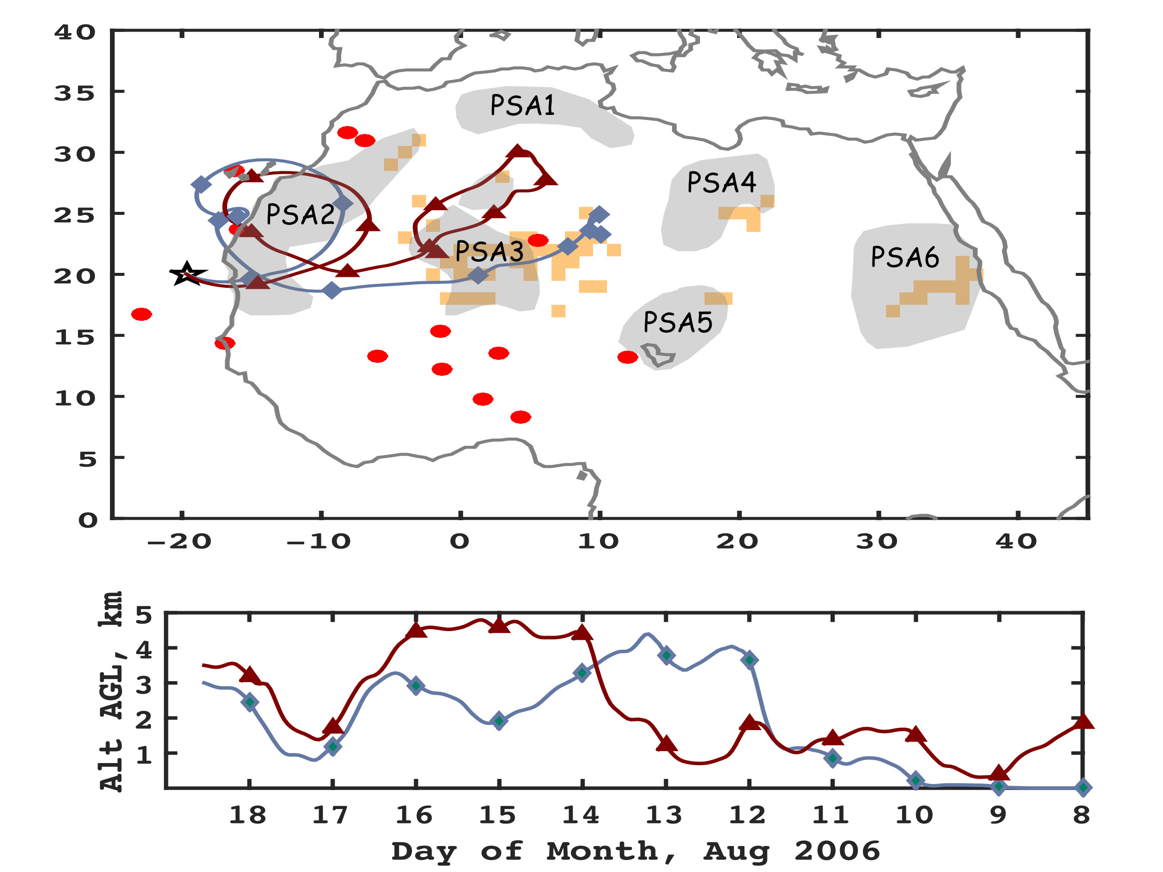

PSA regions from Formenti (ACP, 2011)

How can we Link Measurements to Potential Source Areas?

- Backtrajectories can not quantify the proportion of dust originating from different Potential Source Areas (PSAs).
- Alternative Approach:"Tag" source regions in a transport model (GOCART).

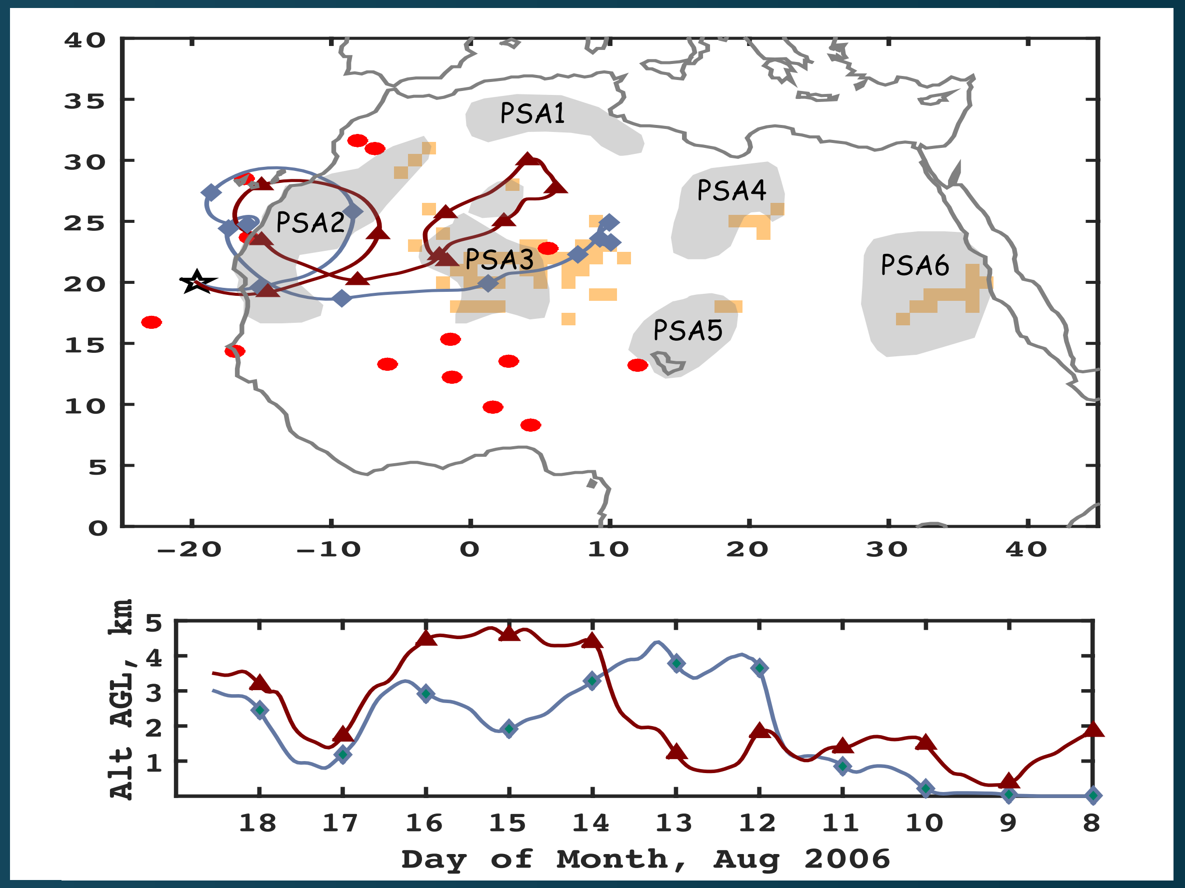

PSA regions from Formenti (ACP, 2011)

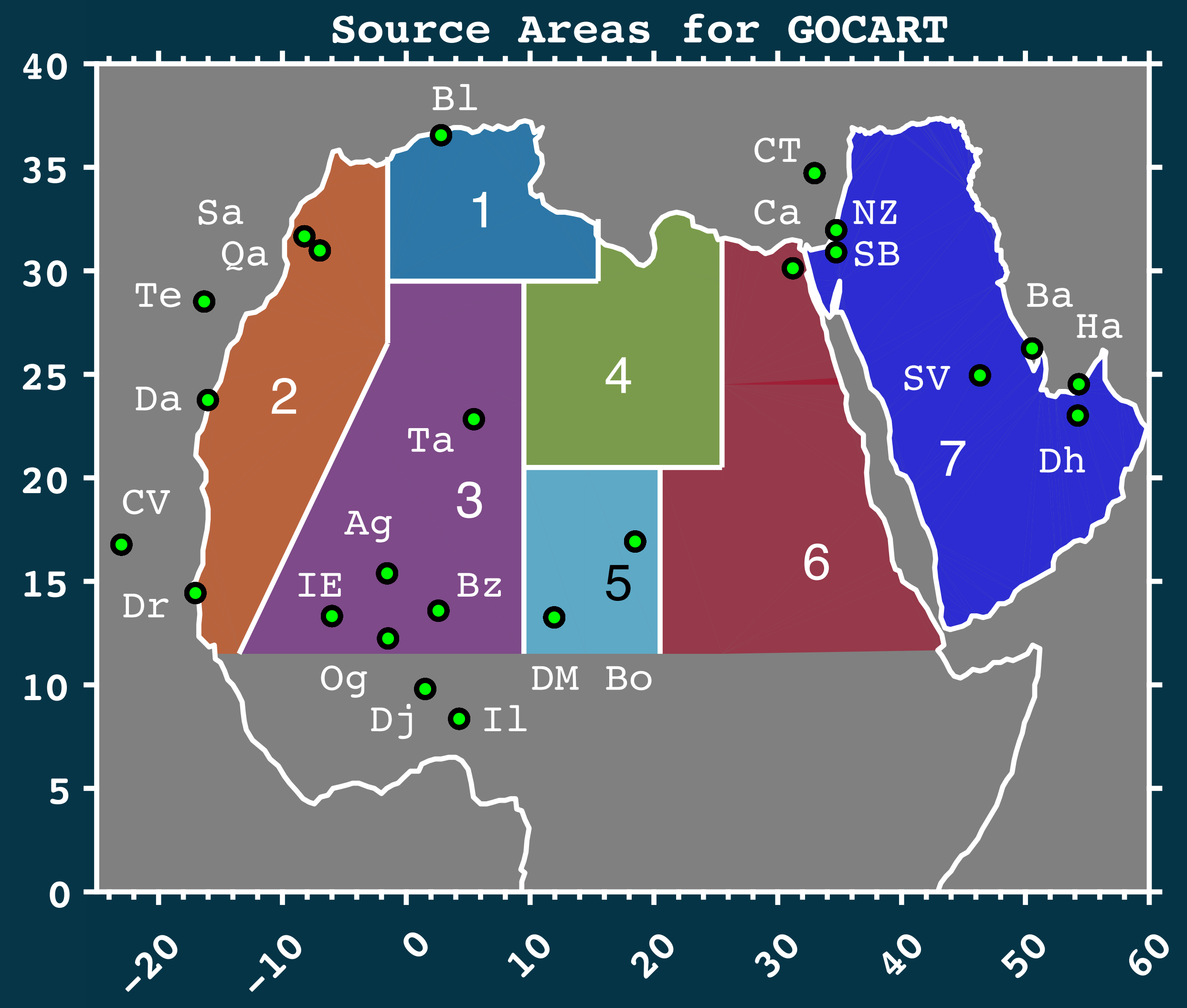

Quantify the Origin of Aeolian Dust Collected over the Atlantic

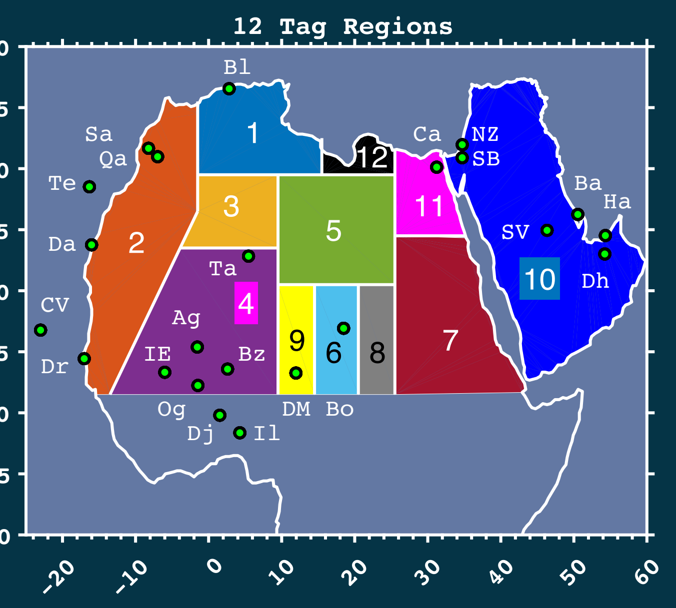

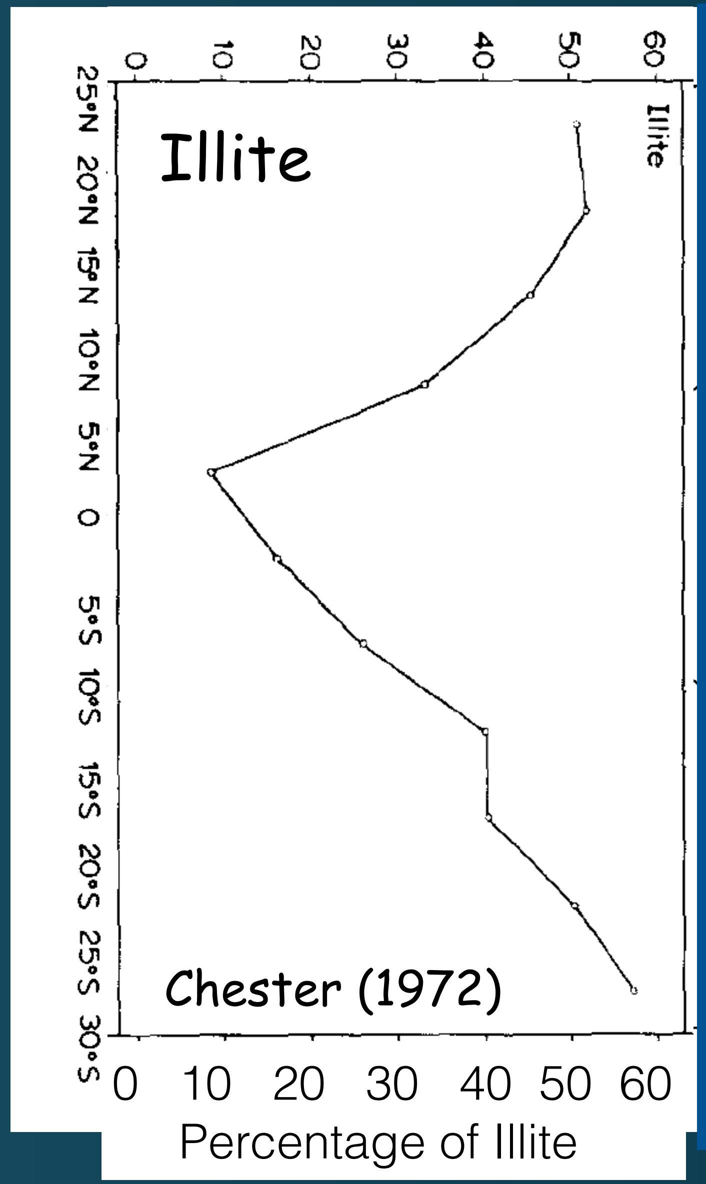

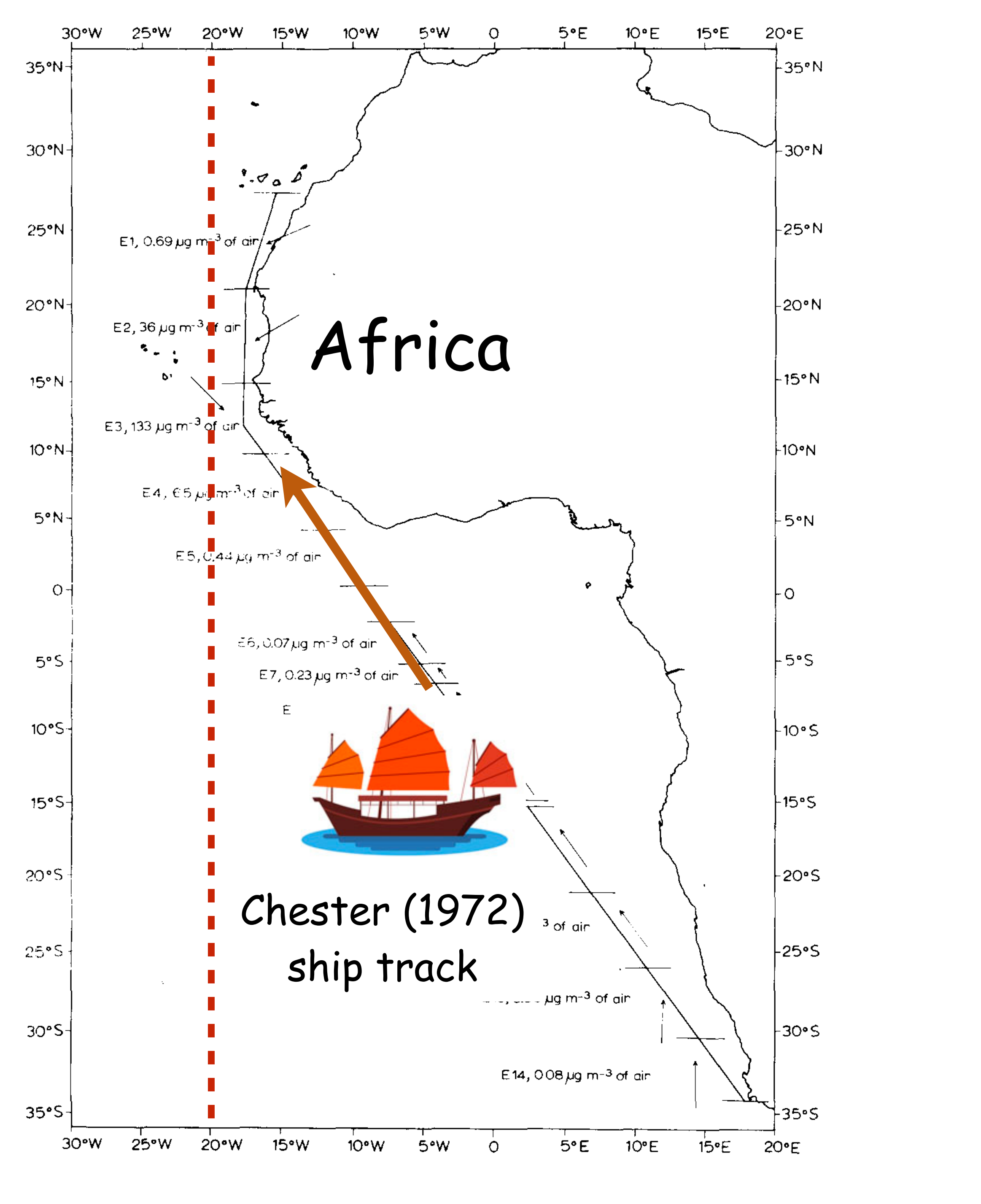

Fig.1. Collection of atmospheric dust made on board M.V. "Elpenor". The solid line indicates the ship's track (which was southwards), and the arrows the averaged wind directions; no average wind direction is given for exposures E4 and E5 where the winds were variable. The sample reference numbers and the dust-loadings are given for each collection; the start and finish of which is indicated by horizontal lines.

Quantify the Origin of Aeolian Dust Collected over the Atlantic

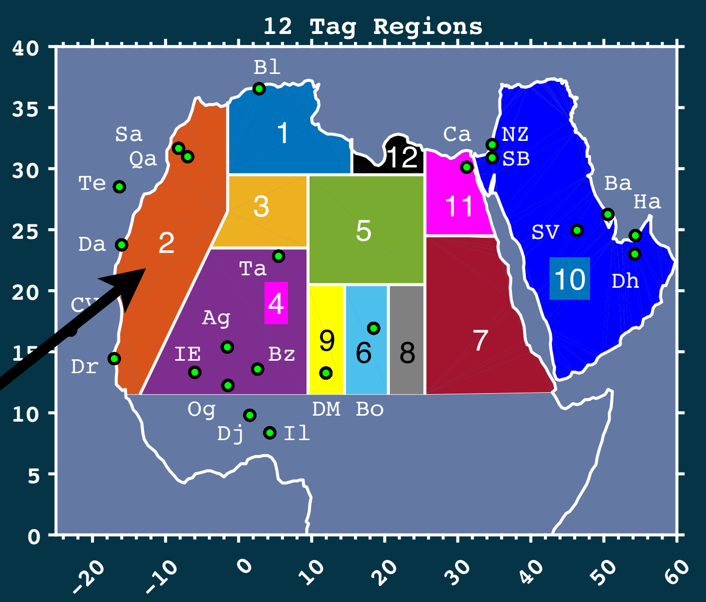

High concentrations of illite in West Africa (Caquineau, JGR 2002)

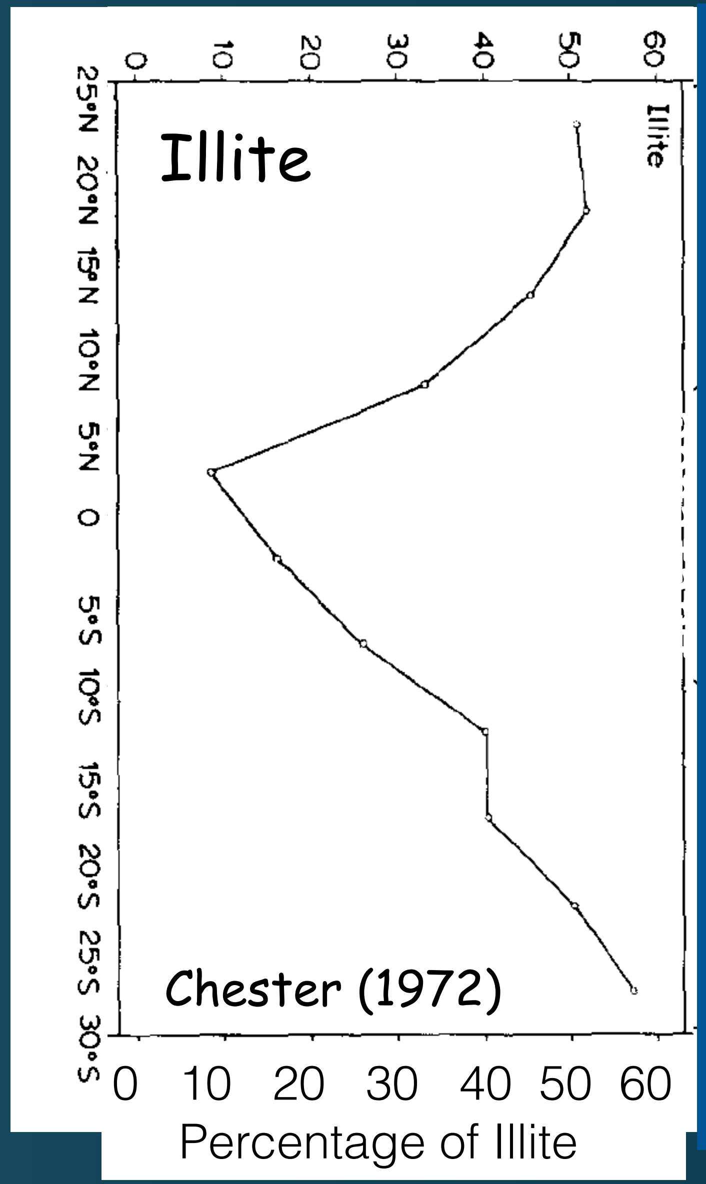

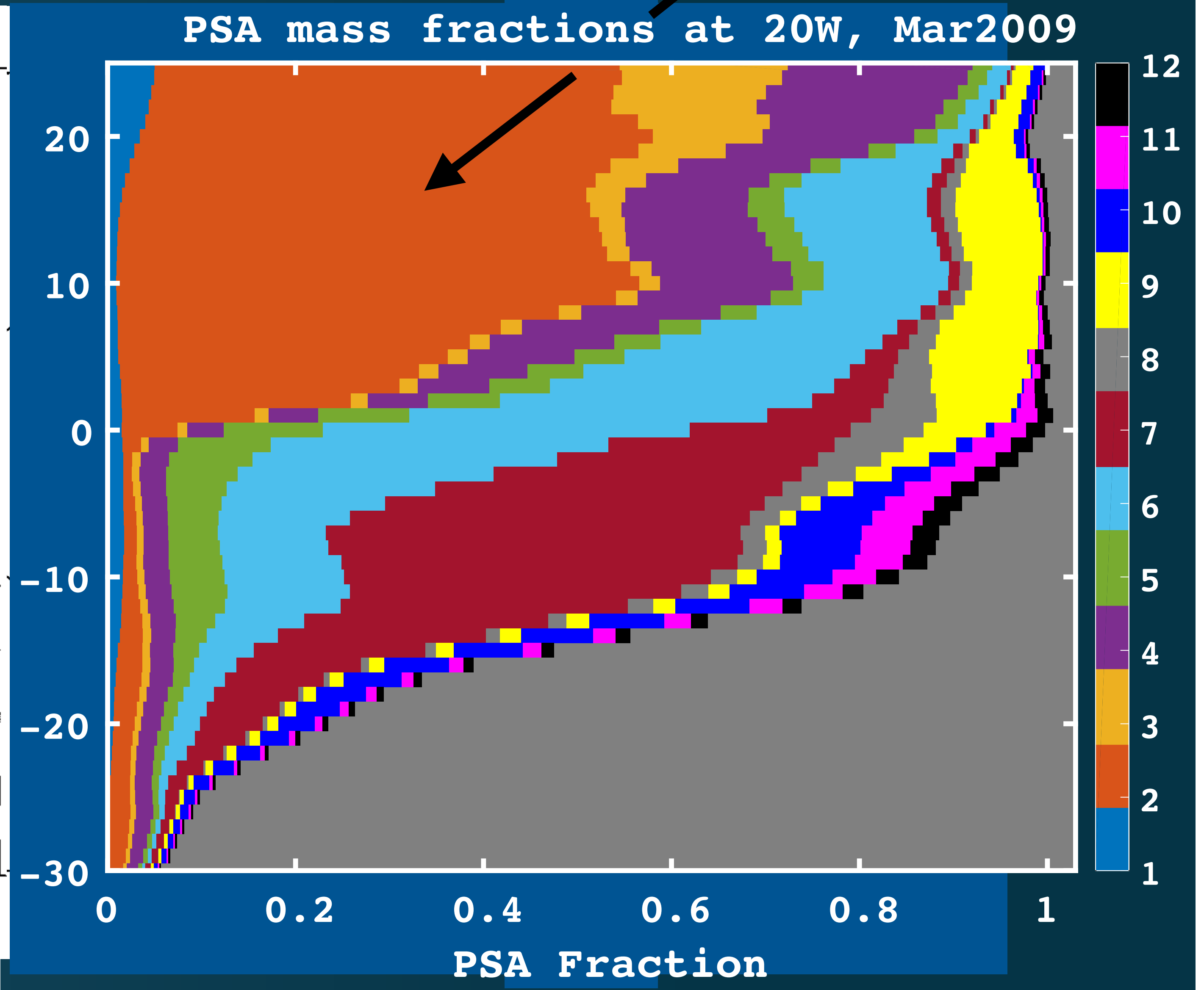

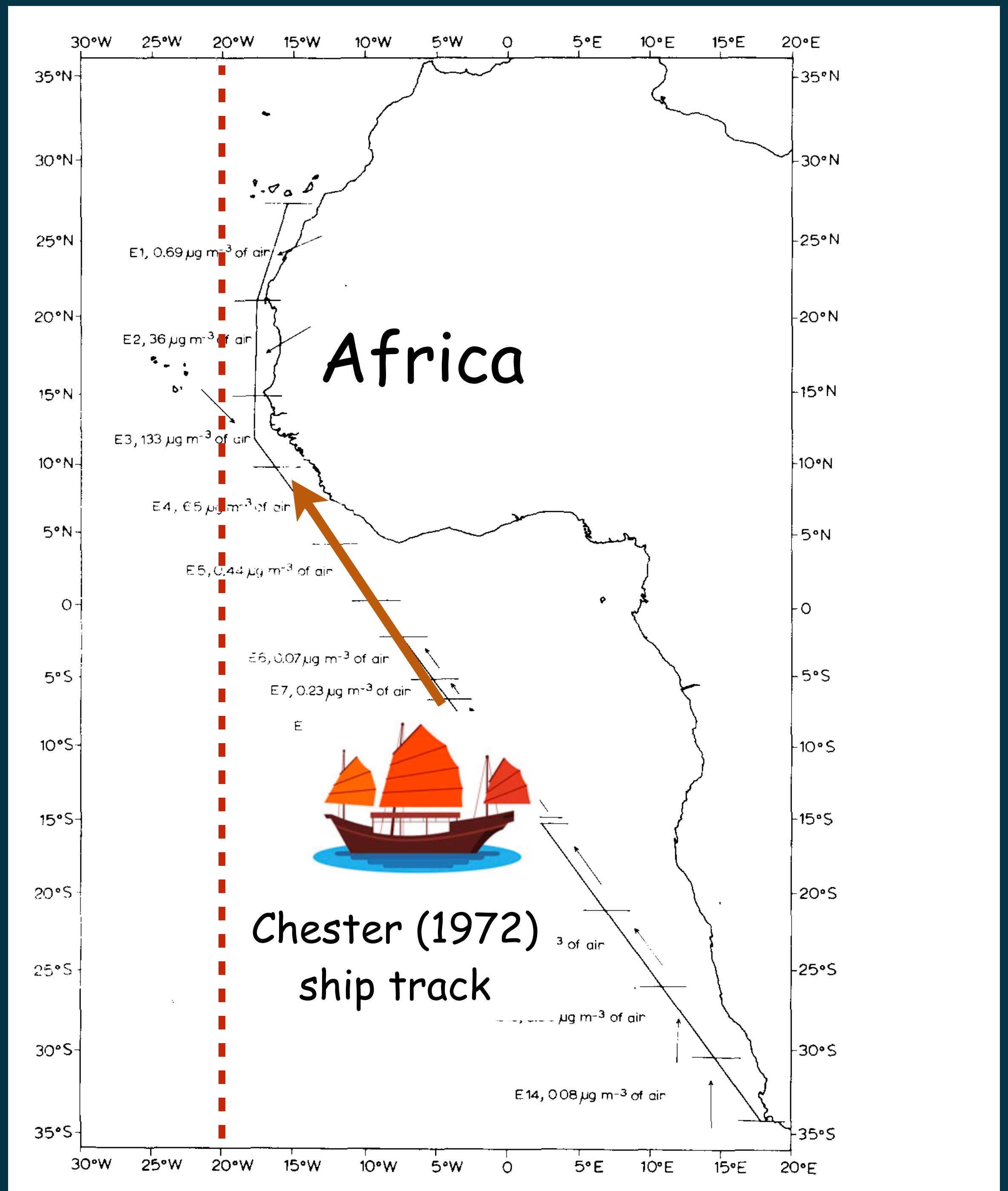

Fig.1. Collection of atmospheric dust made on board M.V. "Elpenor". The solid line indicates the ship's track (which was southwards), and the arrows the averaged wind directions; no average wind direction is given for exposures E4 and E5 where the winds were variable. The sample reference numbers and the dust-loadings are given for each collection; the start and finish of which is indicated by horizontal lines.

Use Generalized Matrix Inverse (GMI) with AERONET retrievals to assign optical properties to each region

GOCART model runs allow us to write:

$$\vec{n}_a = \mathbf{F}\vec{n}_p$$

Real refr index column vector of 7 +1 source regions

M X 8 matrix of PSA fractions at AERONETs (GOCART, 2006-2016)

Real refr index of M AERONET retrievals with $AOT(440) \geq 0.4, dp \geq 0.25, fvf < 0.05$

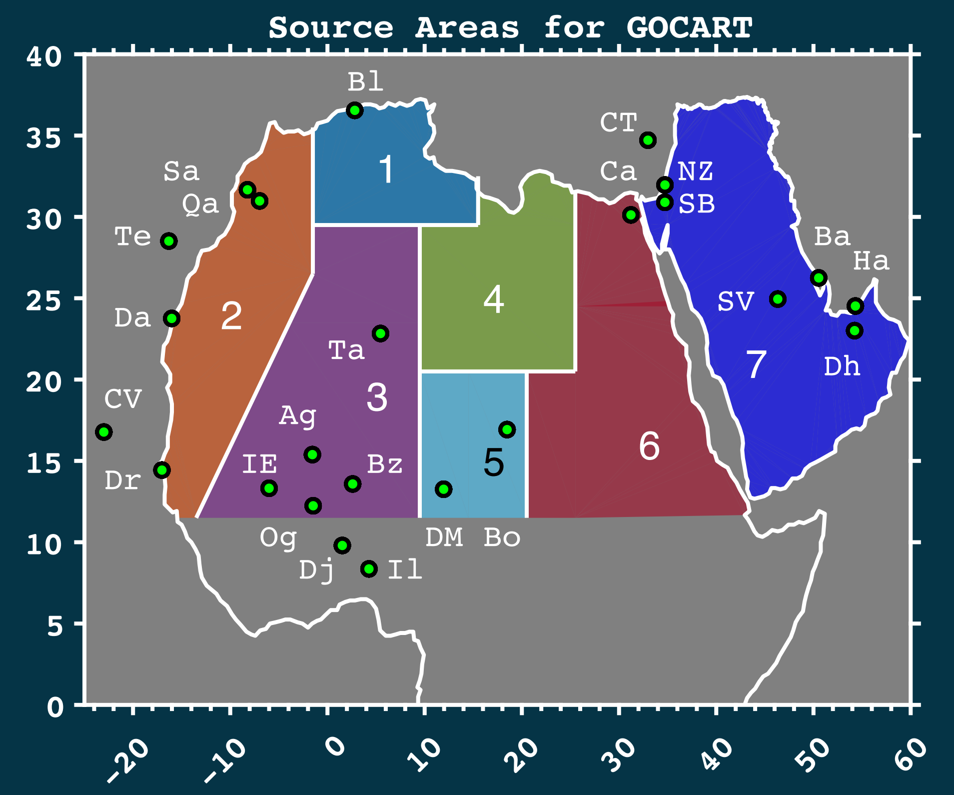

Use Generalized Matrix Inverse (GMI) with AERONET retrievals to assign optical properties to each region

GOCART model runs allow us to write:

✓ ✓

$$\vec{n}_a = \mathbf{F}\vec{n}_p$$

Real refr index column vector of 7 +1 source regions

M X 8 matrix of PSA fractions at AERONETs (GOCART, 2006-2016)

Real refr index of M AERONET retrievals with $AOT(440) \geq 0.4, dp \geq 0.25, fvf < 0.05$

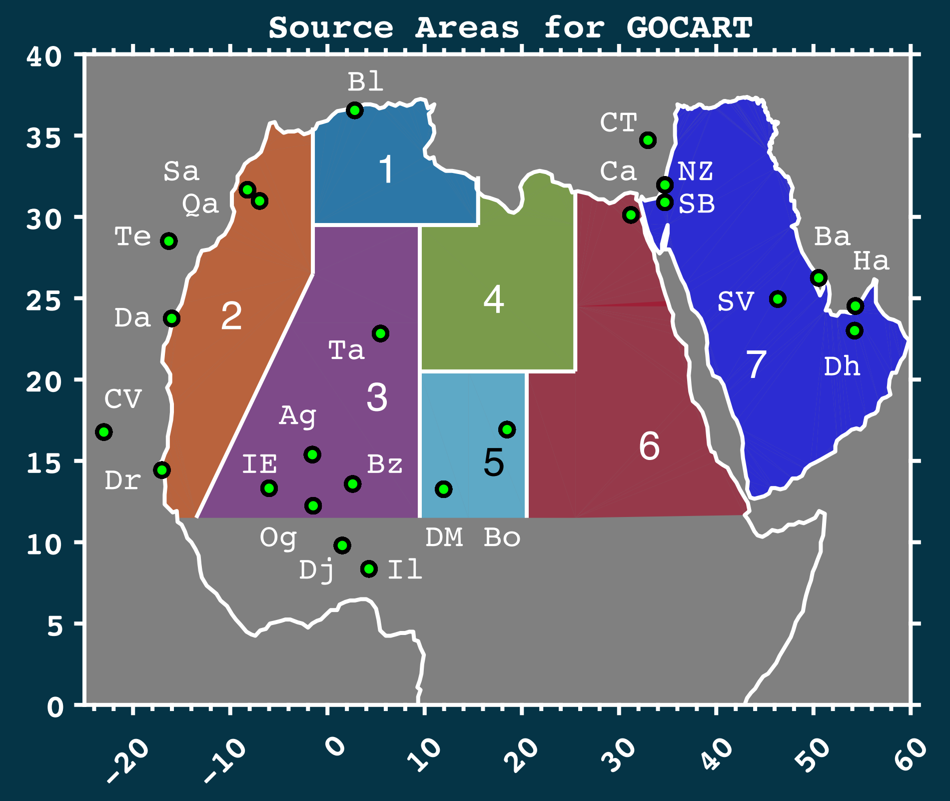

Use Generalized Matrix Inverse (GMI) with AERONET retrievals to assign optical properties to each region

GOCART model runs allow us to write:

$$\vec{n}_a = \mathbf{F}\vec{n}_p$$

Real refr index column vector of 7 +1 source regions

M X 8 matrix of PSA fractions at AERONETs (GOCART, 2006-2016)

Real refr index of M AERONET retrievals with
$AOT(440) \geq 0.4, dp \geq 0.25, fvf < 0.05$

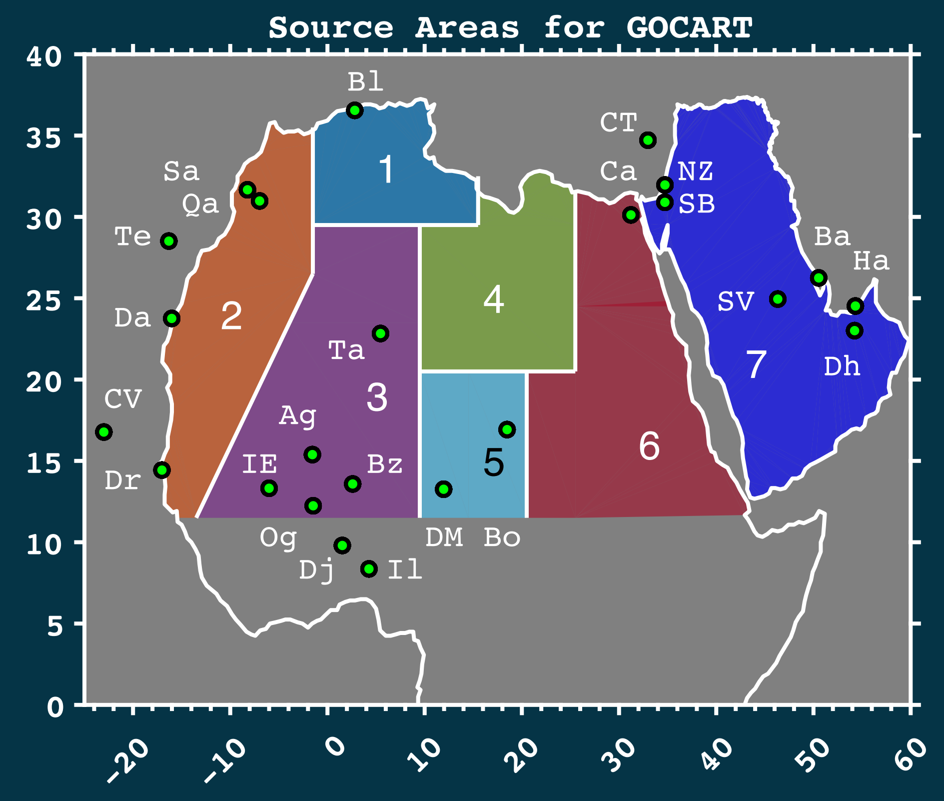

Have M = 1388, so overconstrained (i.e., M > 8). Solve for $\vec{n}_p$

$$\hat{n}_p = (\mathbf{F}^t\mathbf{F})^{-1}\mathbf{F}^t\vec{n}_a$$

Use Generalized Matrix Inverse (GMI) with AERONET retrievals to assign optical properties to each region

GOCART model runs allow us to write:

$$\vec{n}_a = \mathbf{F}\vec{n}_p$$

(✓ above $\vec{n}_a$ and ✓ above $\mathbf{F}$)

Real refr index column vector of 7 +1 source regions

M X 8 matrix of PSA fractions at AERONETs (GOCART, 2006-2016)

Real refr index of M AERONET retrievals with $AOT(440) \geq 0.4, dp \geq 0.25, fvf < 0.05$

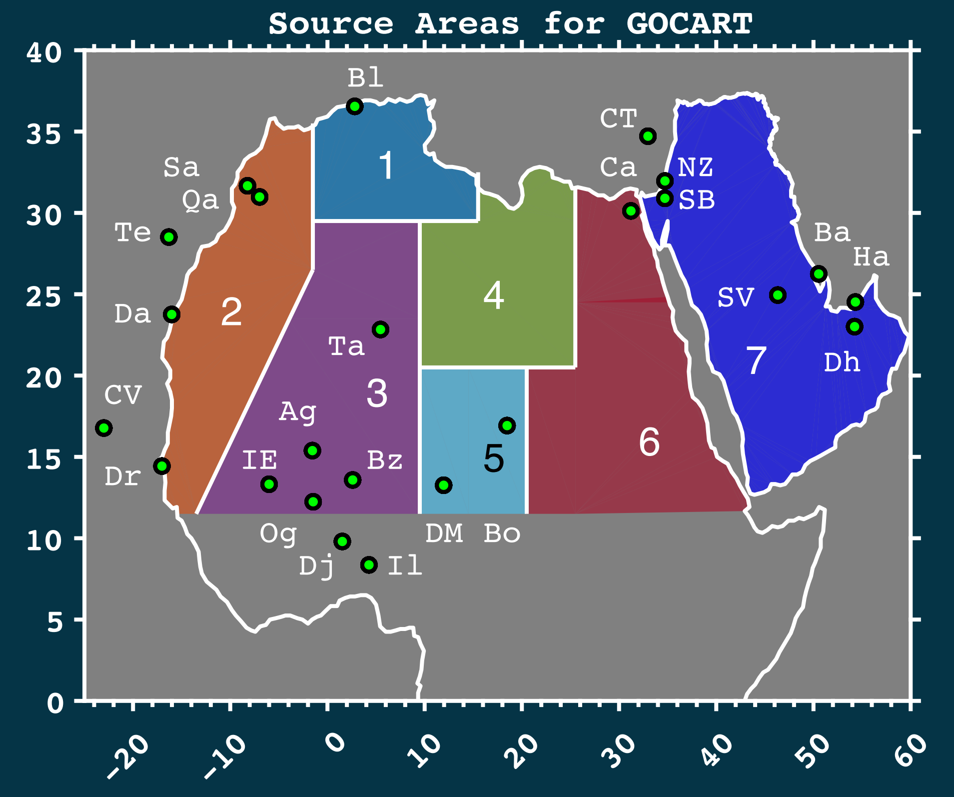

Have M = 1388, so overconstrained (i.e., M > 8). Solve for $\vec{n}_p$

$$\widehat{n}_p = (\mathbf{F}^t\mathbf{F})^{-1}\mathbf{F}^t\vec{n}_a$$

$$\widehat{k}_p = (\mathbf{F}^t\mathbf{F})^{-1}\mathbf{F}^t\,\vec{k}_a$$

Use Generalized Matrix Inverse (GMI) with AERONET retrievals to assign optical properties to each region

GOCART model runs allow us to write:

$$\vec{n}_a = \mathbf{F}\vec{n}_p$$

(✓ marked above $\vec{n}_a$ and $\mathbf{F}$)

Real refr index column vector of 7 +1 source regions

M X 8 matrix of PSA fractions at AERONETs (GOCART, 2006-2016)

Real refr index of M AERONET retrievals with $AOT(440) \geq 0.4, dp \geq 0.25, fvf < 0.05$

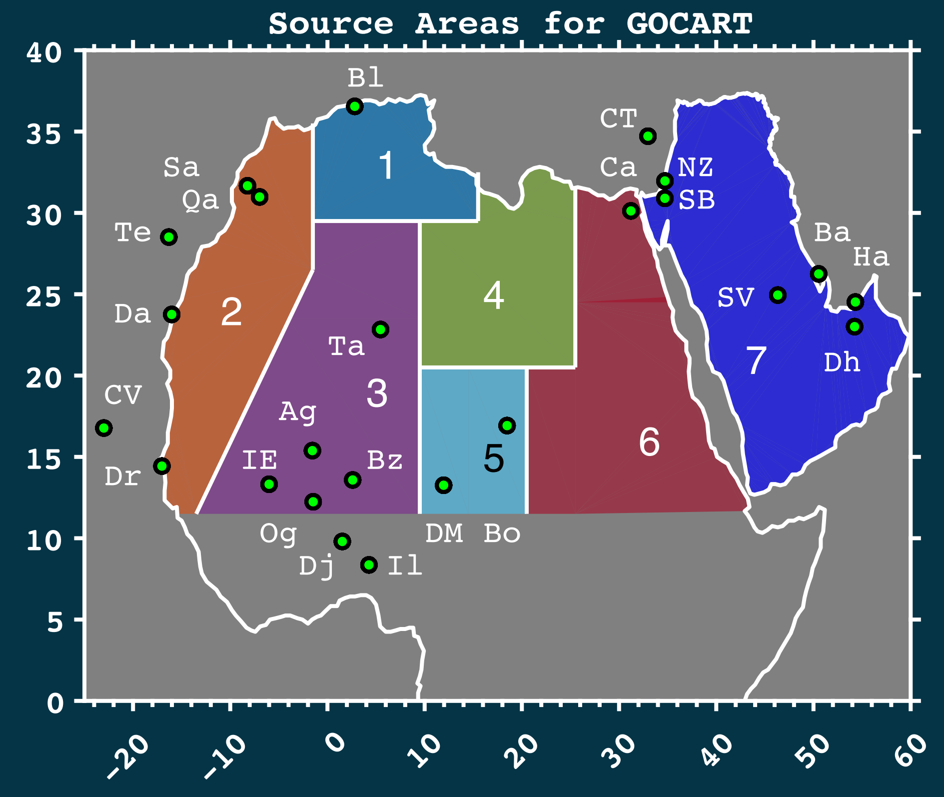

Have M = 1388, so overconstrained (i.e., M > 8). Solve for $\vec{n}_p$

$$\widehat{n}_p = (\mathbf{F}^t\mathbf{F})^{-1}\mathbf{F}^t\vec{n}_a$$

$$\widehat{k}_p = (\mathbf{F}^t\mathbf{F})^{-1}\mathbf{F}^t\,\vec{k}_a$$

Compute S_a from $(\widehat{n}_p, \widehat{k}_p)$ and modeled size distributions

Use Generalized Matrix Inverse (GMI) with AERONET retrievals to assign optical properties to each region

GOCART model runs allow us to write:

$$\vec{n}_a = \mathbf{F}\vec{n}_p$$

(✓ $\vec{n}_a$, ✓ $\mathbf{F}$)

- $\vec{n}_p$: Real refr index column vector of 7 +1 source regions
- $\mathbf{F}$: M X 8 matrix of PSA fractions at AERONETs (GOCART, 2006-2016)
- $\vec{n}_a$: Real refr index of M AERONET retrievals with $AOT(440) \geq 0.4, dp \geq 0.25, fvf < 0.05$

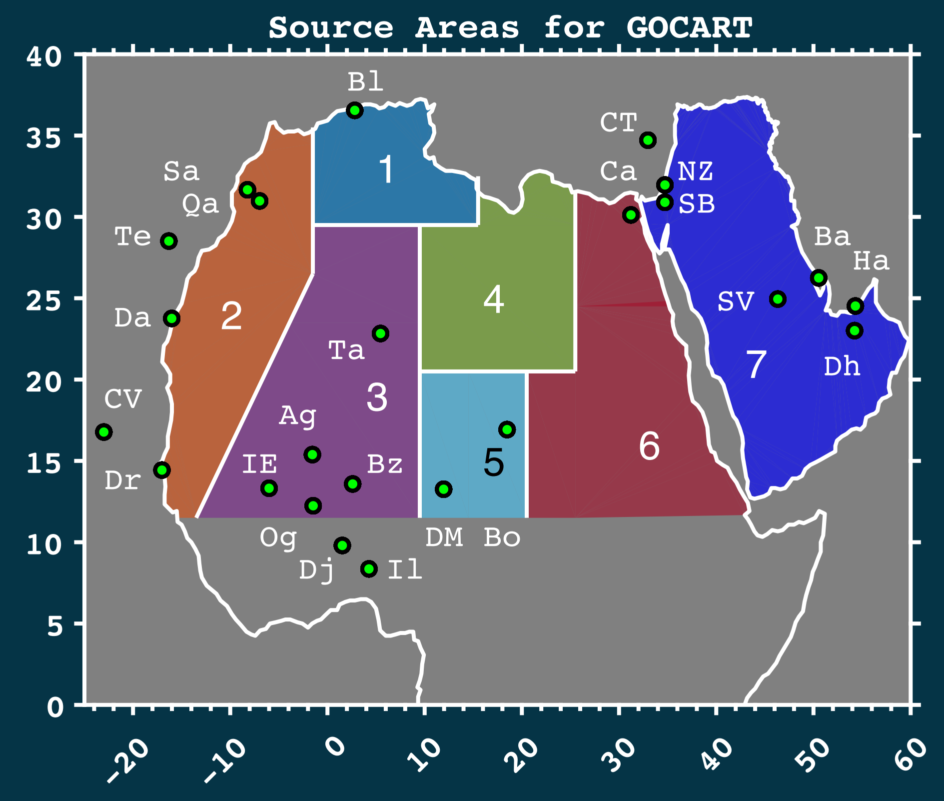

Have M = 1388, so overconstrained (i.e., M > 8). Solve for $\vec{n}_p$

$$\widehat{n}_p = (\mathbf{F}^t\mathbf{F})^{-1}\mathbf{F}^t\vec{n}_a$$

$$\widehat{k}_p = (\mathbf{F}^t\mathbf{F})^{-1}\mathbf{F}^t\vec{k}_a$$

Compute S_a from $(\widehat{n}_p, \widehat{k}_p)$ and modeled size distributions

$$\widehat{S}_p = (\mathbf{F}^t\mathbf{F})^{-1}\mathbf{F}^t\vec{S}_a \rightarrow S_a = \sum_i F_i(S_p)_i$$

Empirical approach

Regional Refractive Indices and Lidar Ratios from GMI

$$\widehat{n}_p = (F^t F)^{-1} F^t \overrightarrow{n_a}$$
$$\widehat{k}_p = (F^t F)^{-1} F^t \overrightarrow{k_a}$$

$$\widehat{S}_p = (F^t F)^{-1} F^t \overrightarrow{S_a}$$

Refractive Index

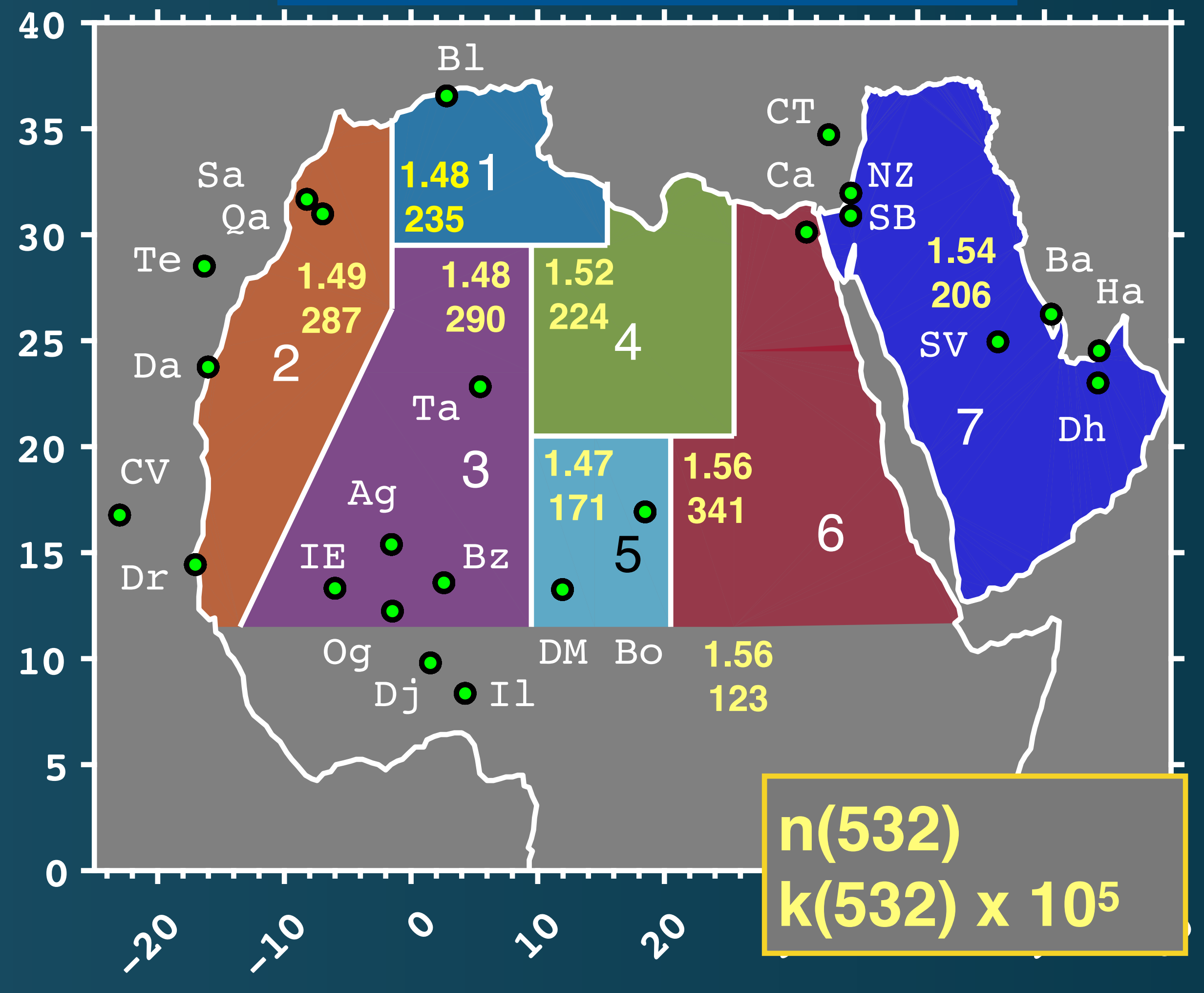

Compute S_a with GOCART:
(n_p, k_p) and GOCART dn/dr => Lidar Ratio S_a

Lidar Ratio, 532 nm

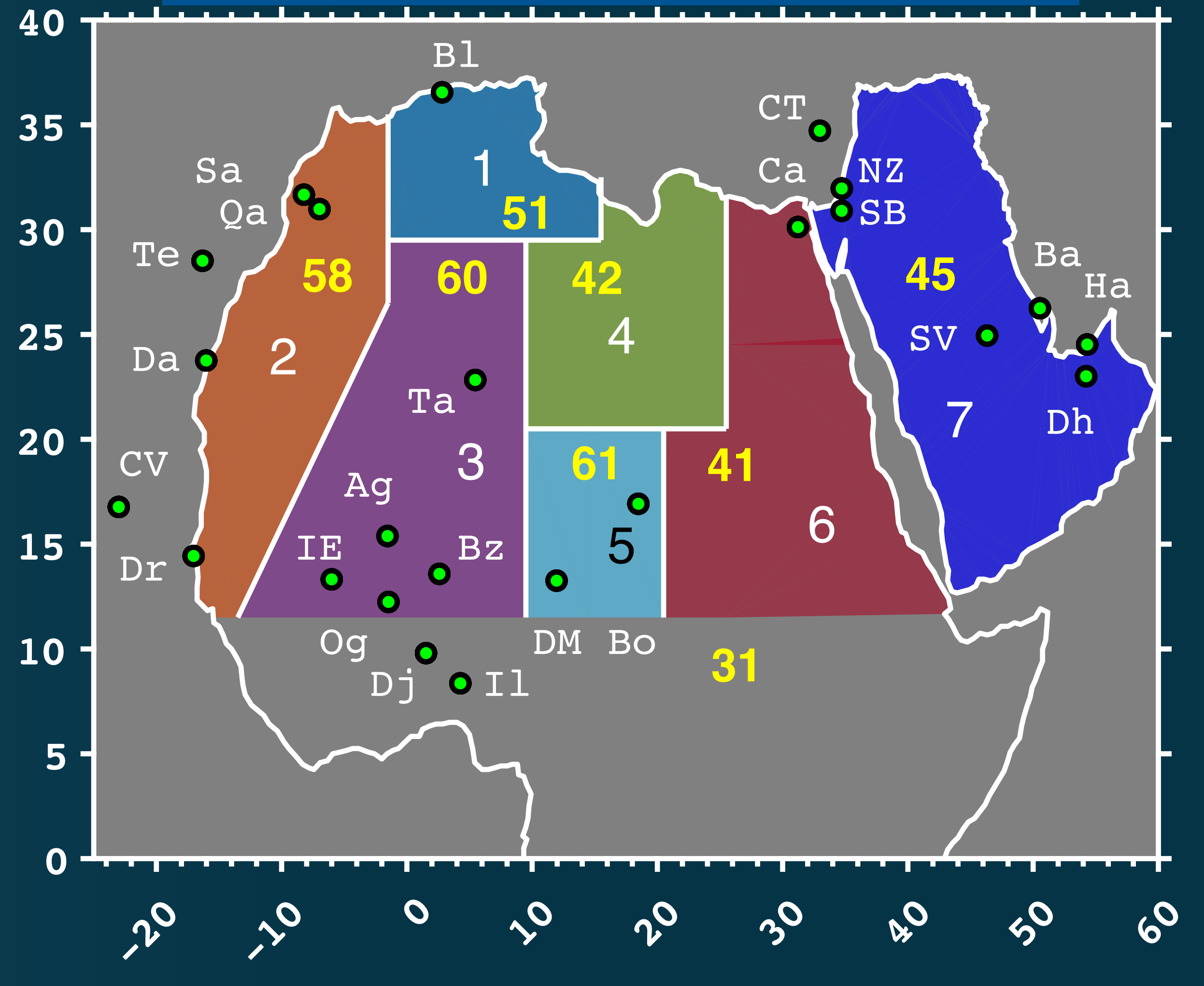

Empirical Approach: $S_a = \sum_i F_i (S_p)_i$

Reference k-values:

GOCART *k x 10⁵*:	550
AERONET *k_min x 10⁵*:	50

Computing Lidar Ratios from Modeled Size Distributions in the GOCART Transport Model

Traditional Approach

- Eight dust size distributions (modes)
- Modes are transported according to size
- Identical refractive indices for all modes
- Identical refractive indices for all sources
- Spherical particles (frequently)

This Approach

- Eight dust size distributions (modes)
- Modes are transported according to size
- Identical refractive indices for all modes
- Different refractive indices for 8 sources (7 PSA + ROW)
- Spheroids (with code provided by O. Dubovik and T. Lapyonok)

Requires separate optics computations for each source (mass extinction efficiencies, etc.) . Lidar ratio is computed for spheroids from modeled size distributions (Dubovik, GRL 2002; JGR 2006):

$$S = \frac{\int Q_{ext}(r, m, \lambda)\pi r^2 n(r) dr}{\int Q_{sca}(r, m, \lambda)\pi r^2 n(r)(P_{11}(r, m, \lambda, \pi)/4\pi) dr}$$

Example of Modeled and Empirical lidar ratios

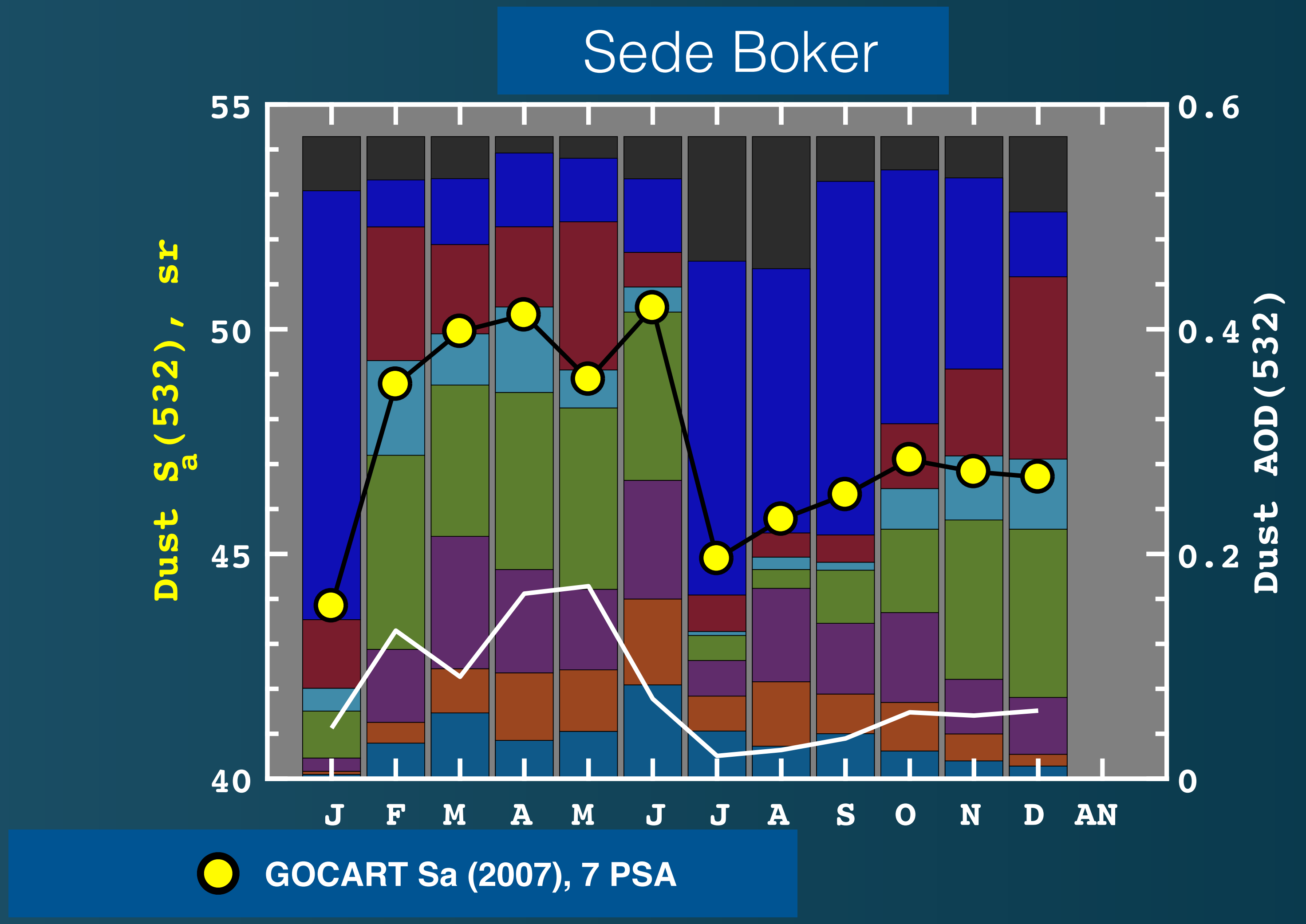

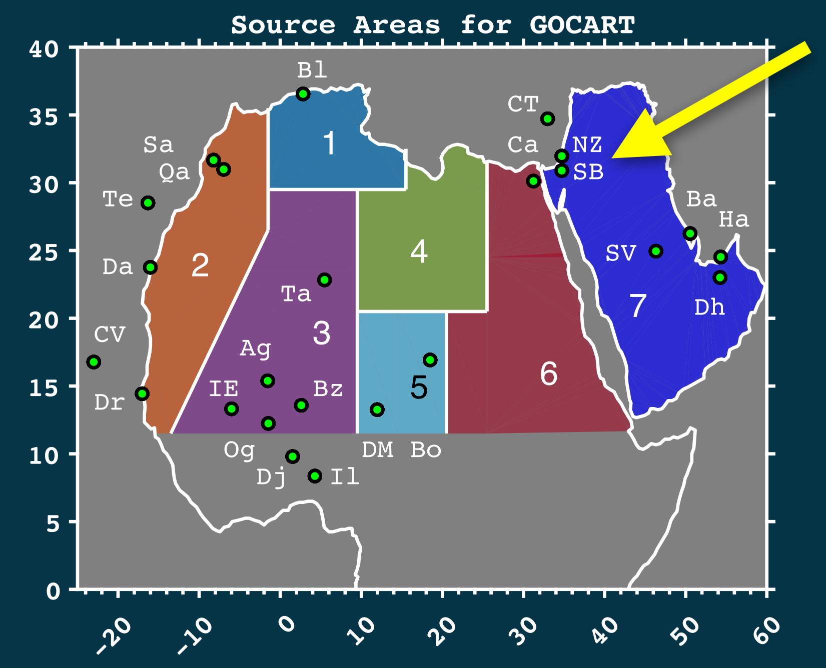

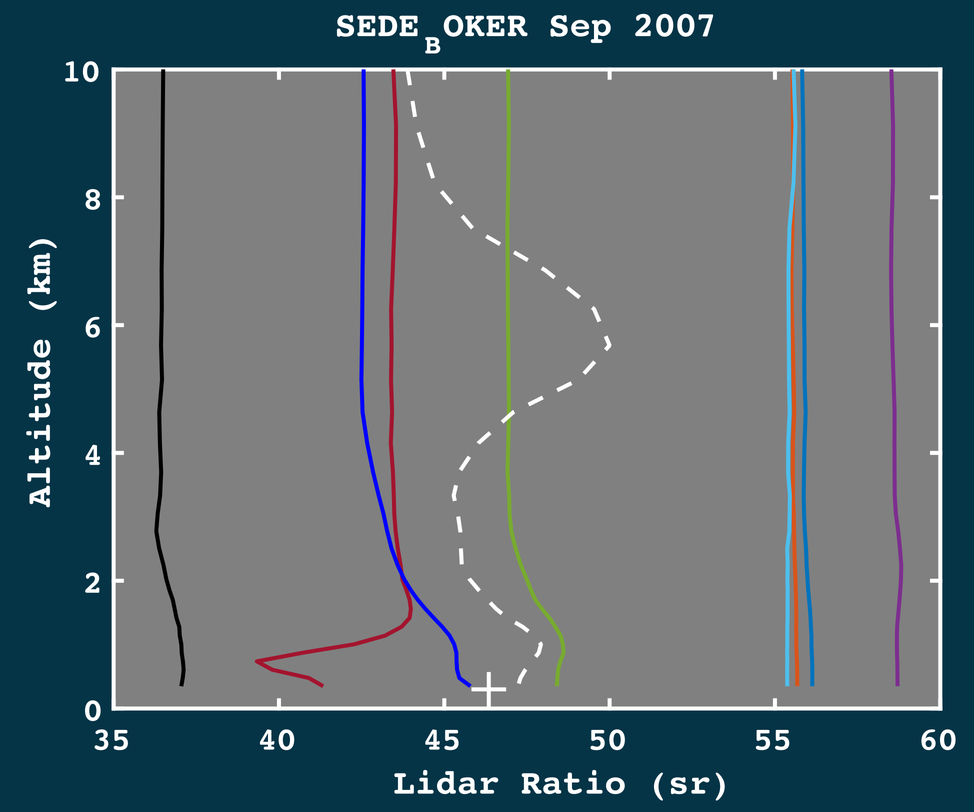

Example of Modeled and Empirical lidar ratios

Sede Boker

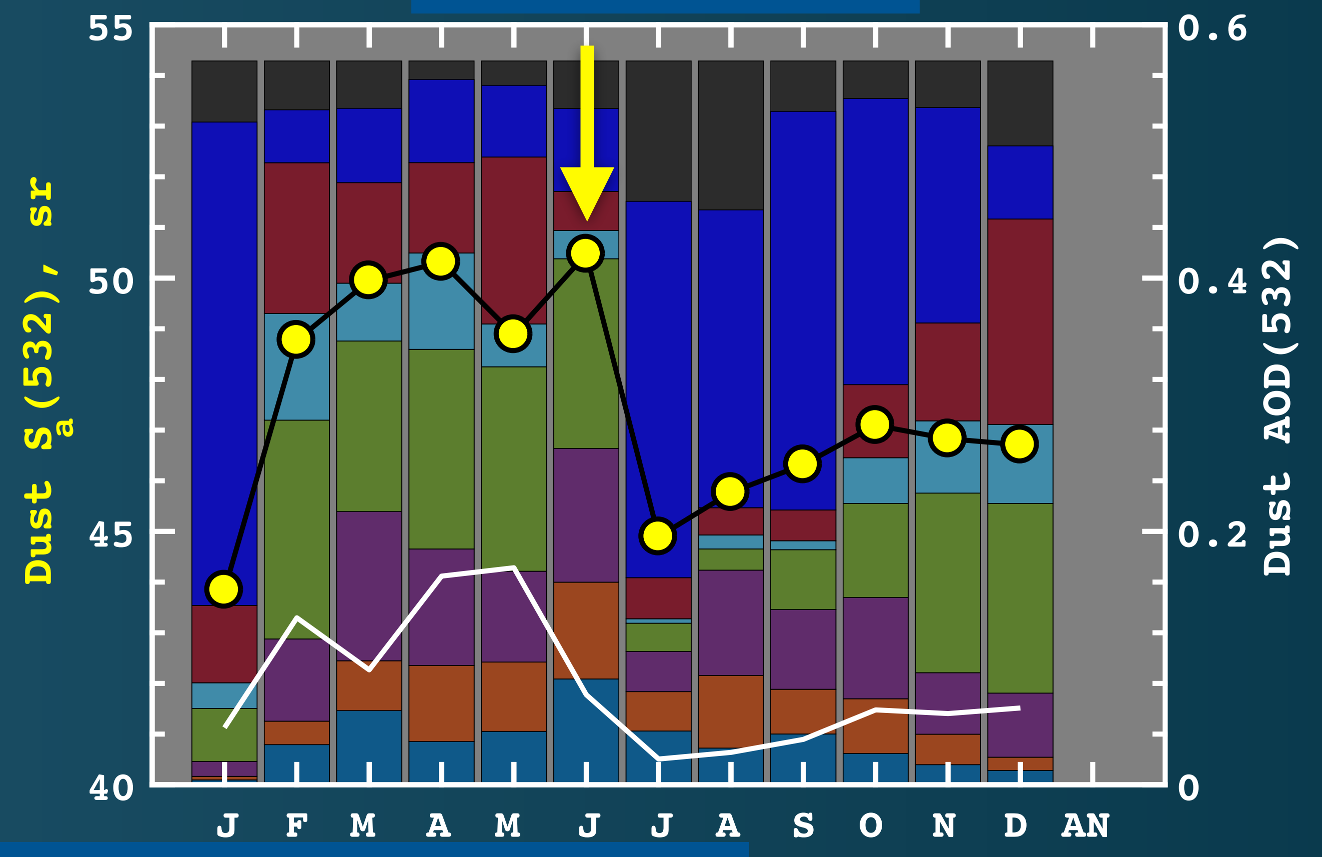

GOCART Sa (2007), 7 PSA

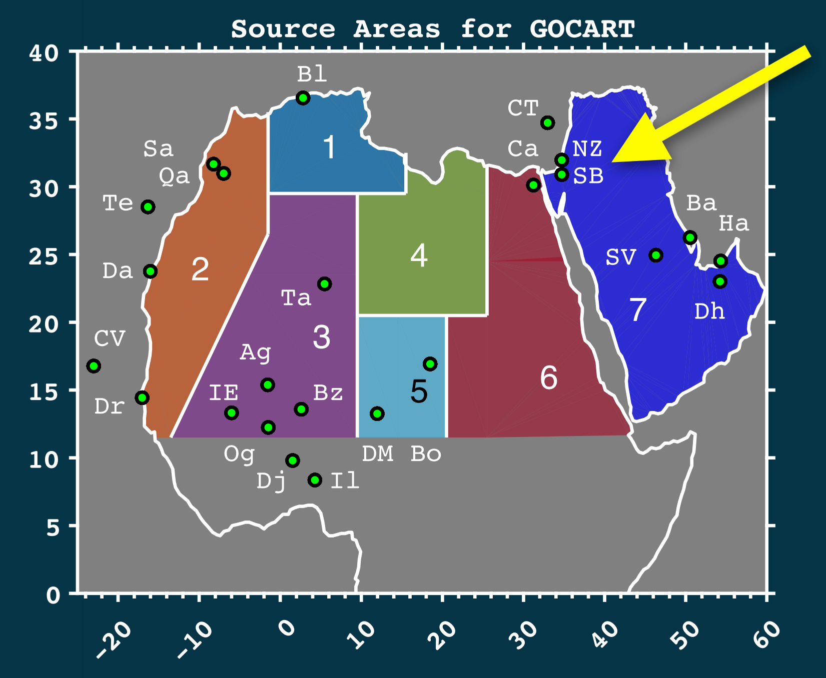

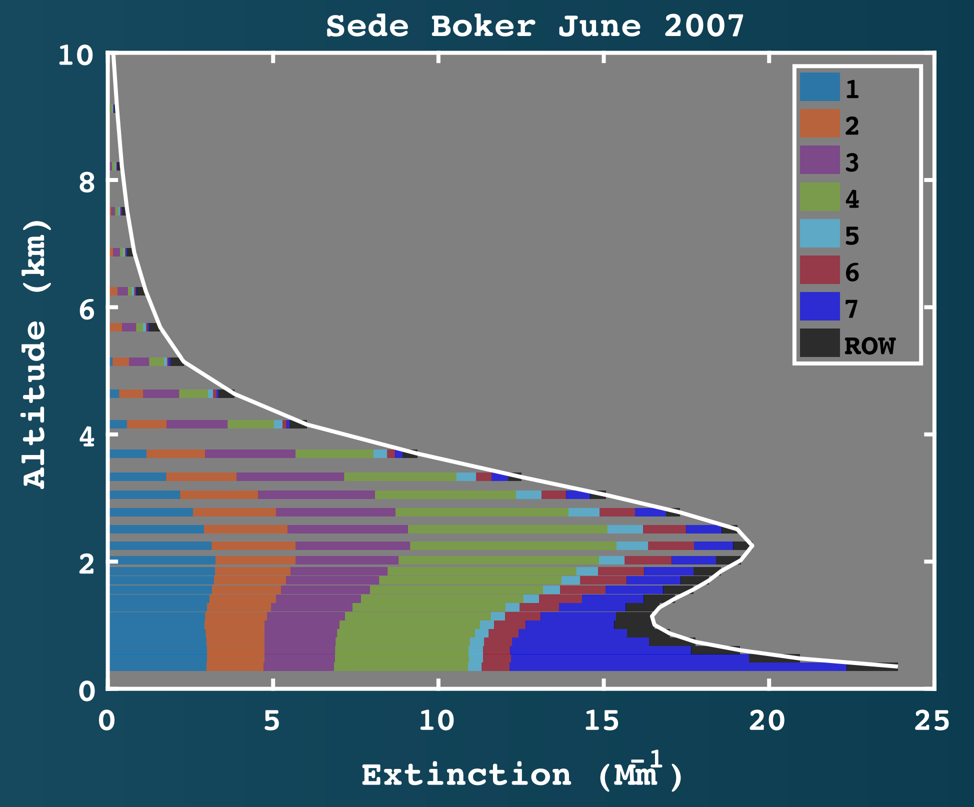

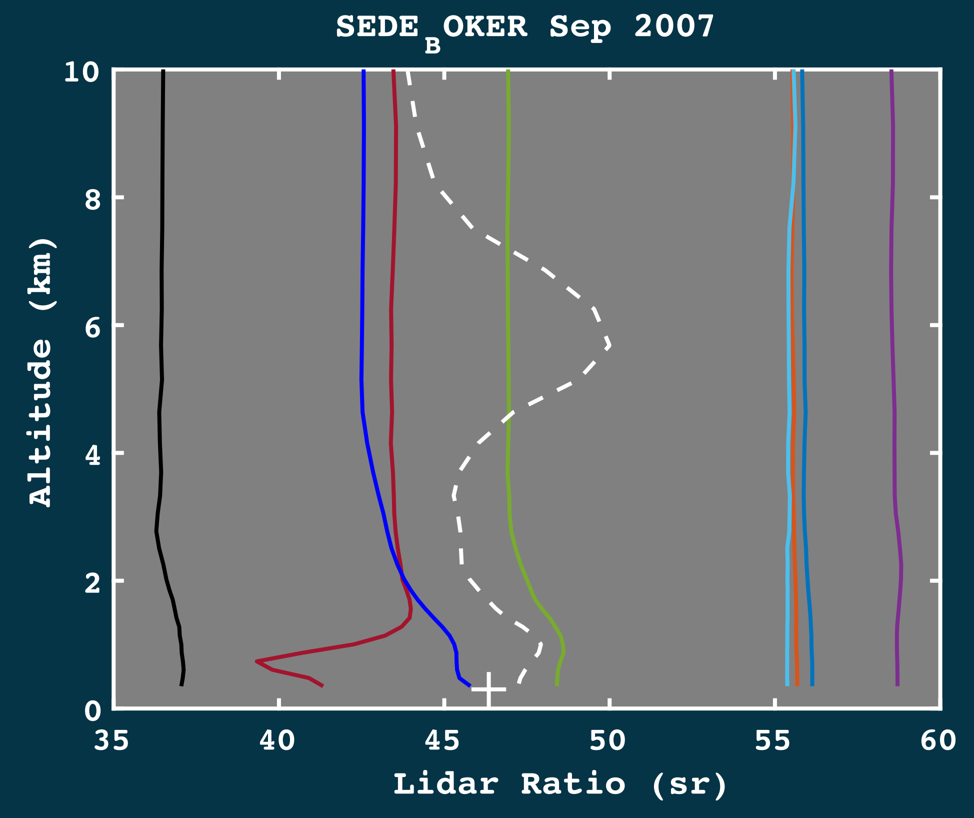

Example of Modeled and Empirical lidar ratios

Sede Boker

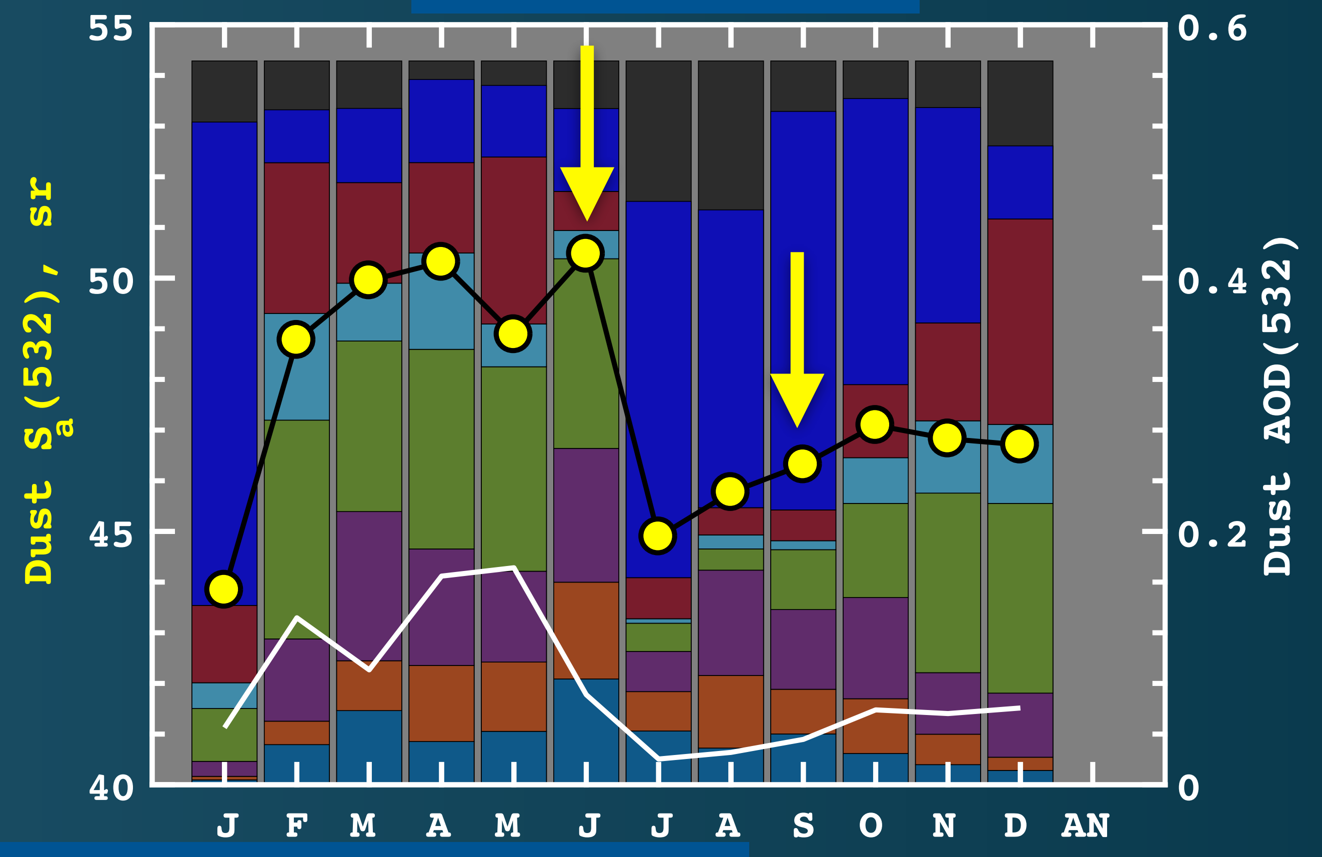

GOCART Sa (2007), 7 PSA

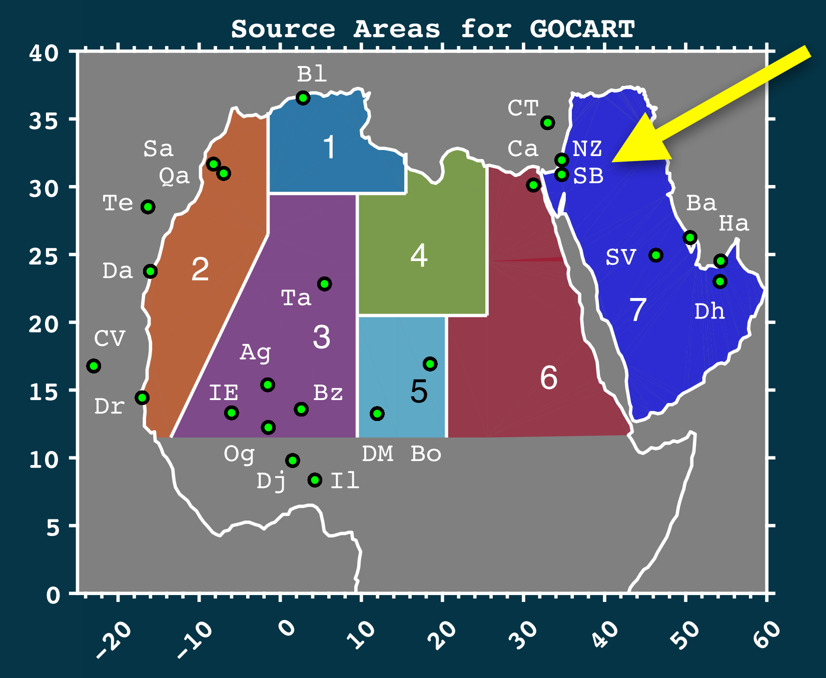

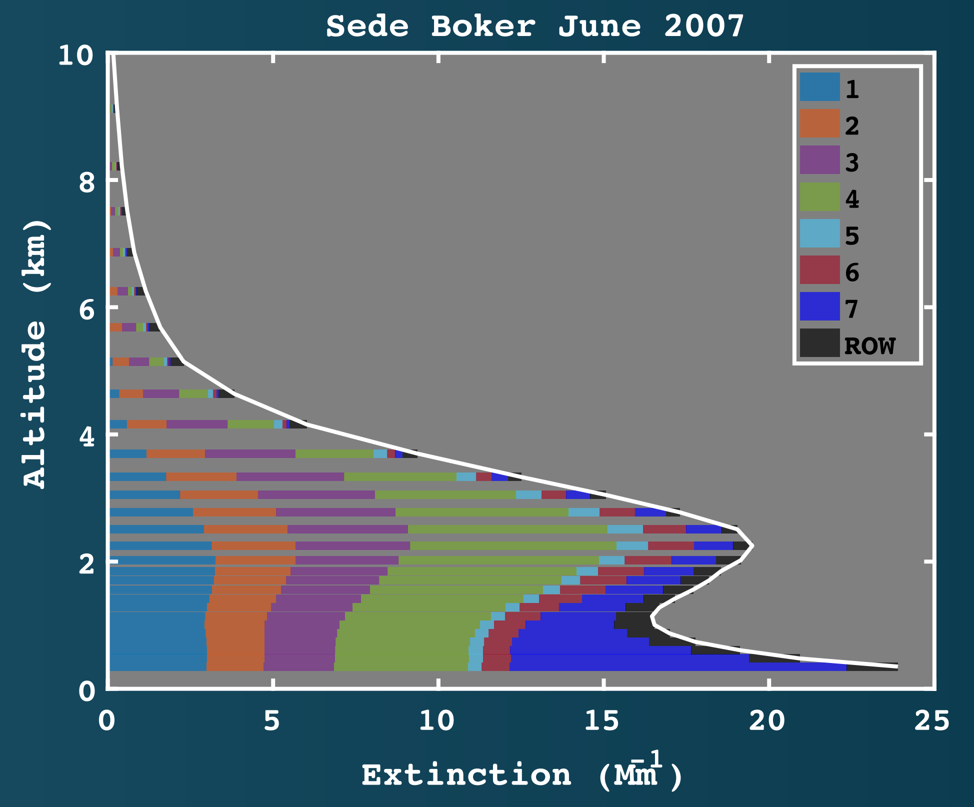

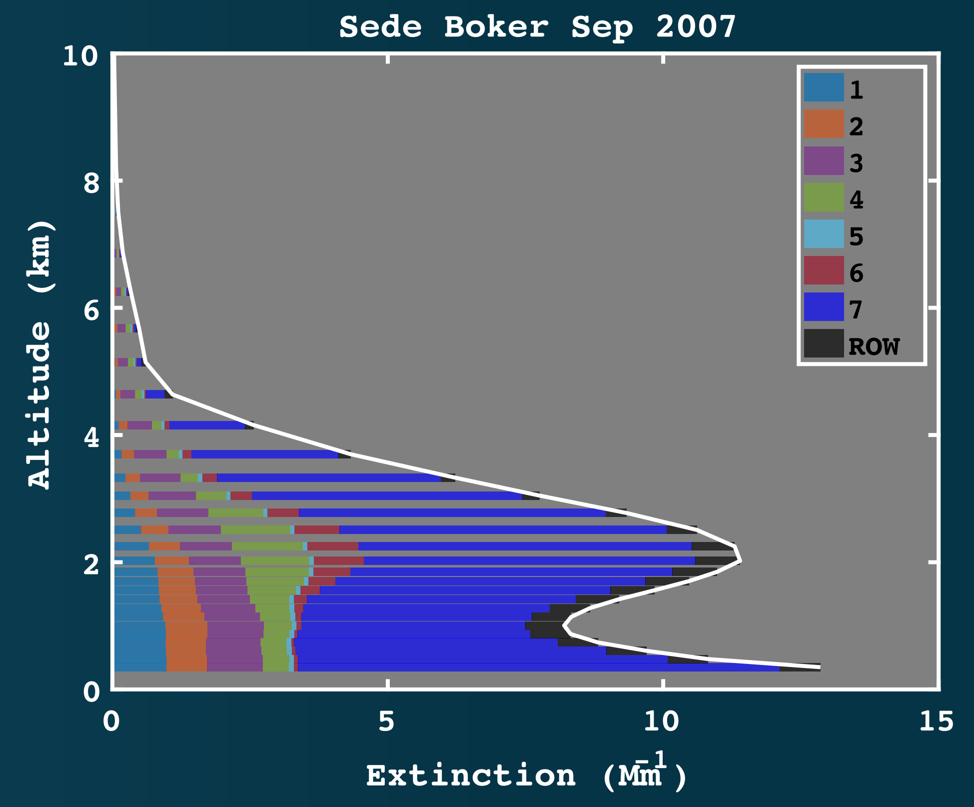

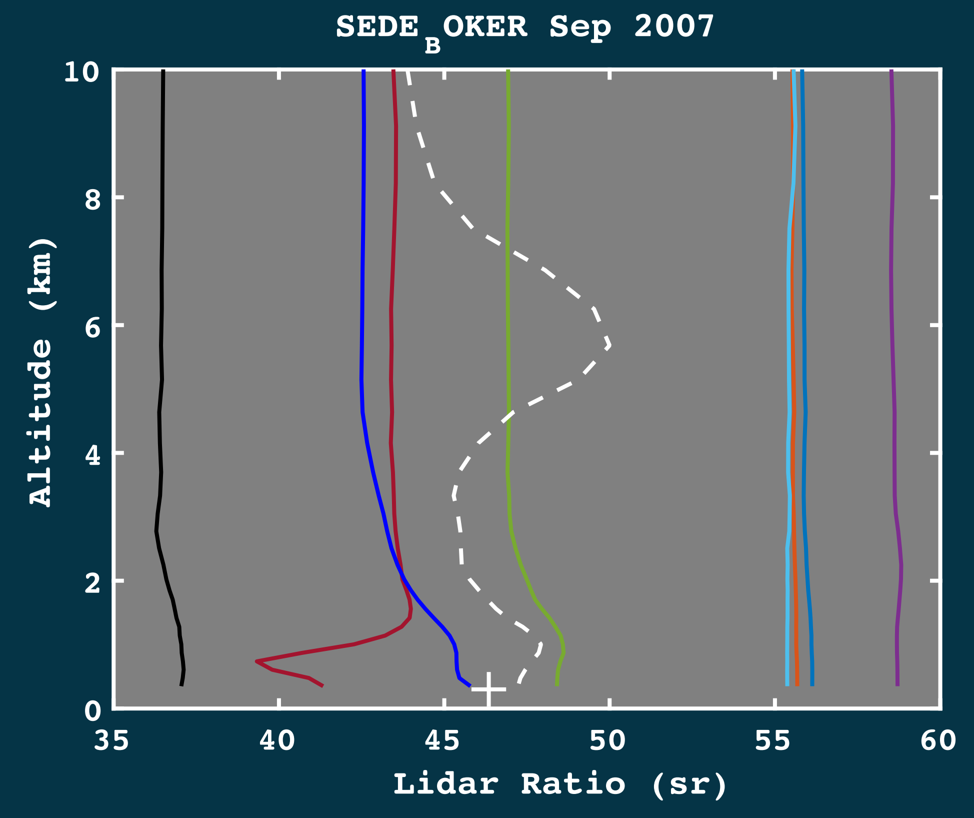

Example of Modeled and Empirical lidar ratios

Sede Boker

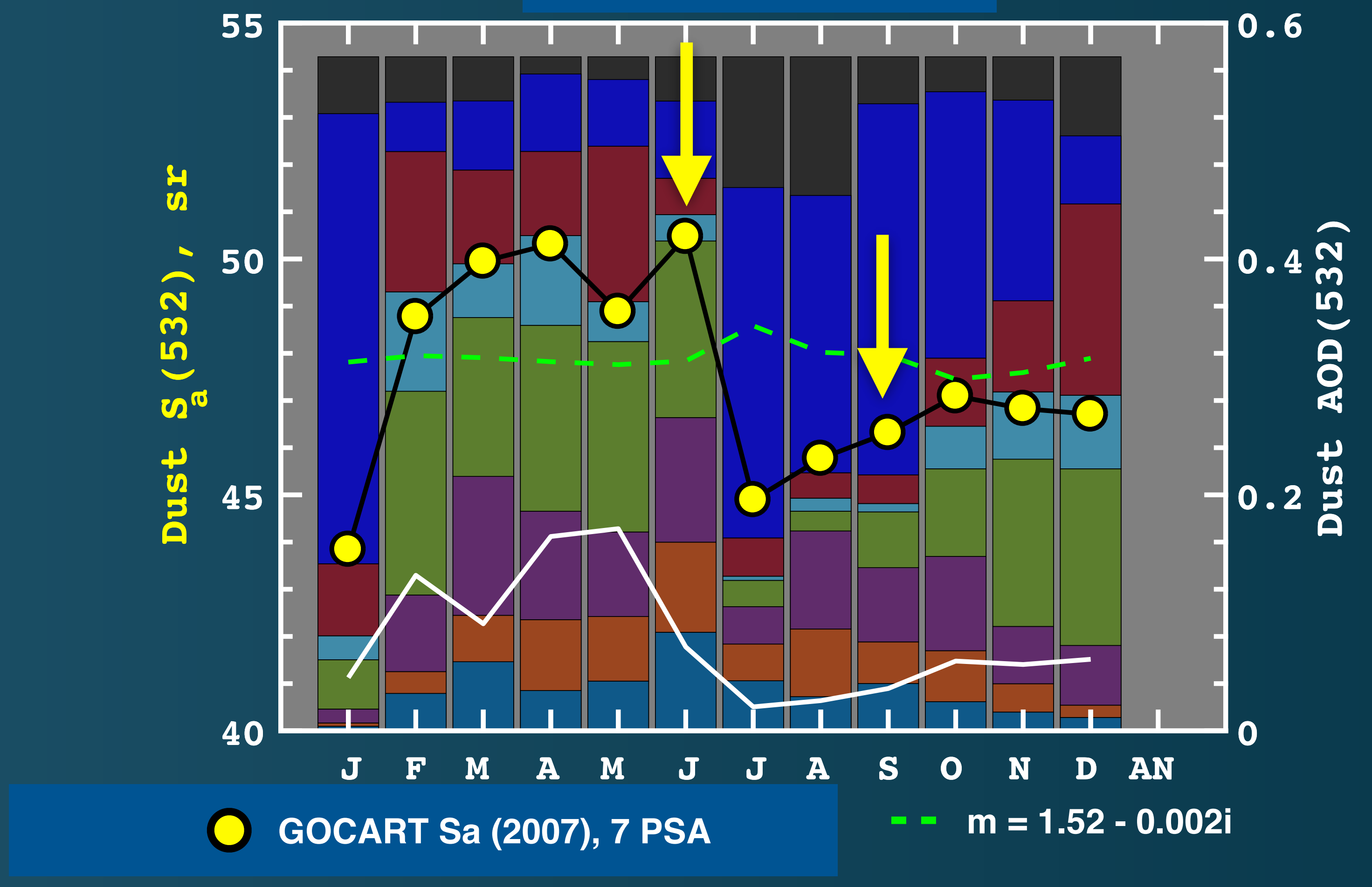

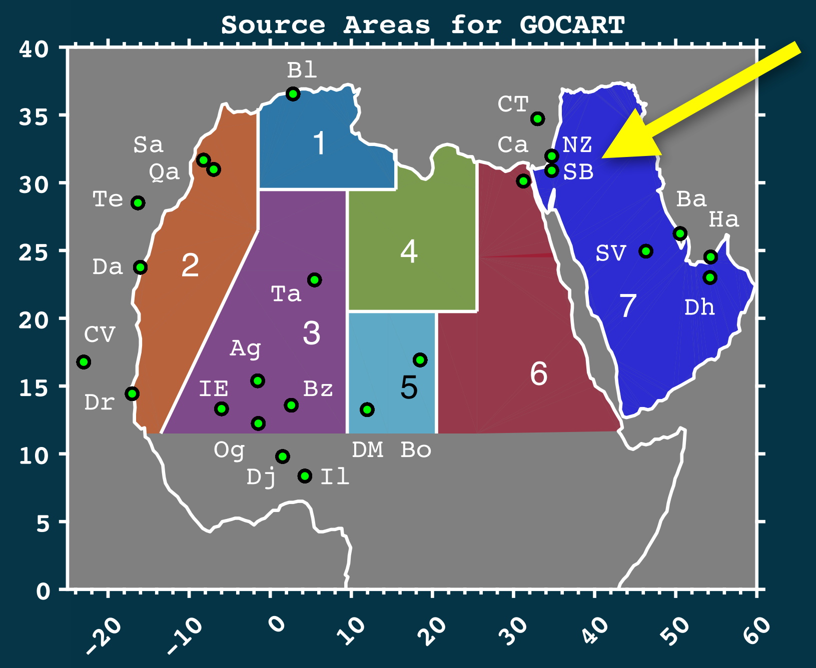

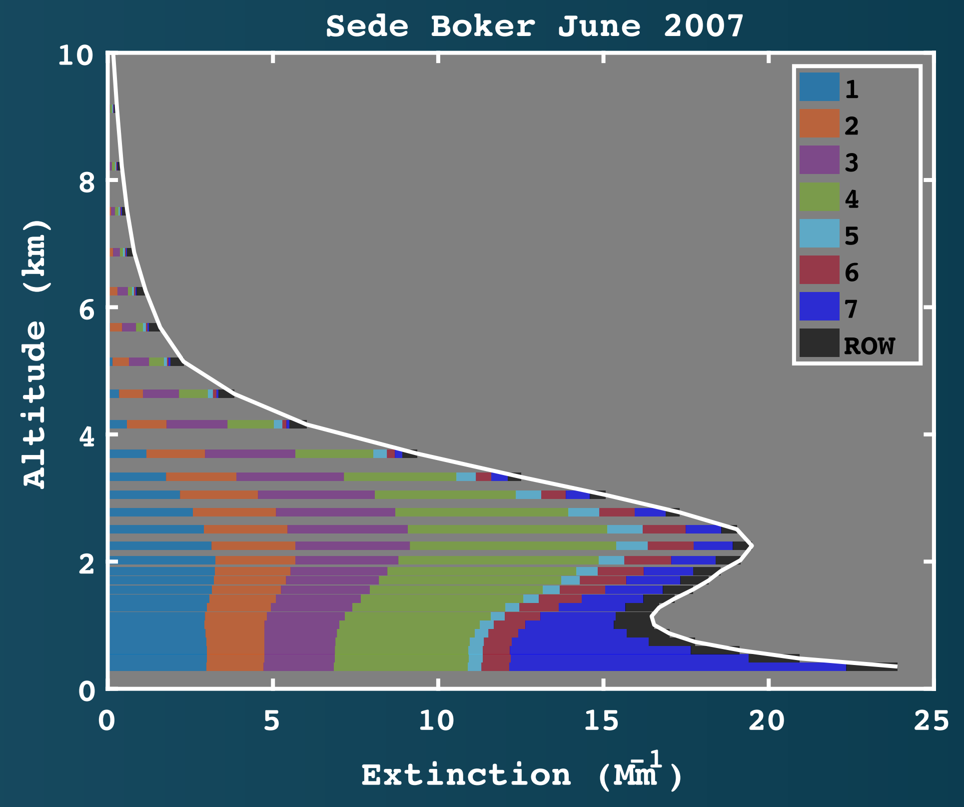

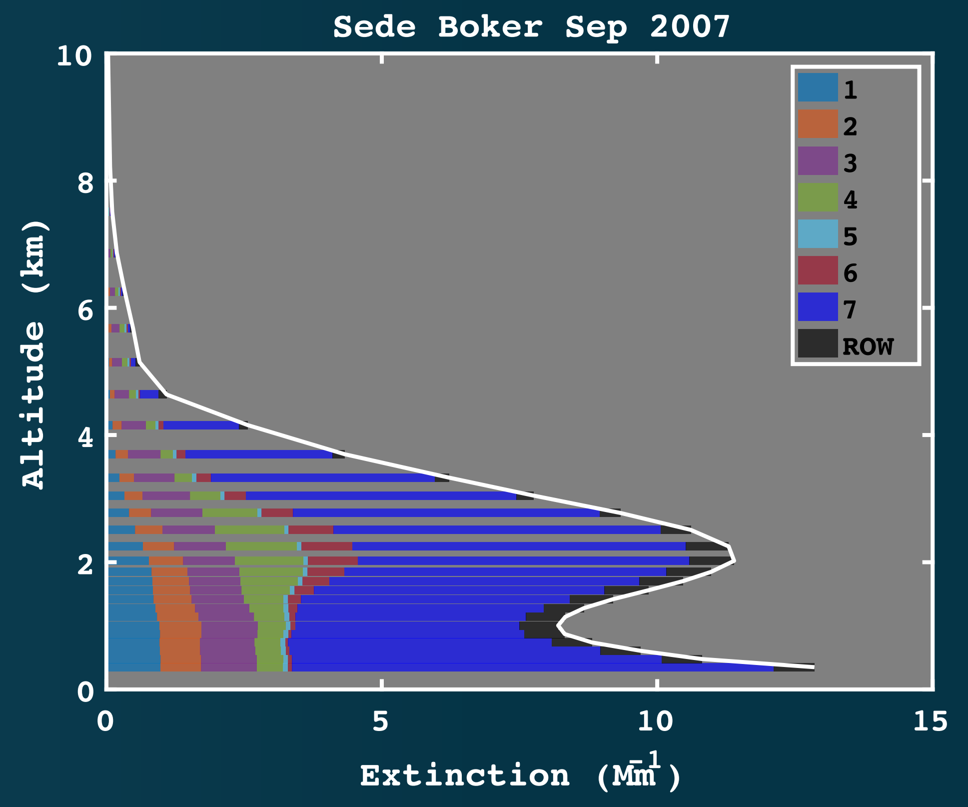

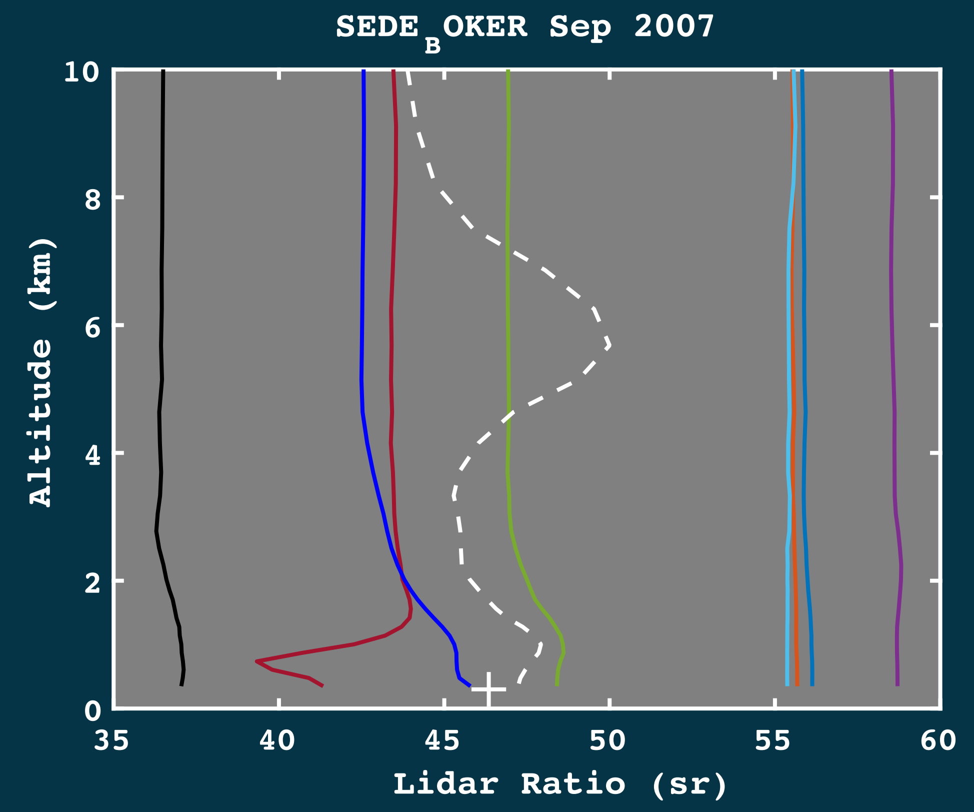

Source region impact on dust single-scatter albedo and AOD

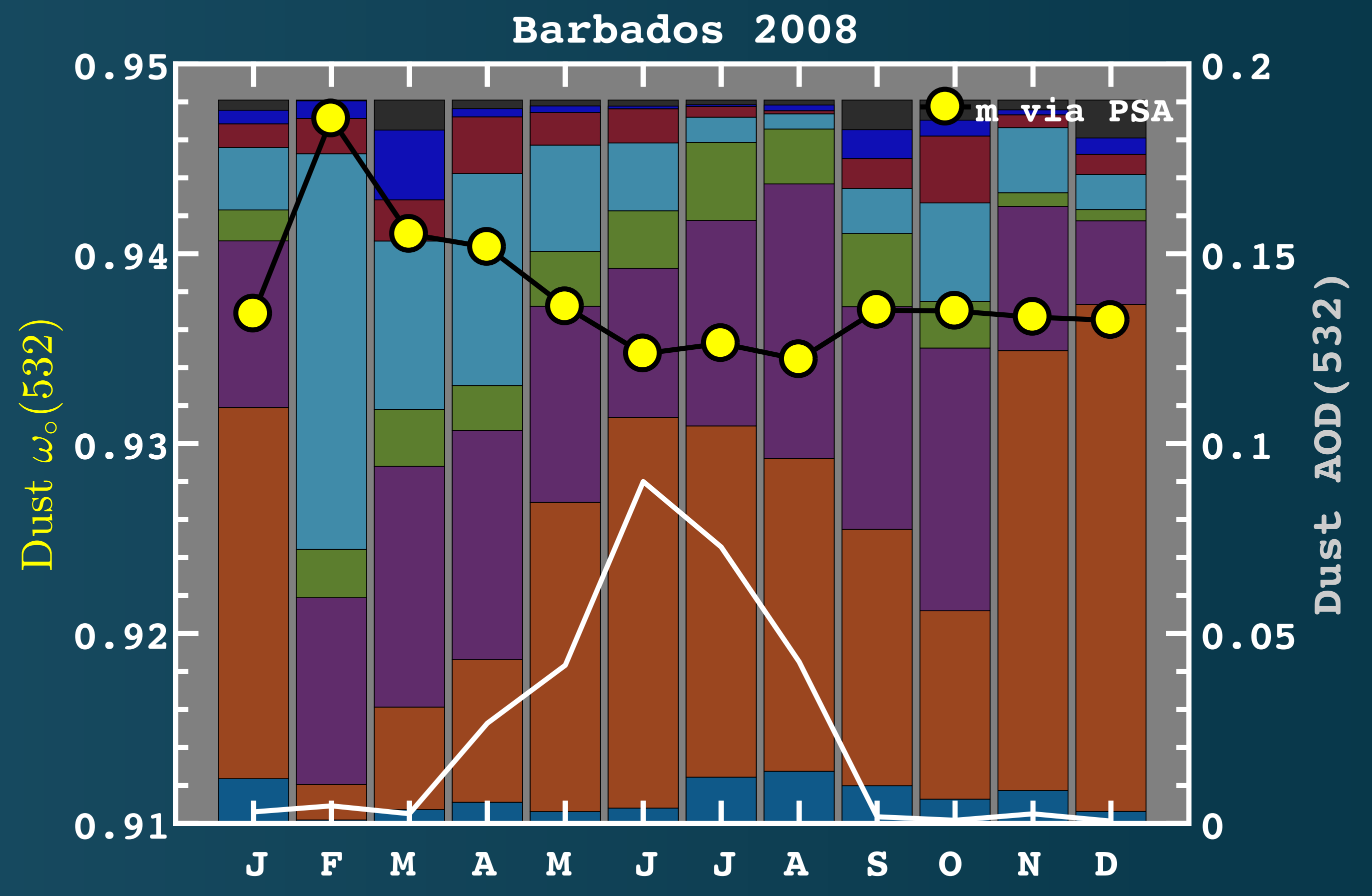

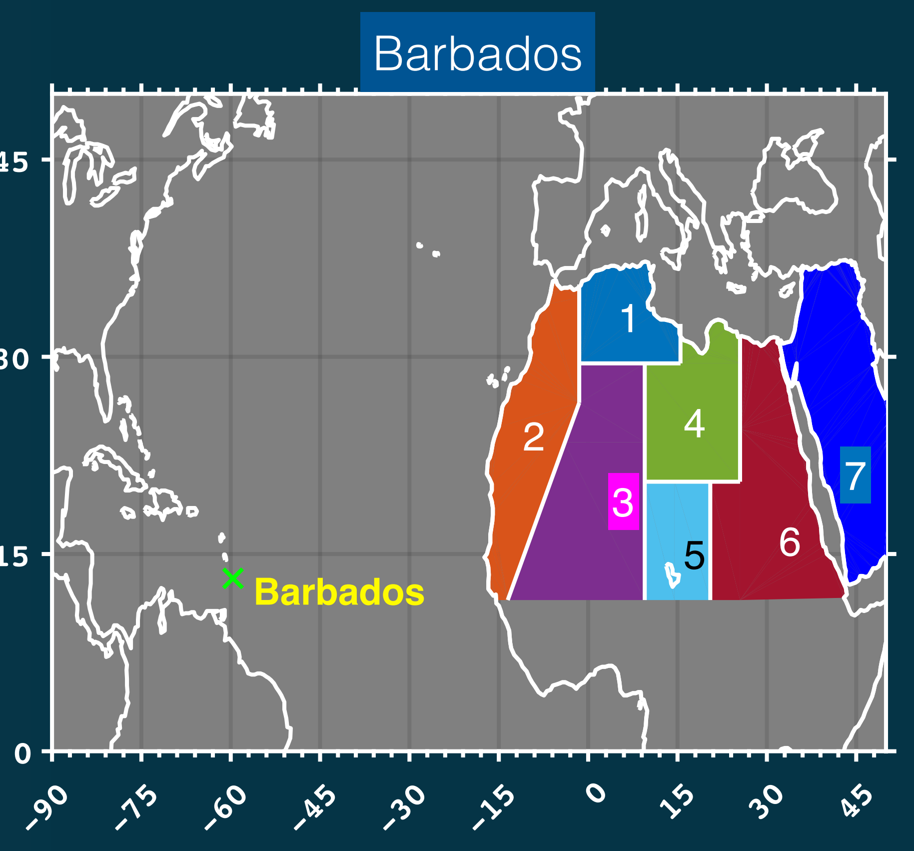

Source region impact on dust single-scatter albedo and AOD

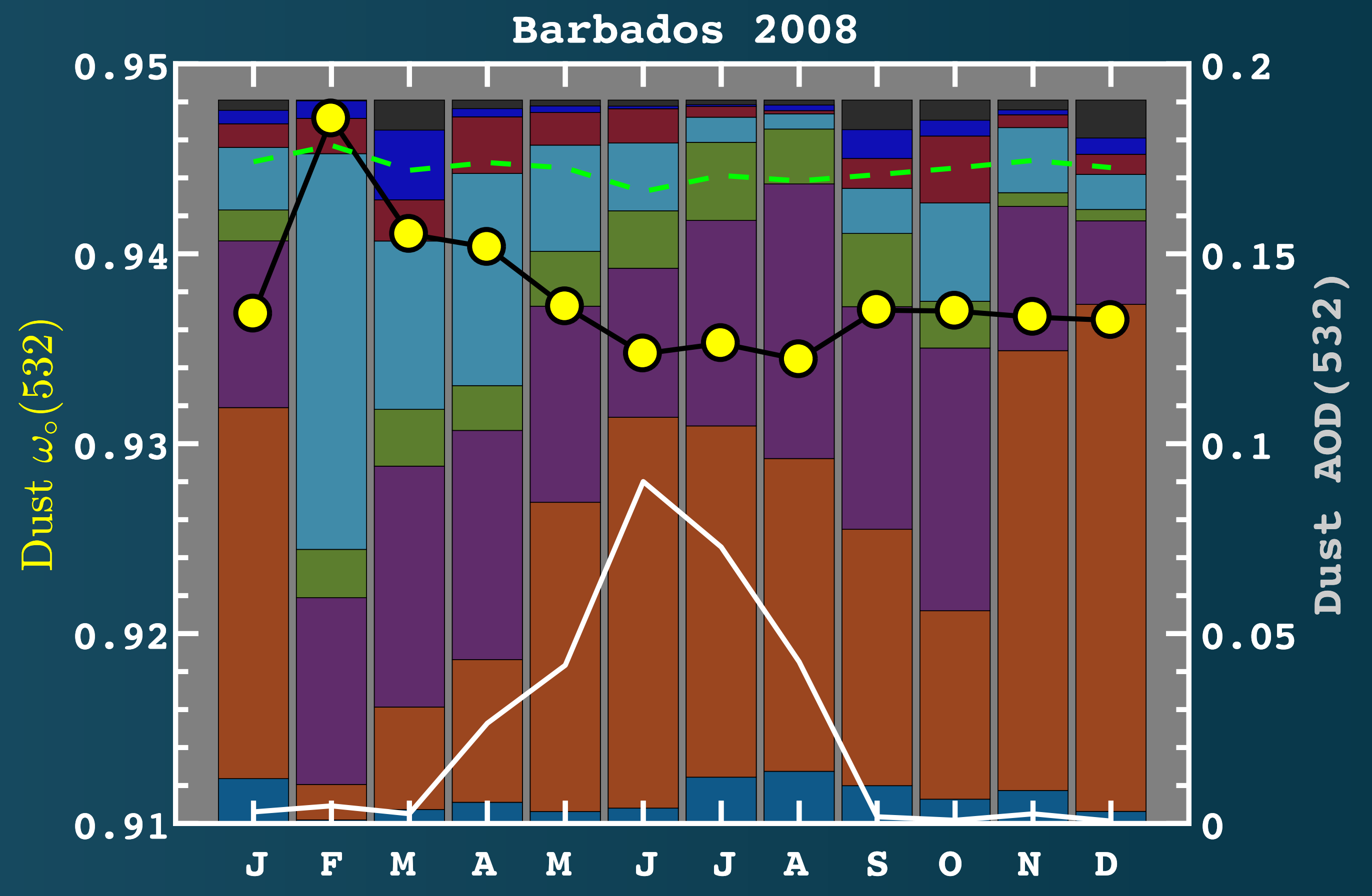

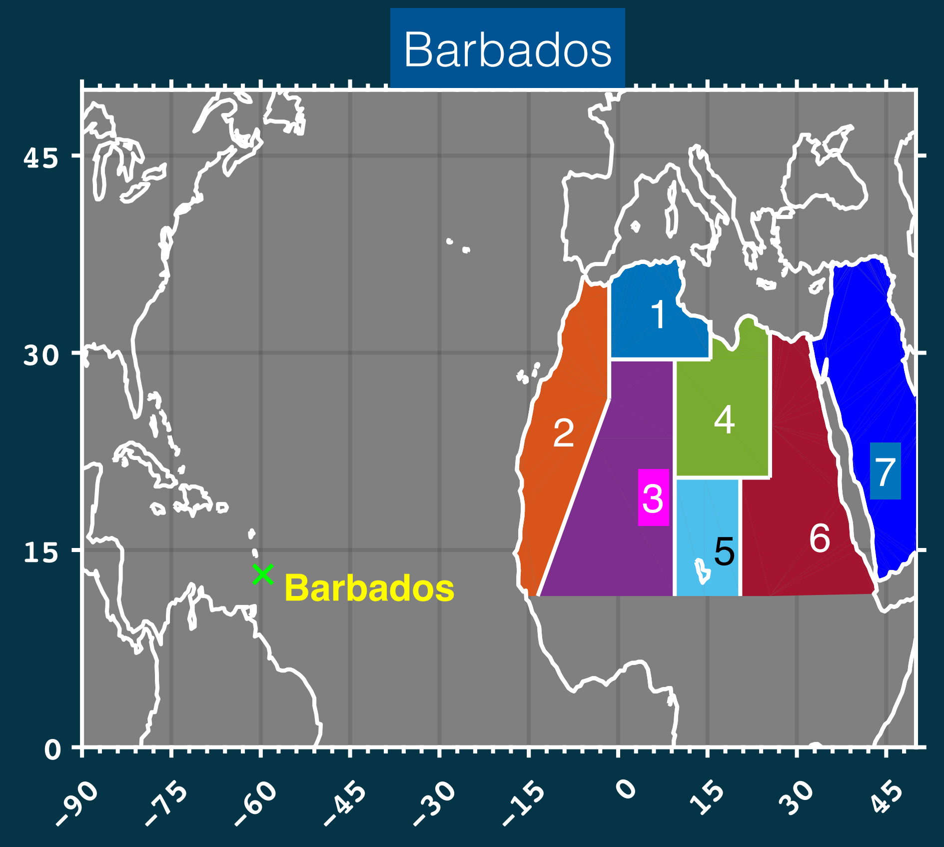

Source region impact on dust single-scatter albedo and AOD

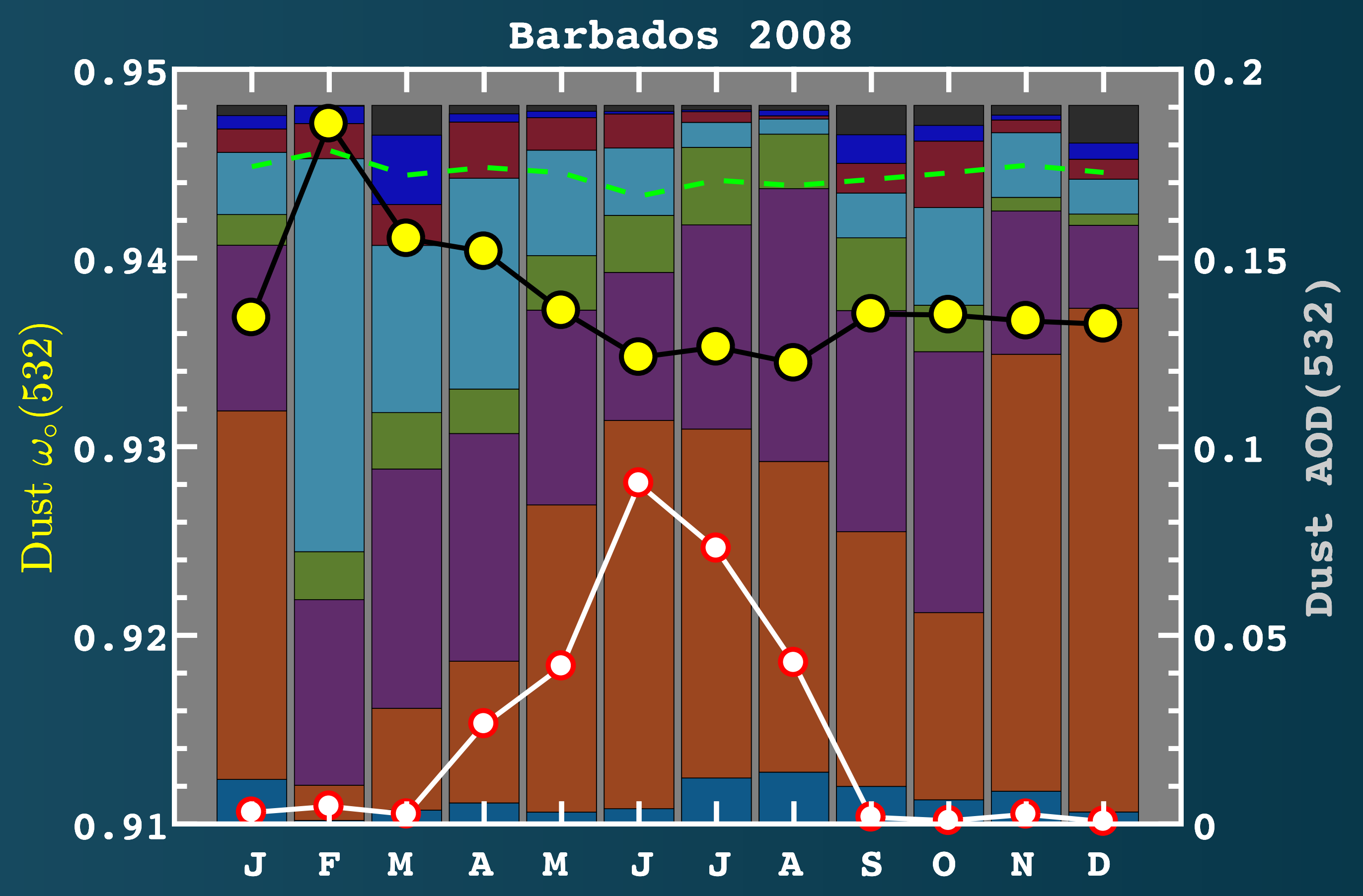

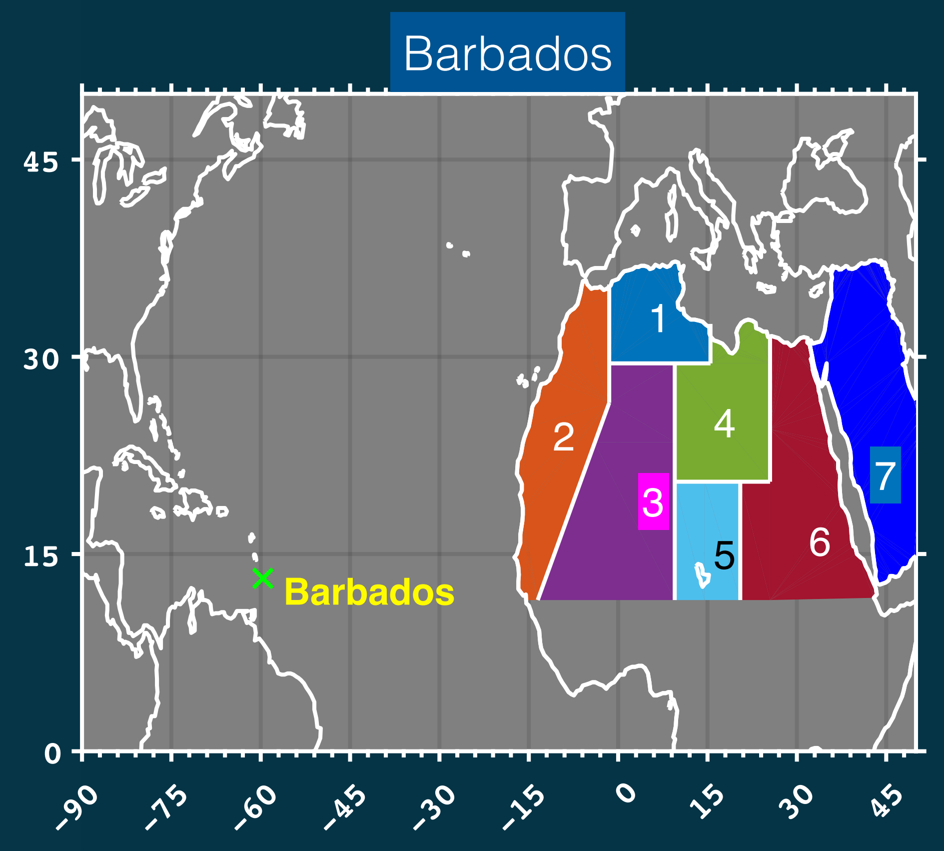

Source region impact on dust single-scatter albedo and AOD

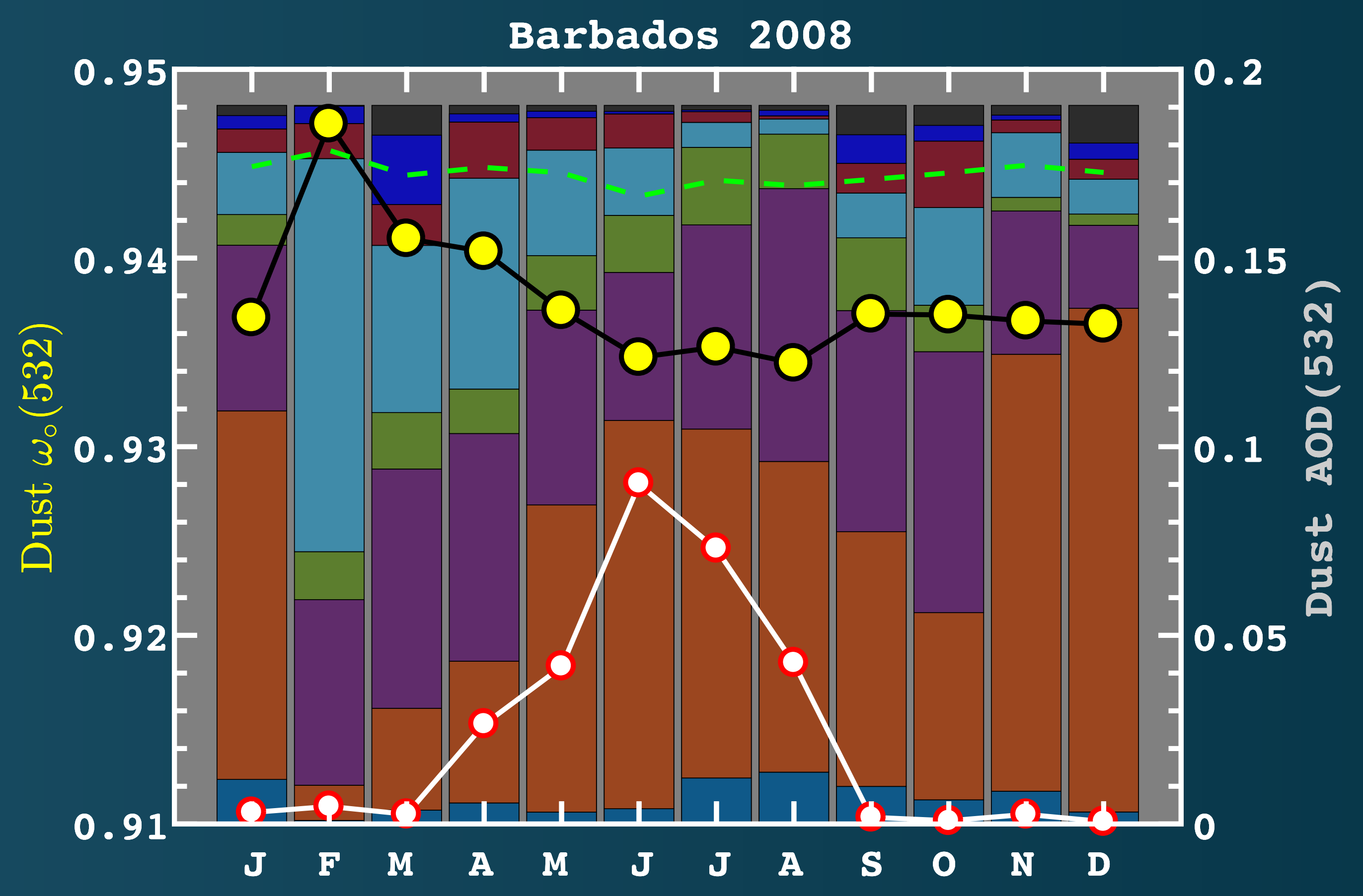

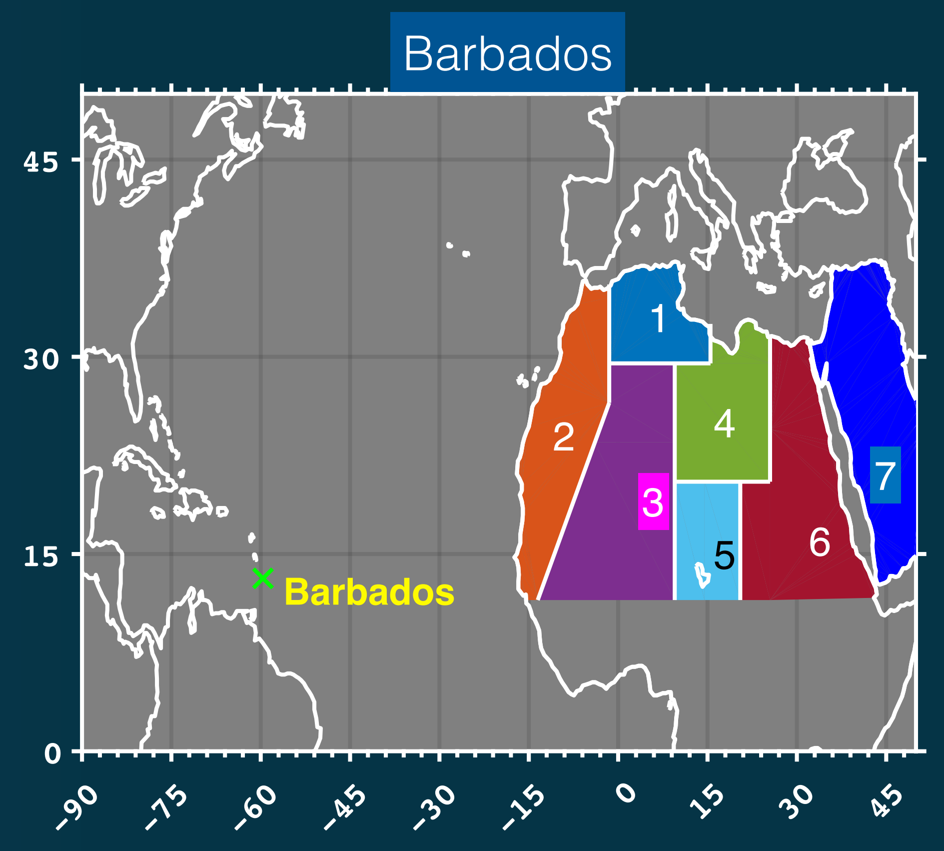

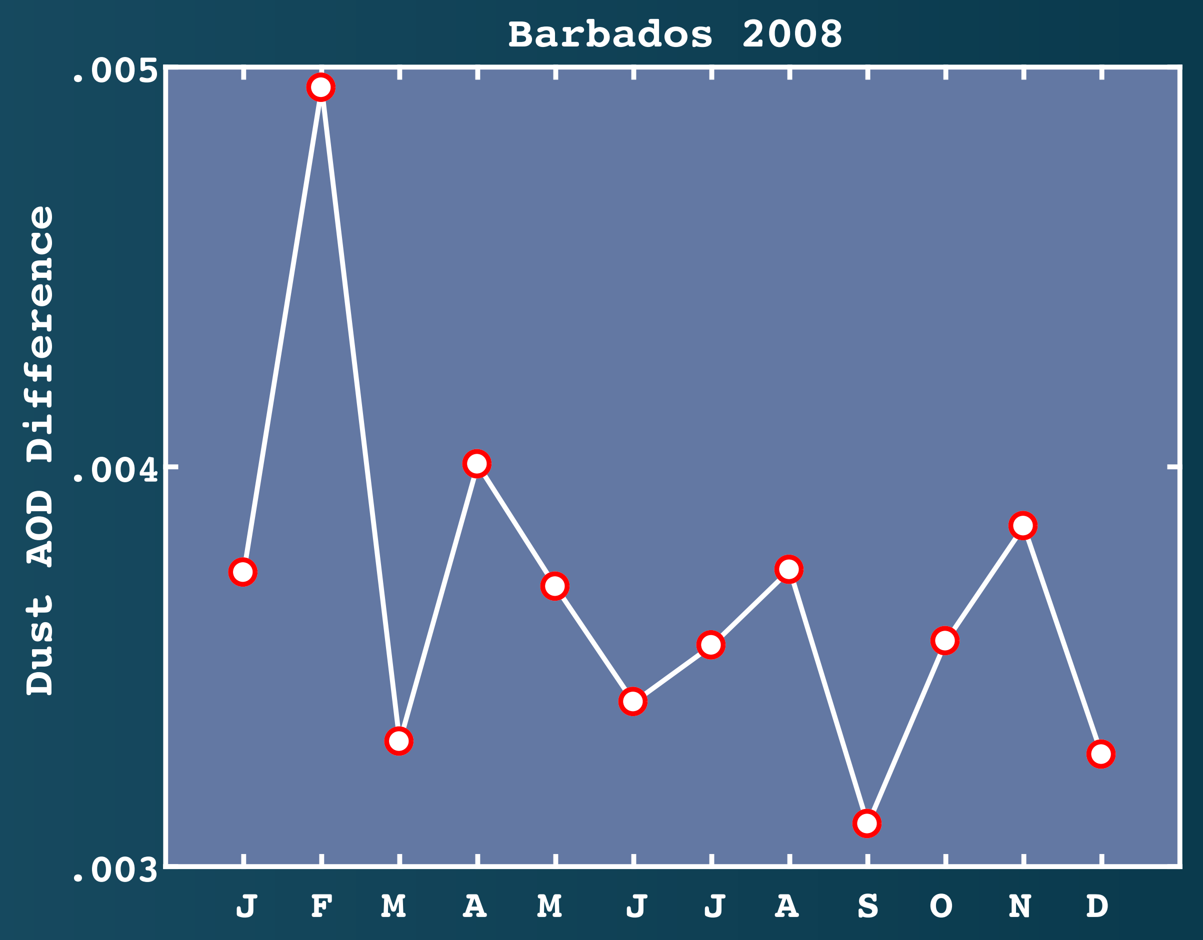

Source region impact on dust single-scatter albedo and AOD

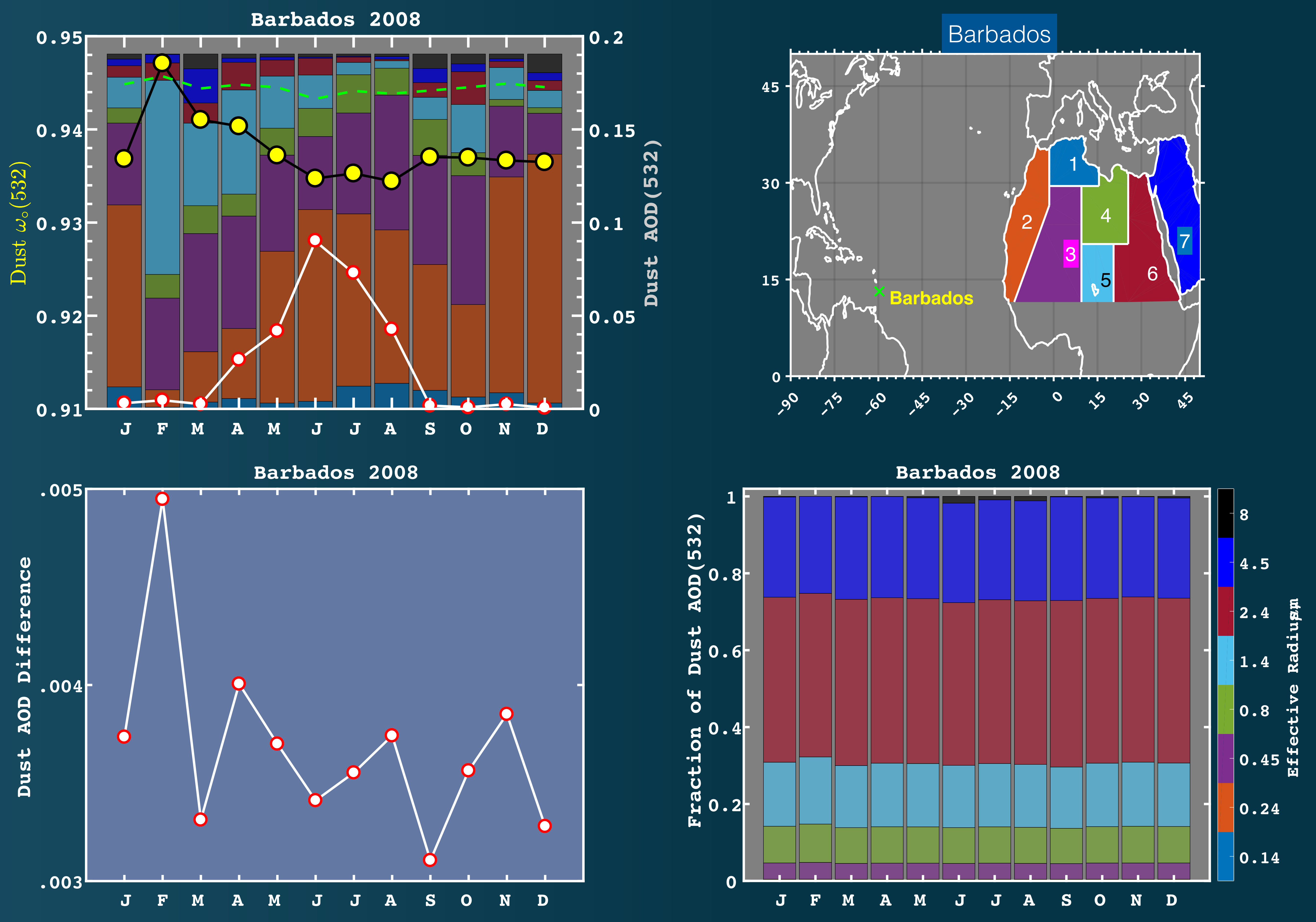

Regional Variability of the Lidar Ratio for Dust

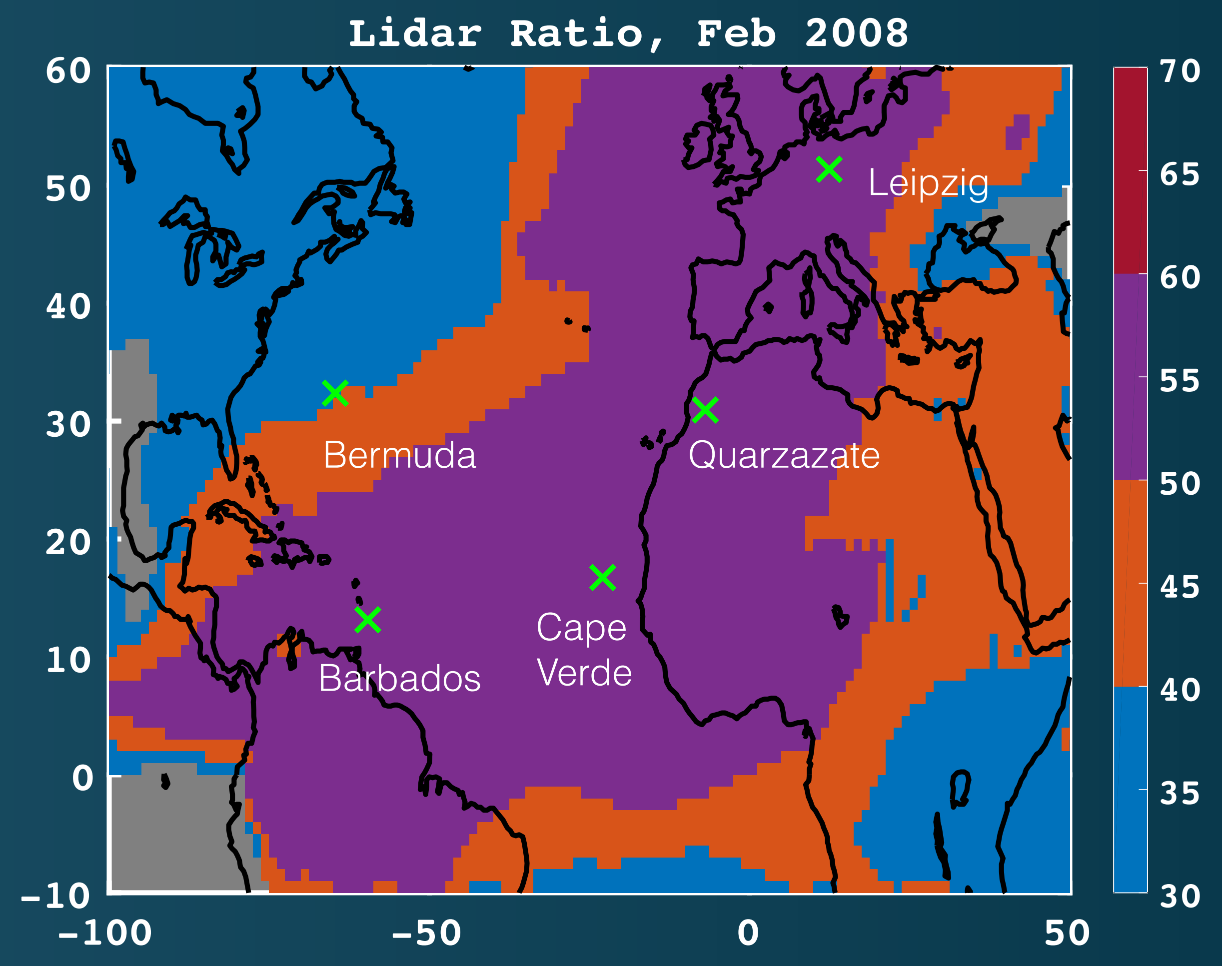

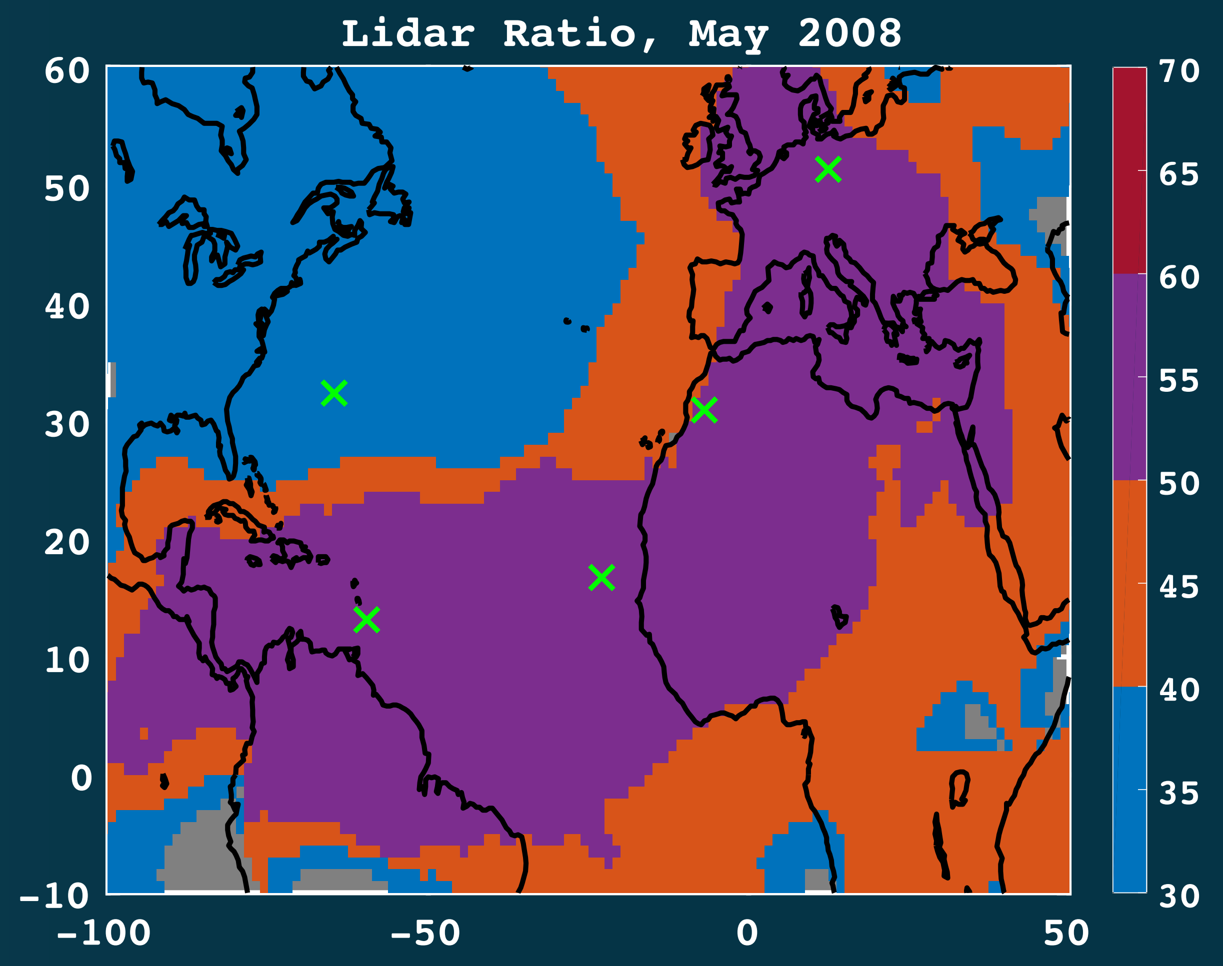

- SAMUM -1 took place near Quarzazate (Morroco) in May/June 2006
- SAMUM-2 took place in Cape Verde in Jan/Feb and May/June 2008
- SALTRACE took place in Barbados in Aug 2013

Recap

- CALIOP retrievals of dust AOD require accurate dust lidar ratios.
- Dust lidar ratios are sensitive to the real refractive index (i.e., mineralogy).
- We used the GOCART aerosol transport model and AERONET to assign refractive index and lidar ratios to seven regions in Africa and Middle East.
- Model output indicates that downstream mineralogy and lidar ratios vary regionally and seasonally.
- Single-scatter albedo varies by ~0.015.
- Dust AOD varies by less than 0.01.

Acknowledgements

- We appreciate the efforts of the AERONET and PHOTONS (Service d'Observation from LOA/USTL/CNRS) principal investigators, and the entire AERONET, PHOTONS, and CALIPSO teams.
- We thank O. Dubovik and T. Lapyonok for providing the forward scattering code.
- This work is supported by NASA's Earth Science Enterprise through the CALIPSO project.

Measurements Needed to Constrain Lidar Ratios for CALIPSO Retrievals

- Lidar ratio measurements are great, but we need concurrent mineralogy (or refractive index) and size distributions.
- Need these concurrent measurements near source regions in Middle East and Asia, and in transport regions over the Atlantic and Carribean.
- Refractive index measurements for "pure" African clays (illite, kaolinite, montmorillonite, and goethite).
- Studies to determine any changes in dust refractive indices during transport.

Appendix

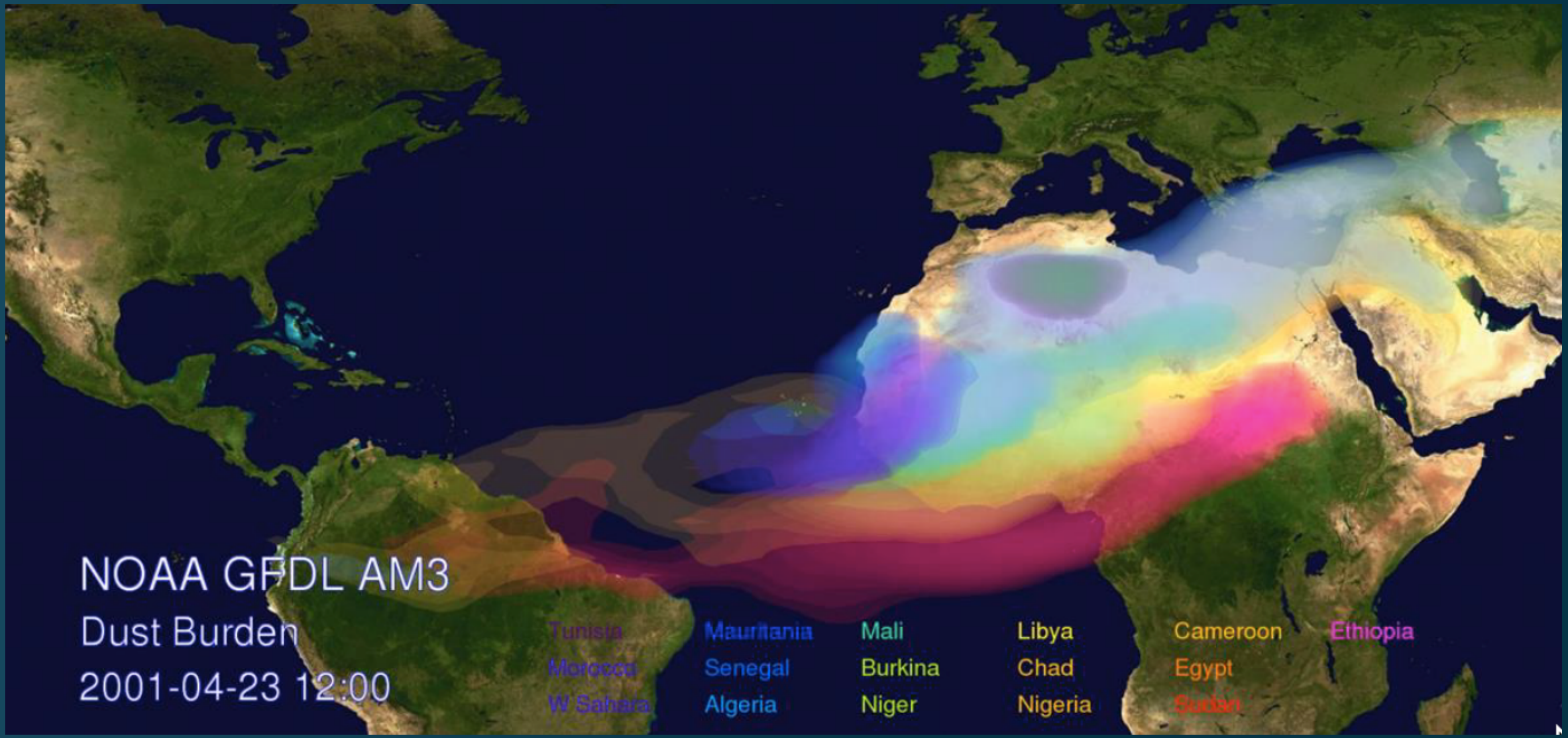

African dust sources presented by Joe Prospero at DUST 2014. Model run by Paul Ginoux

Mineral	n(532)	Reference
Hematite	3.18	Chen and Cahan (1981)
Calcite	1.58	Ghosh (1999)
Quartz	1.55	Ghosh (1999)
Gypsum	1.52	Roush (2007)
Montomorillonite	1.52	Egan and Hilgeman (1979)
Kaolinite	1.49	Egan and Hilgeman (1979)
★ Illite*	1.41	Egan and Hilgeman (1979)

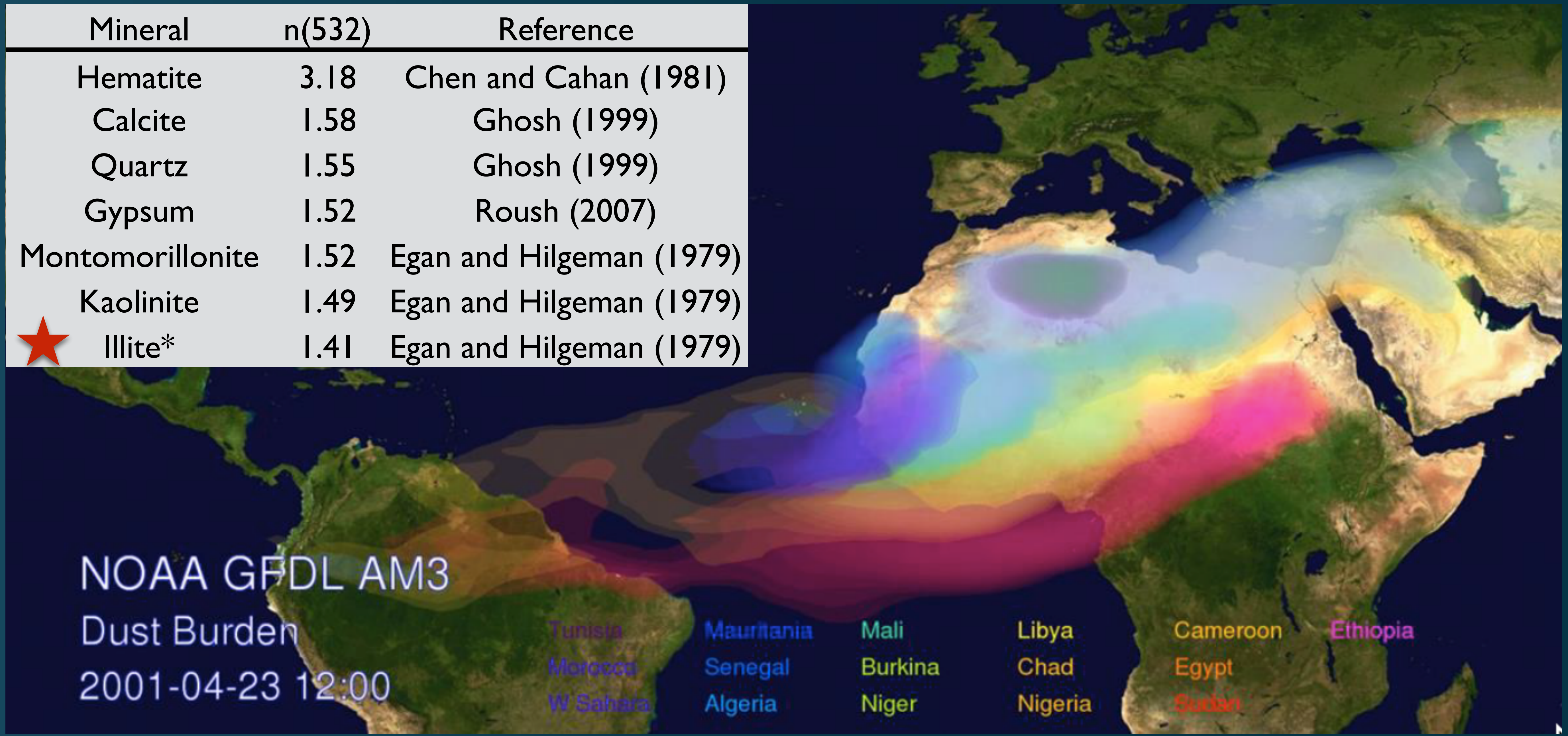

African dust sources presented by Joe Prospero at DUST 2014. Model run by Paul Ginoux

Comparison to HSRL and Raman Lidars in West Atlantic

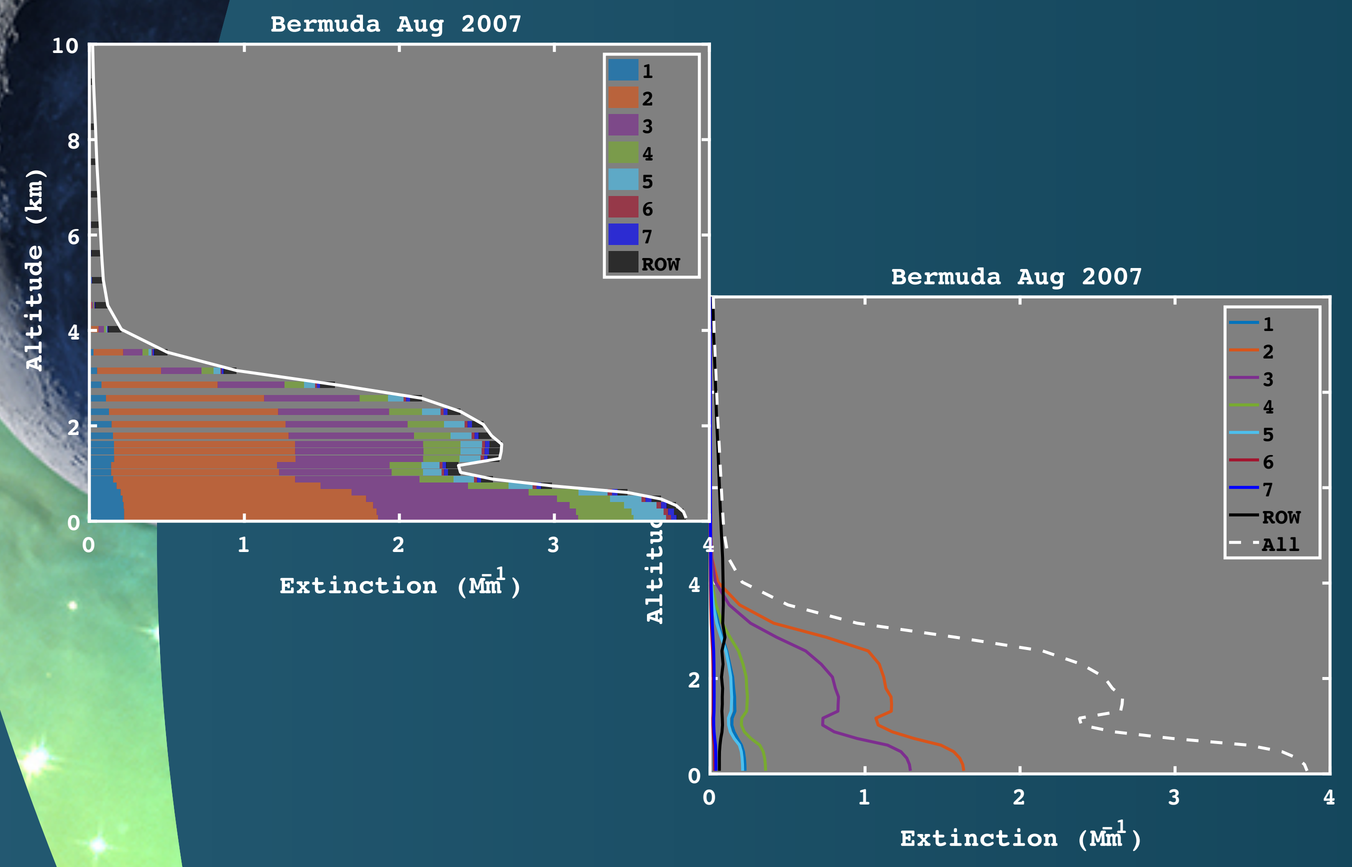

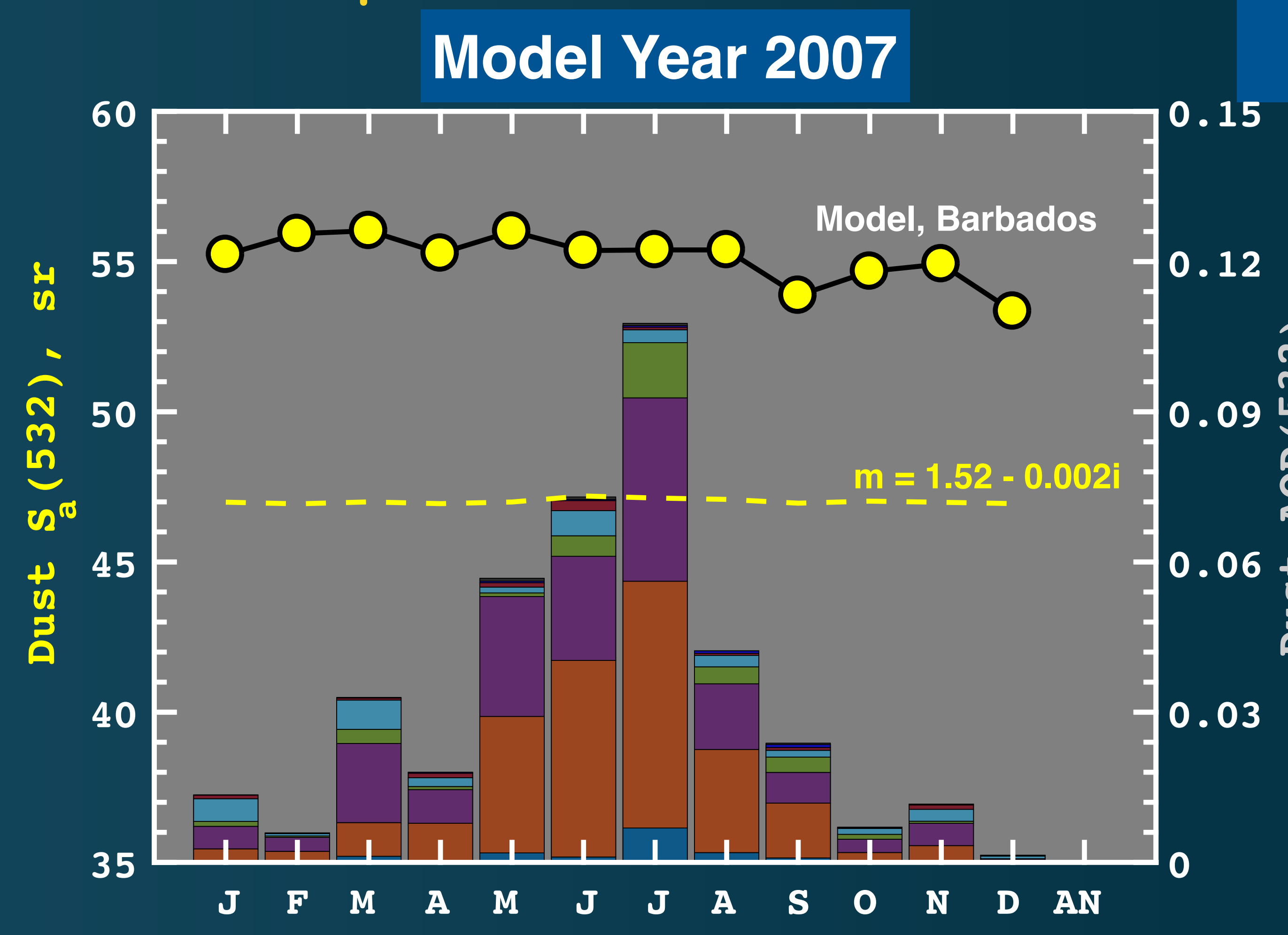

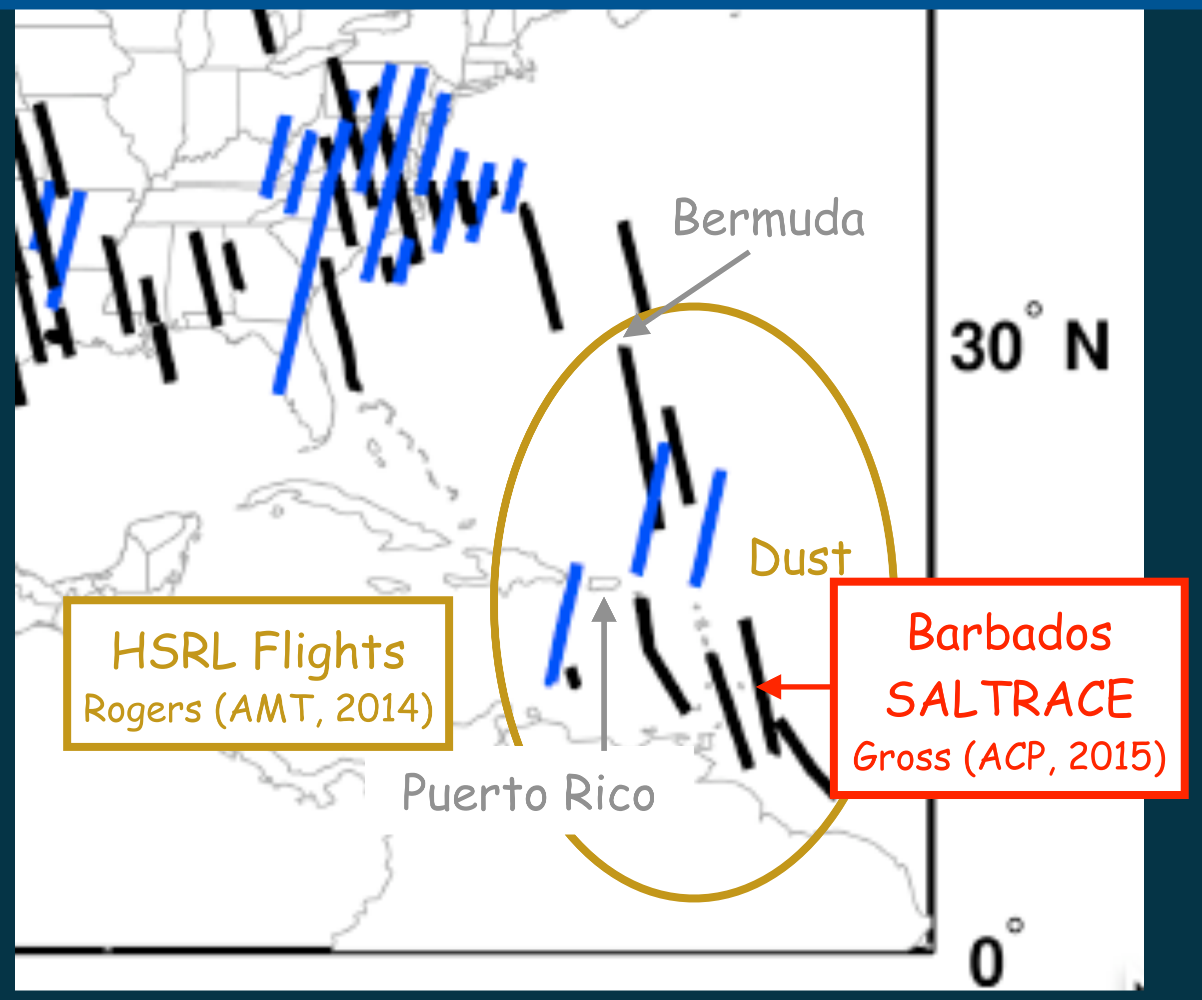

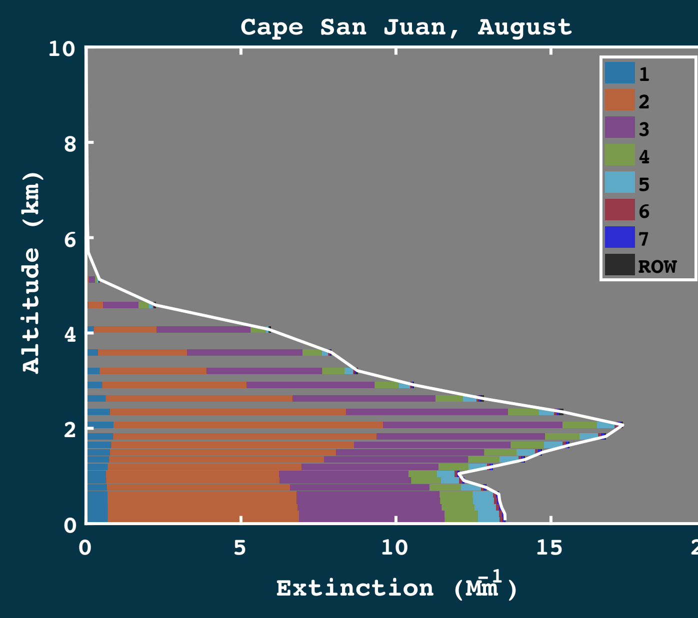

Comparison to HSRL and Raman Lidars in West Atlantic

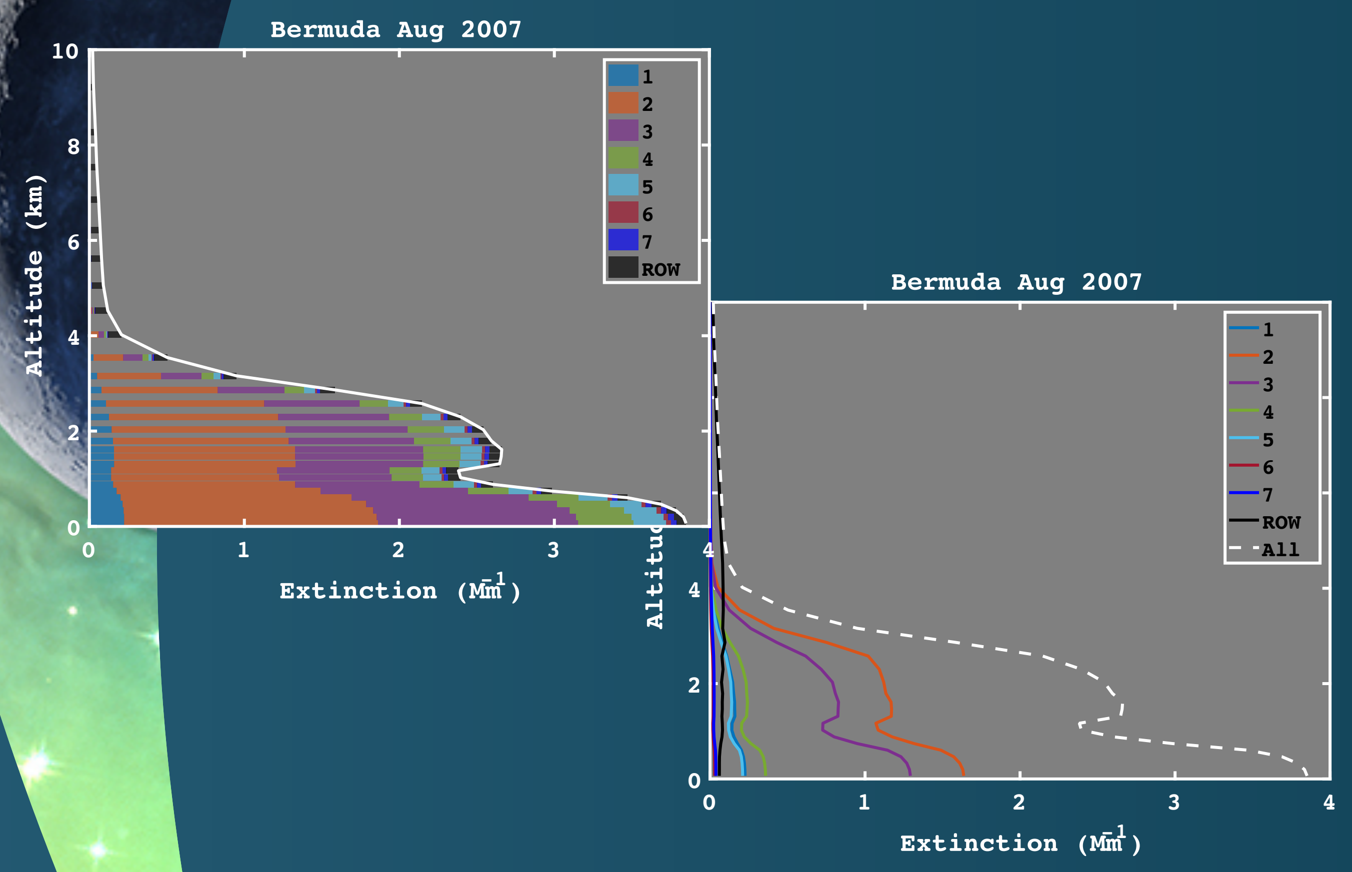

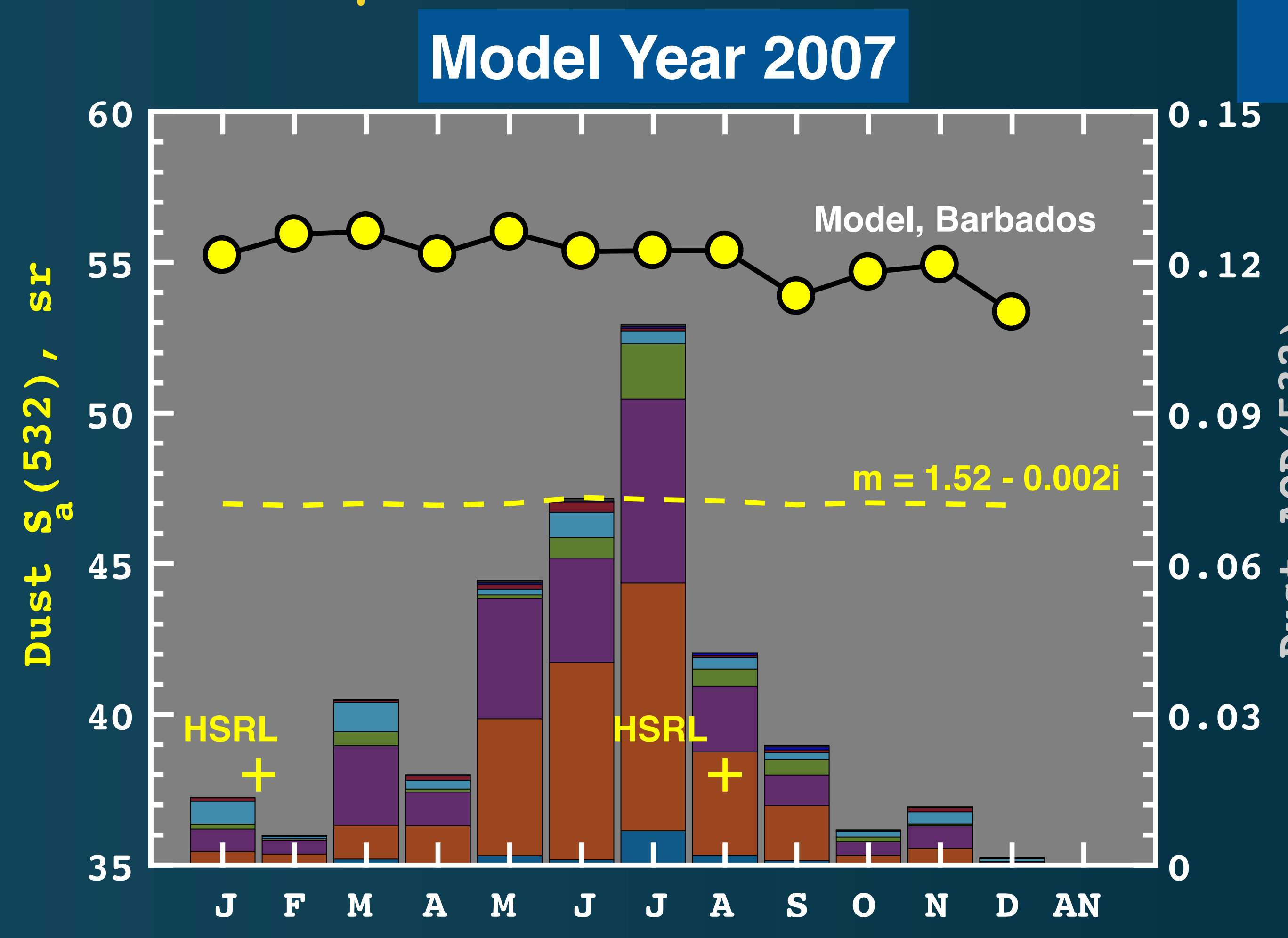

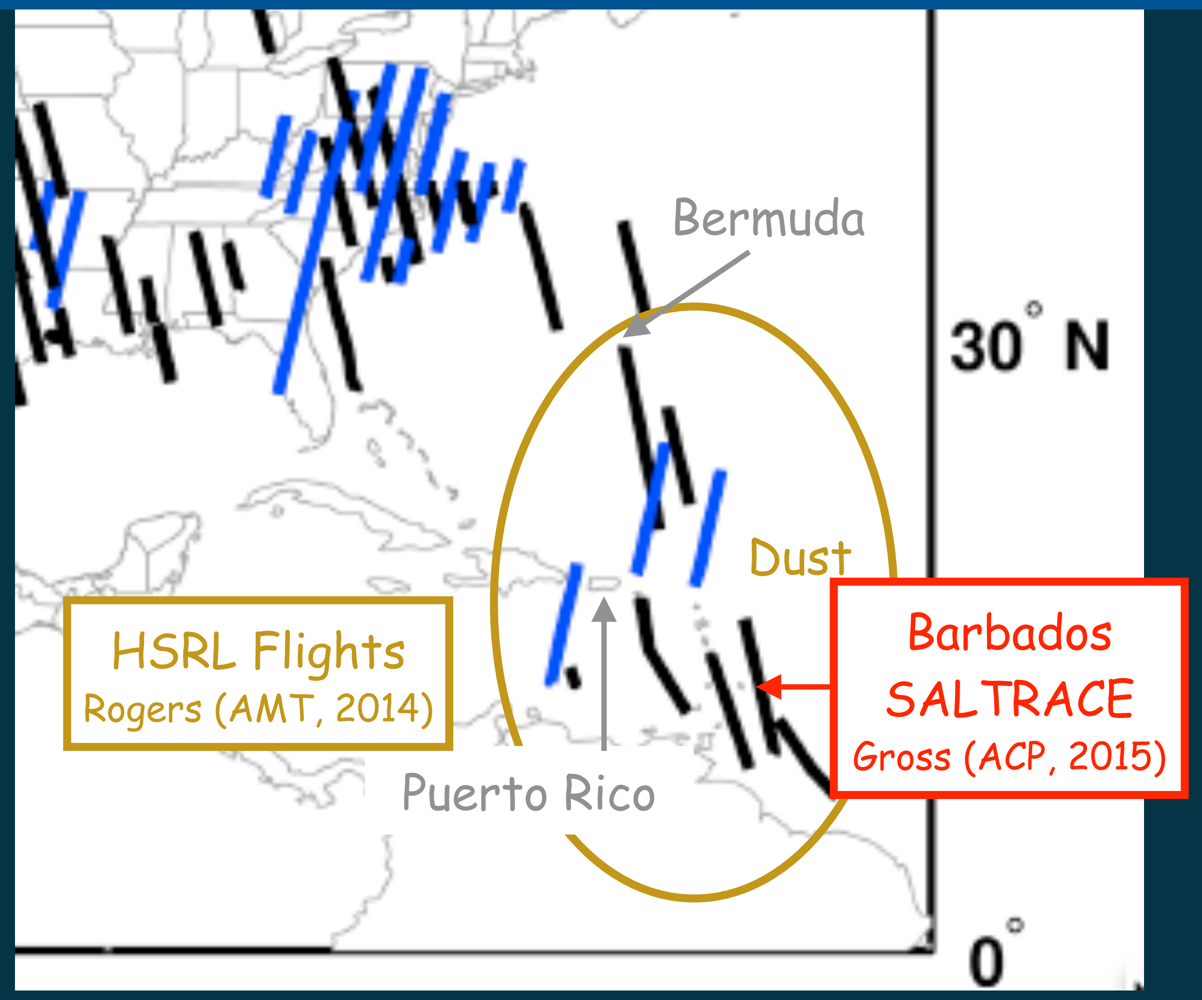

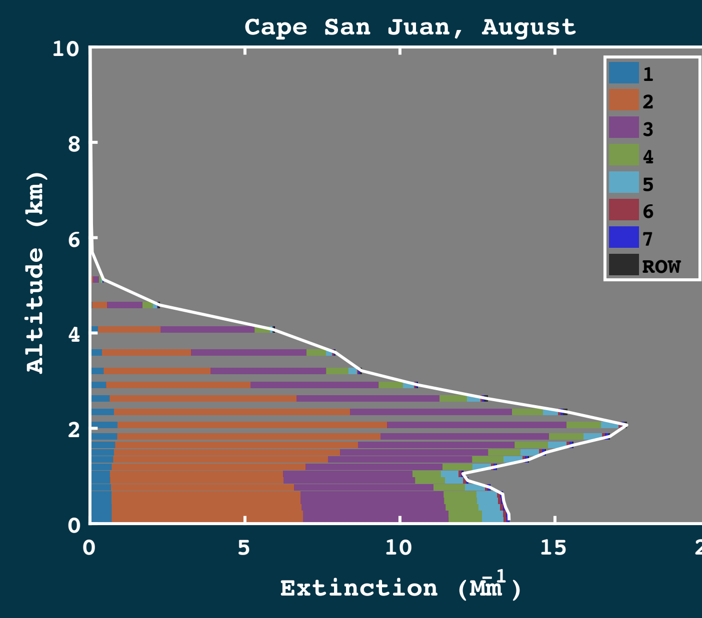

Comparison to HSRL and Raman Lidars in West Atlantic

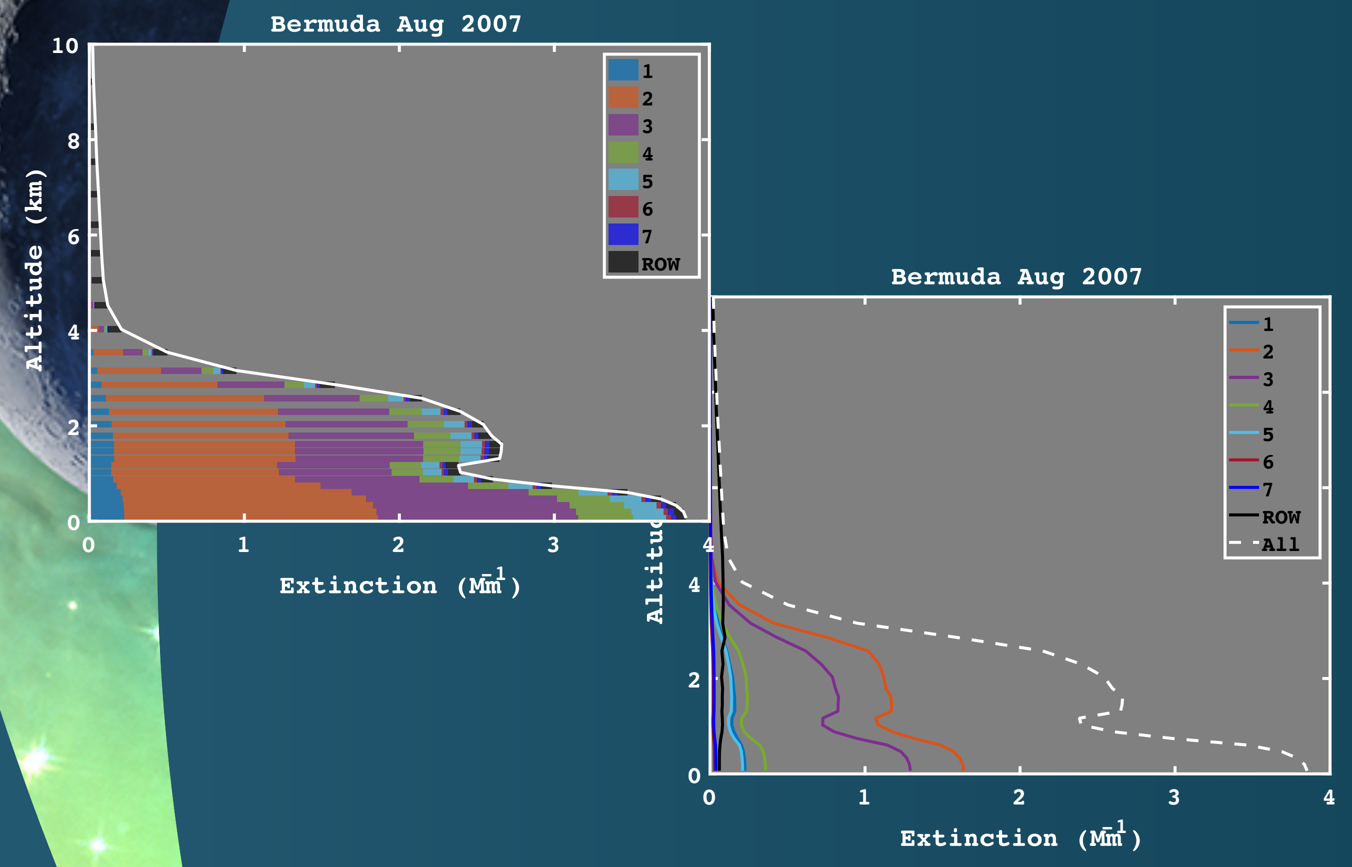

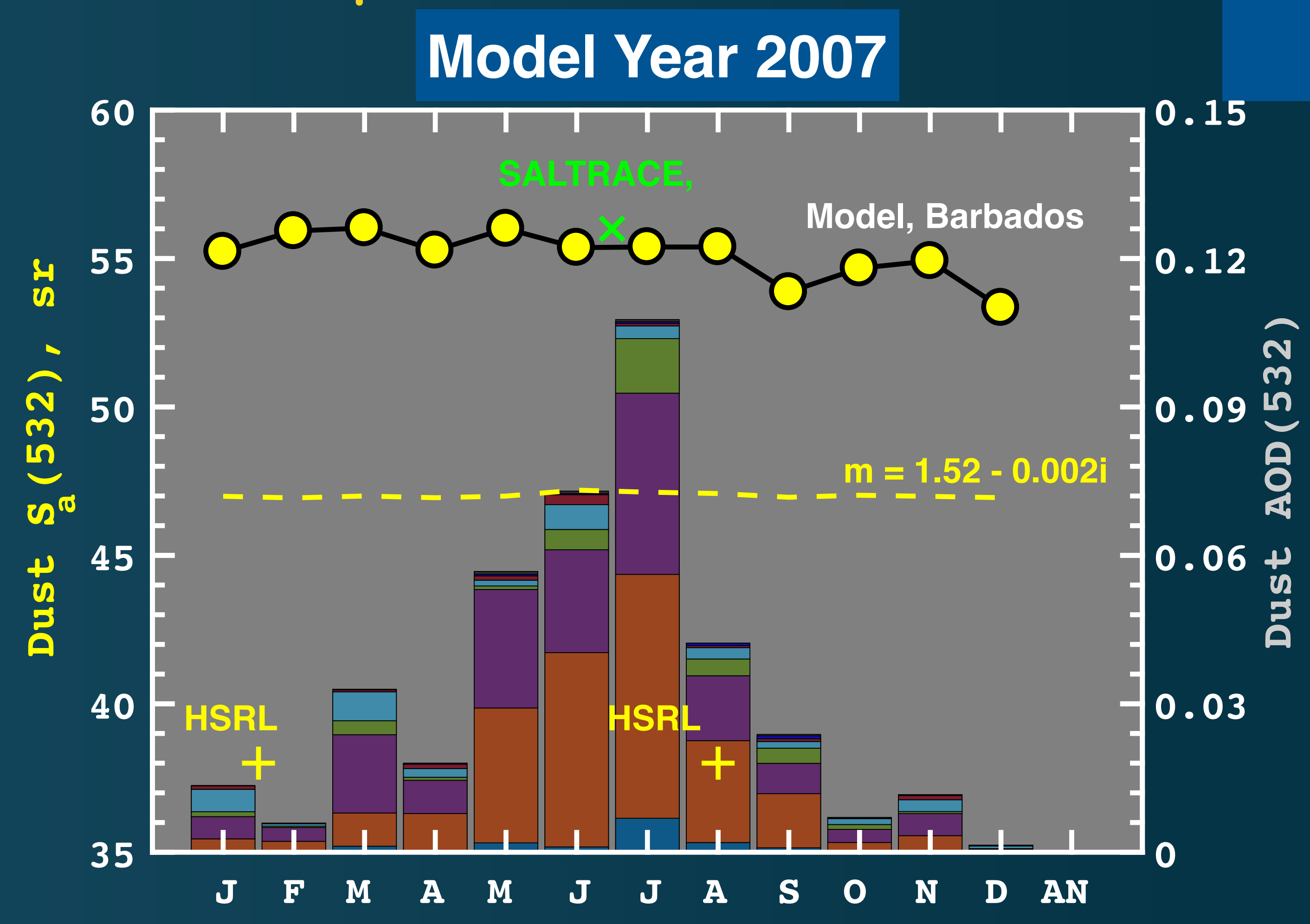

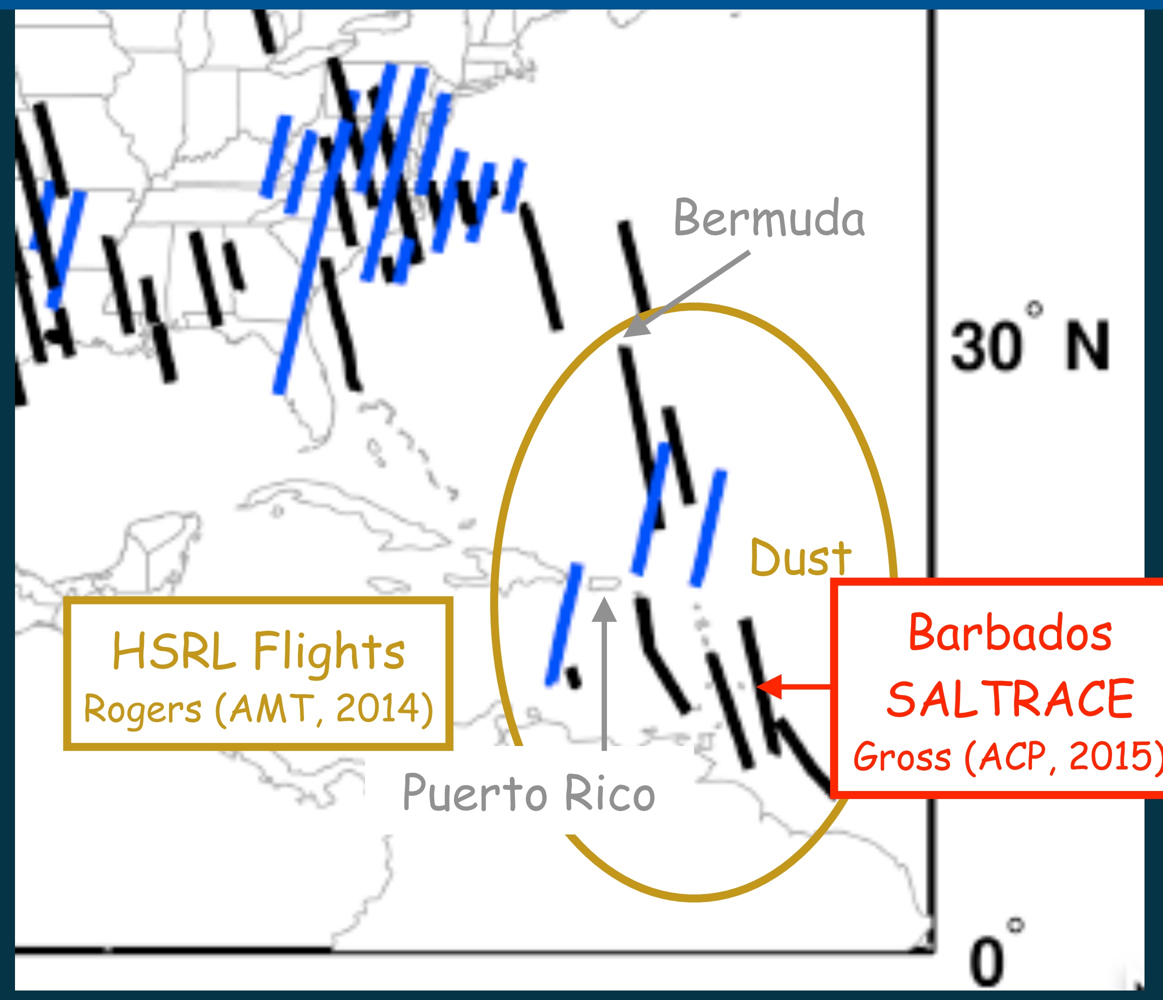

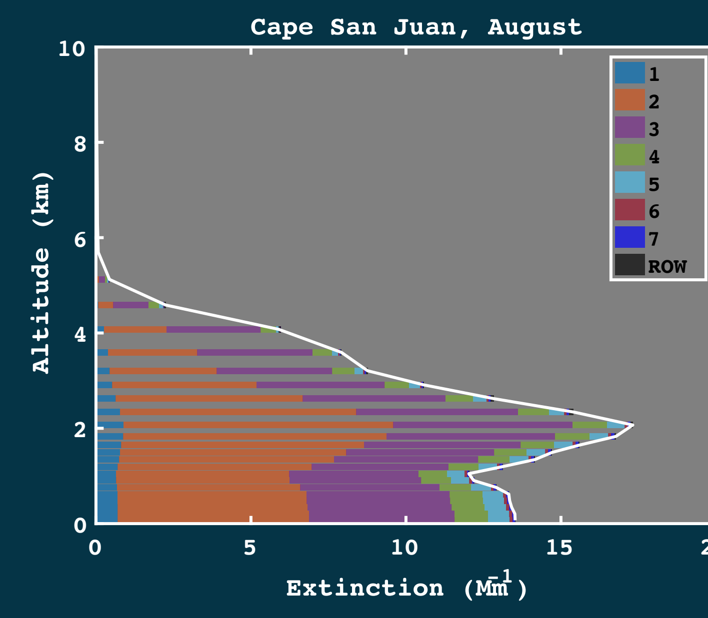

Comparison to HSRL and Raman Lidars in West Atlantic

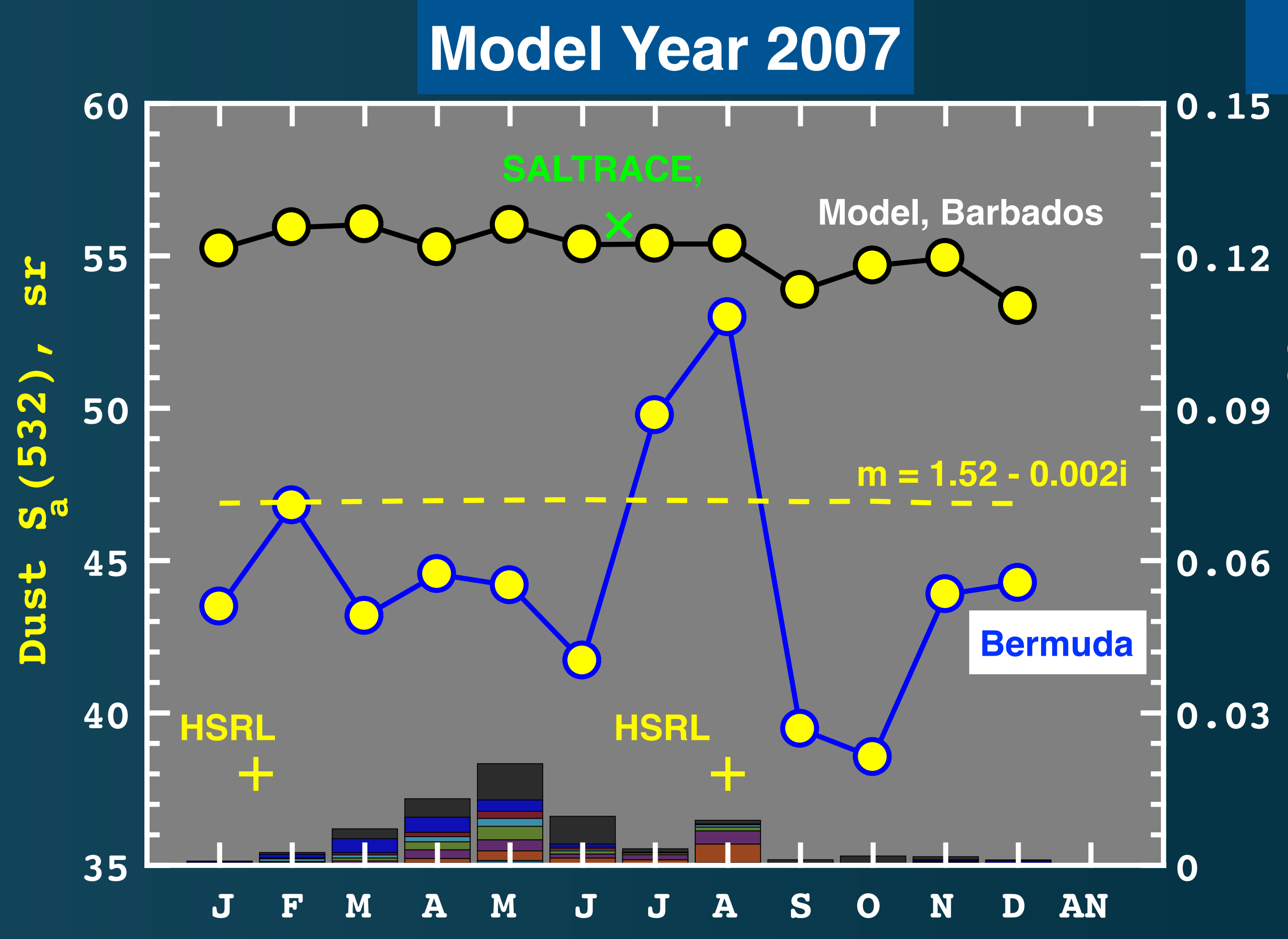

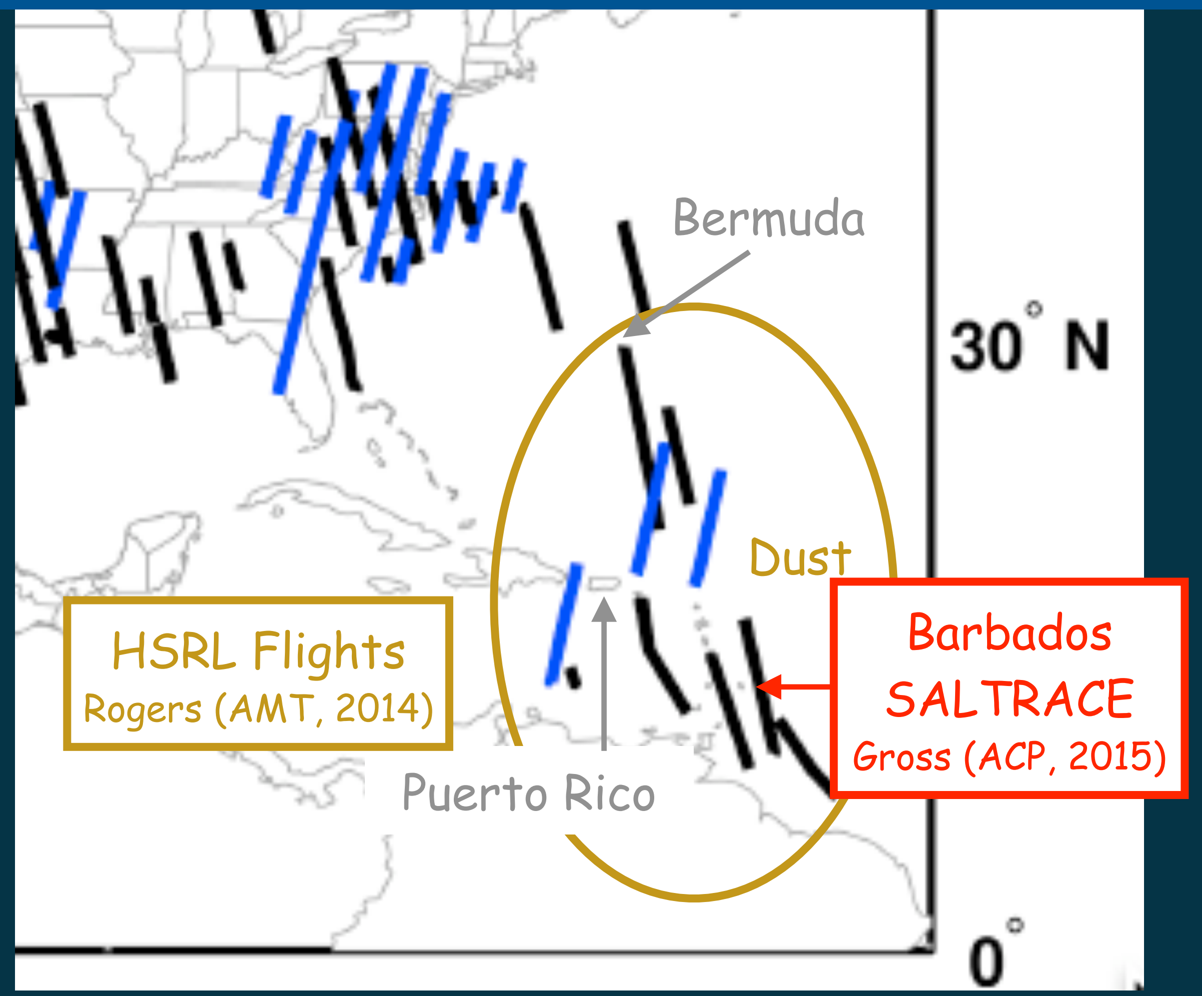

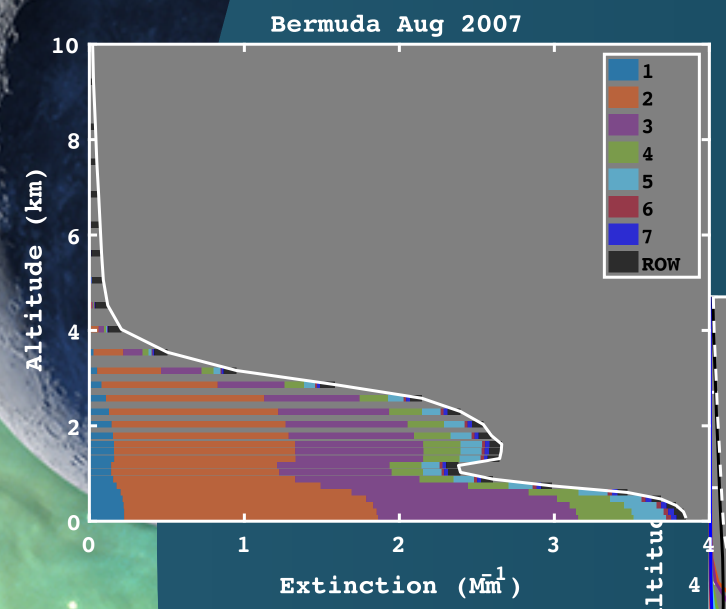

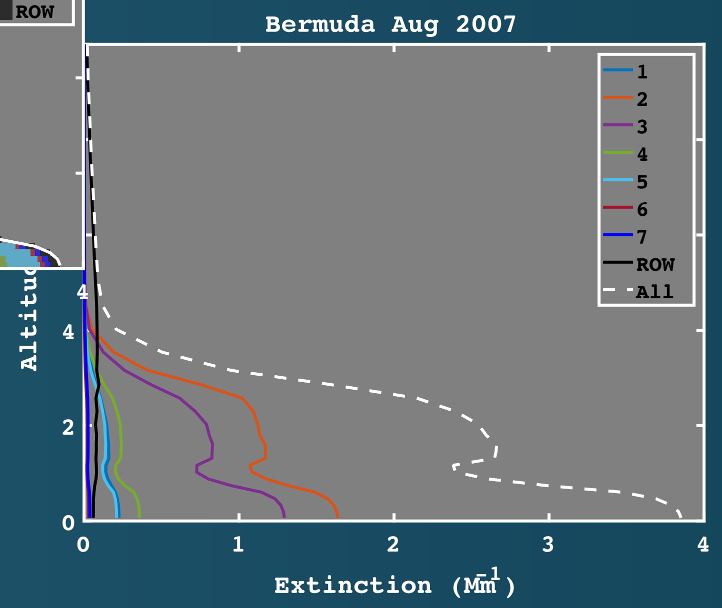

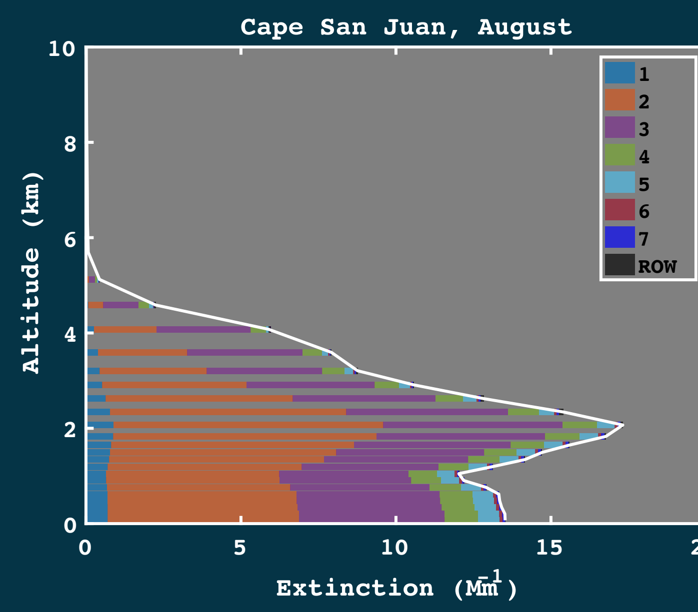

Comparison to HSRL and Raman Lidars in West Atlantic

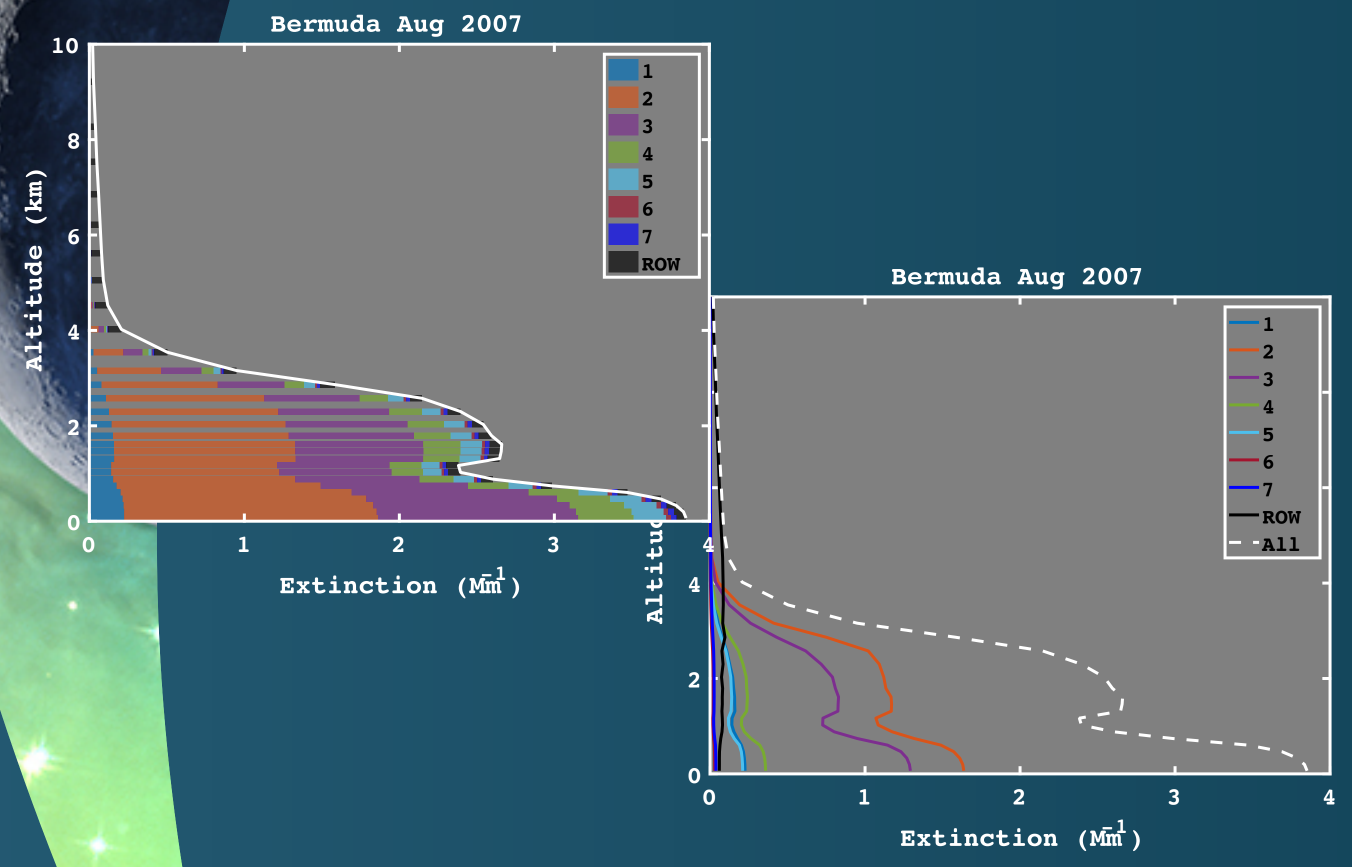

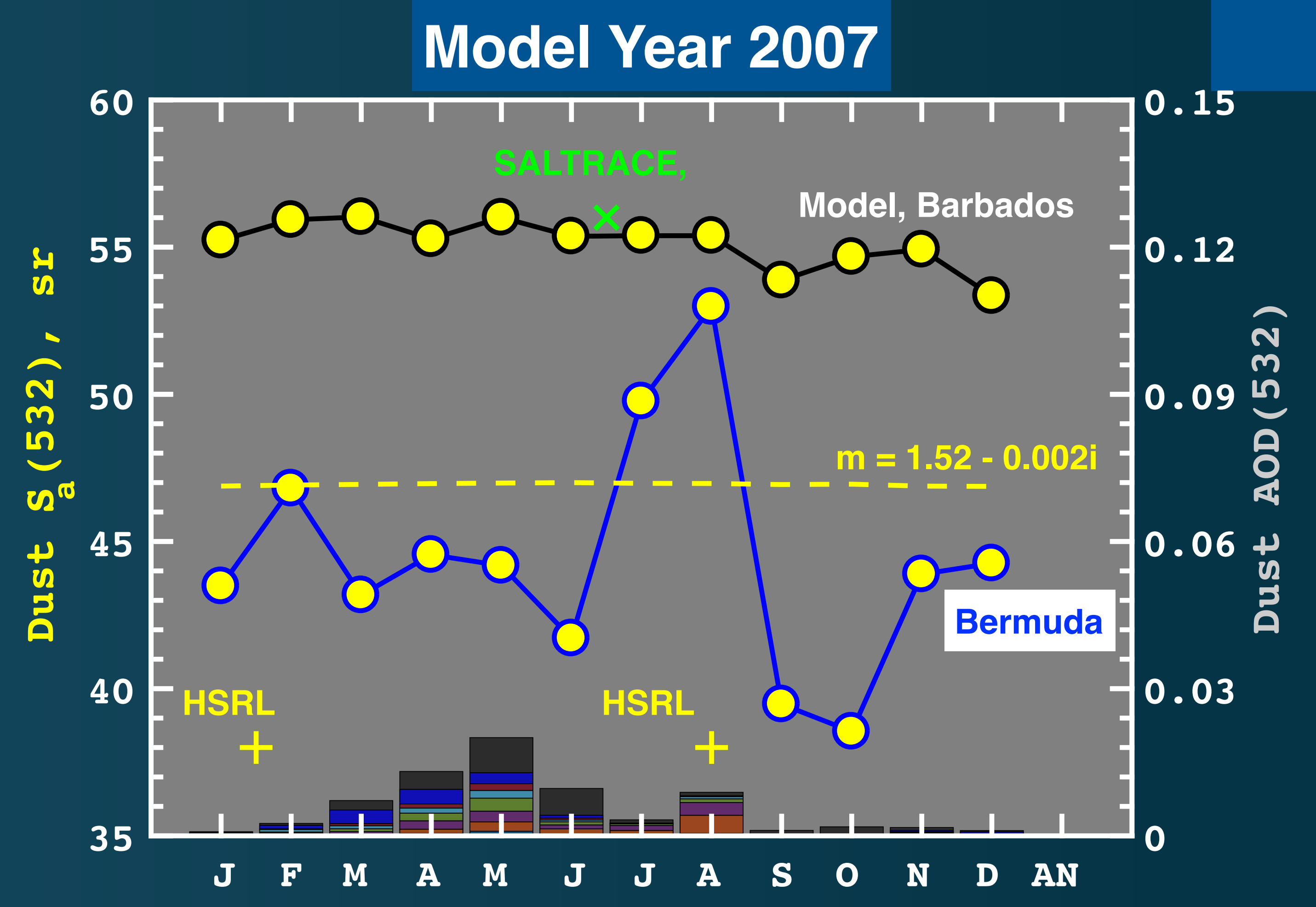

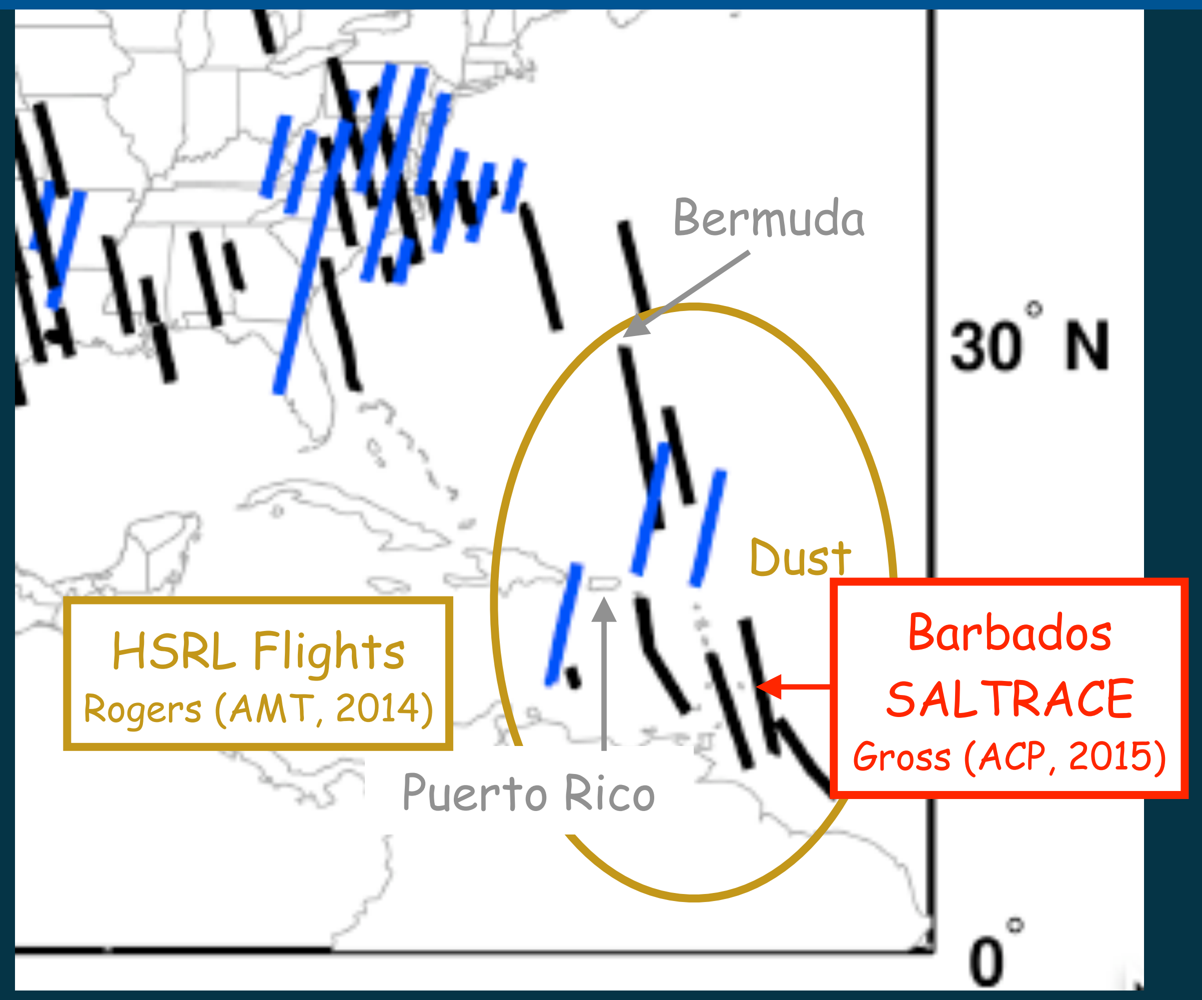

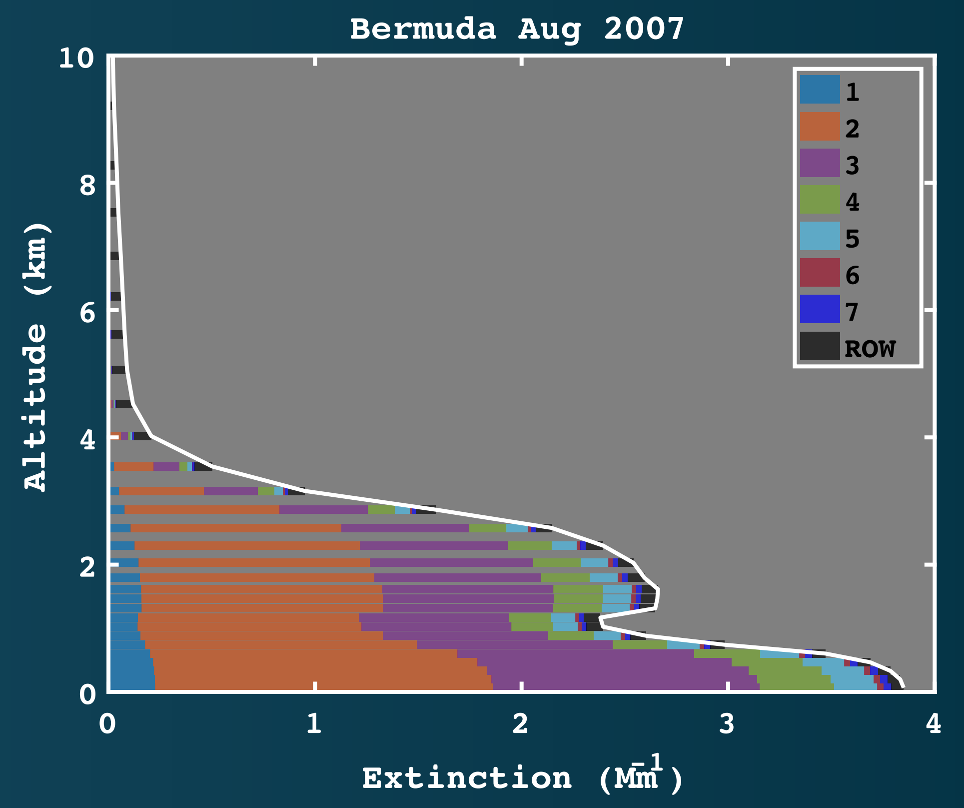

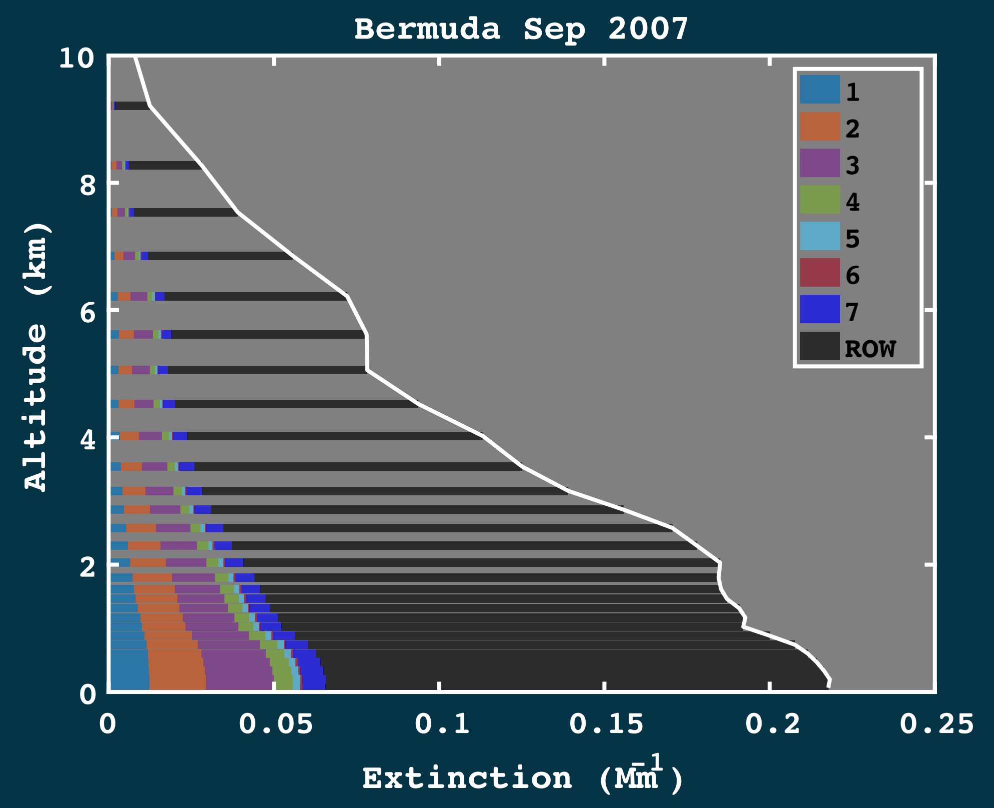

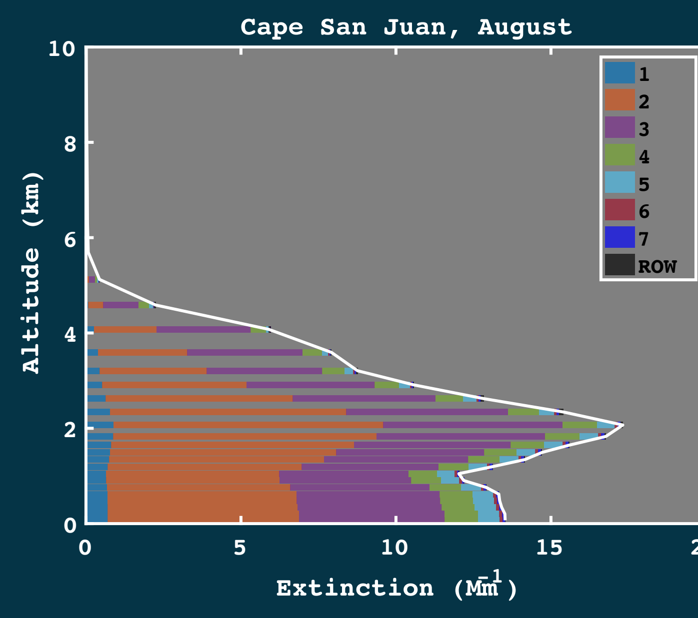

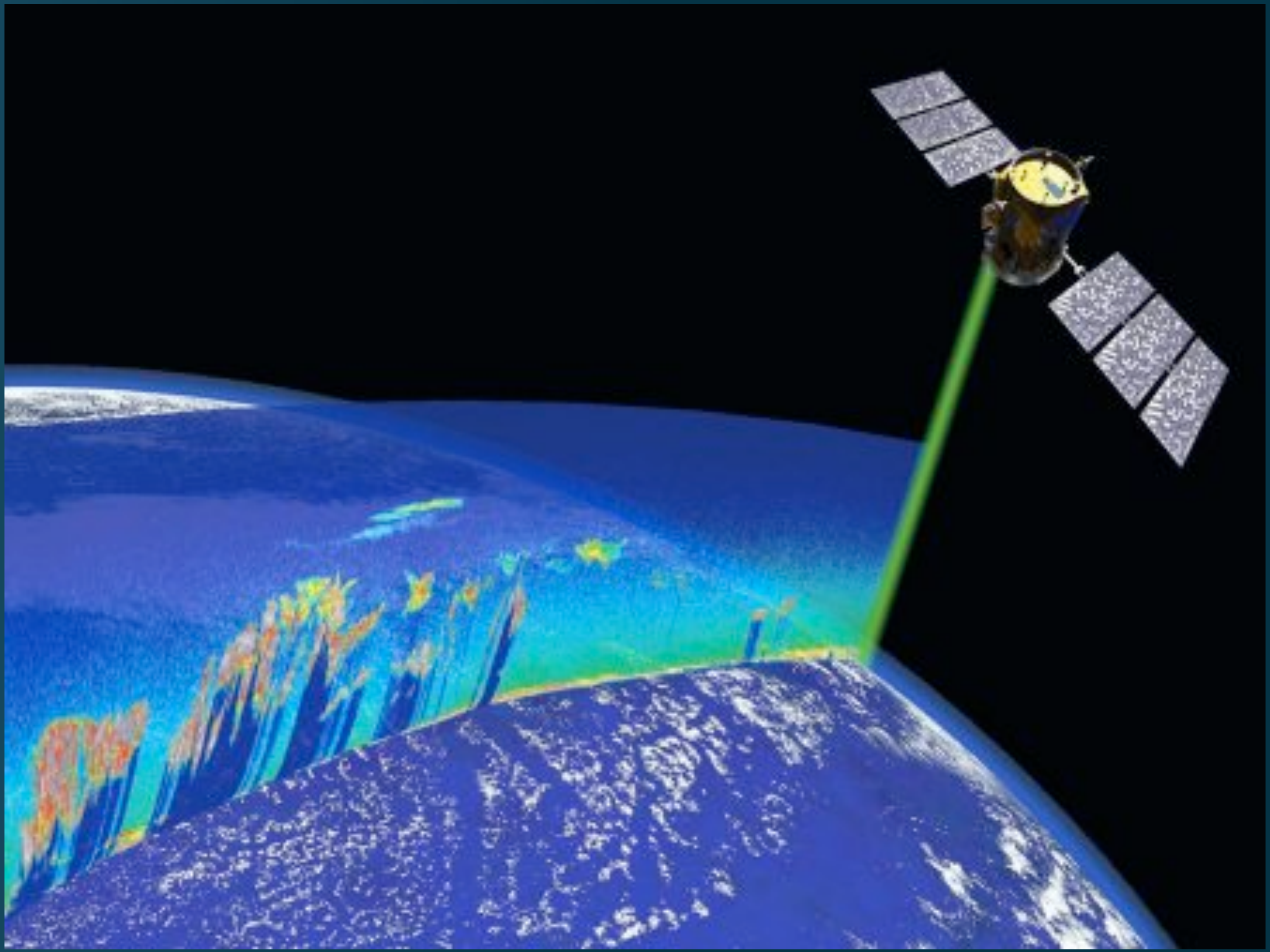

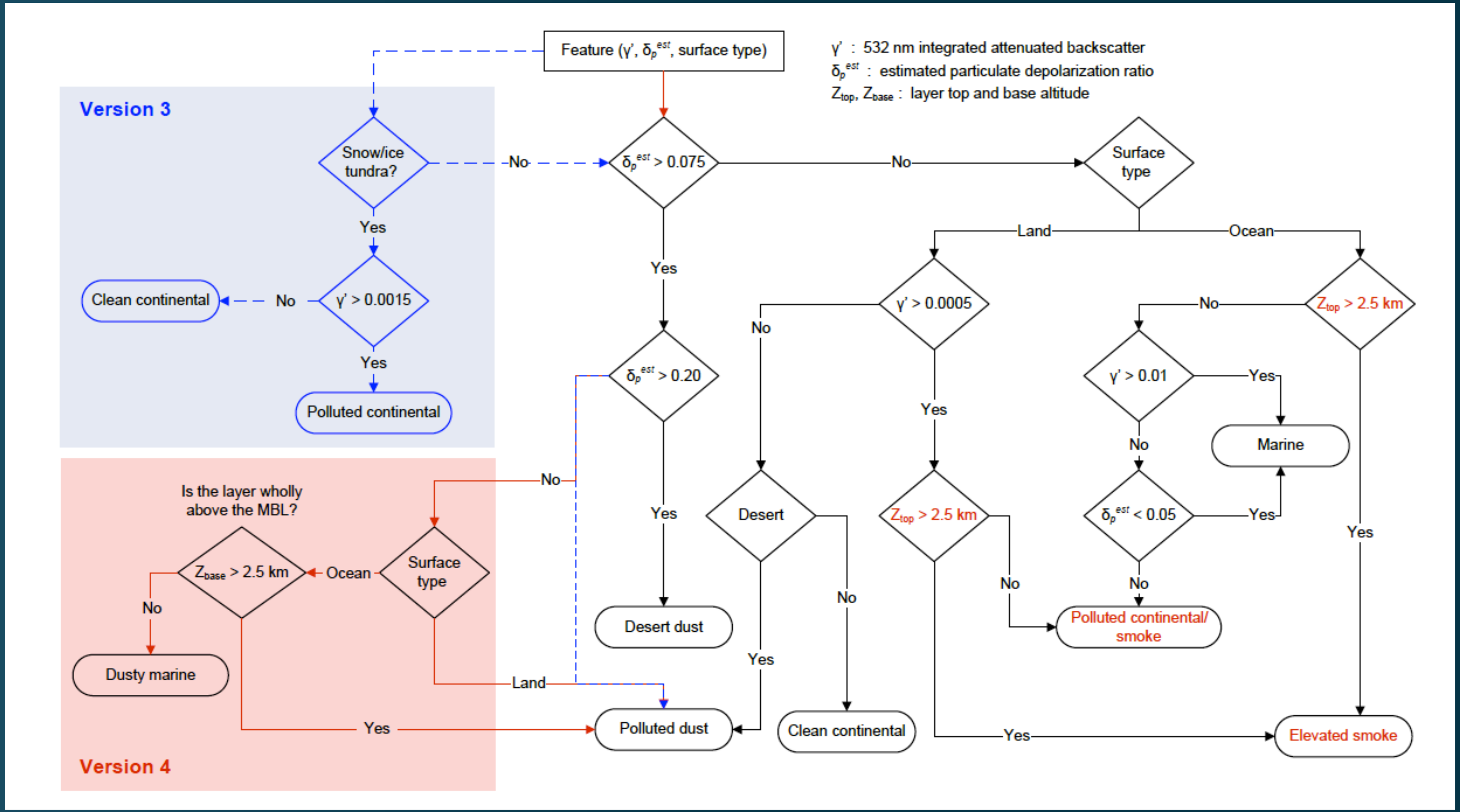

Kim et al (AMT, 2018)

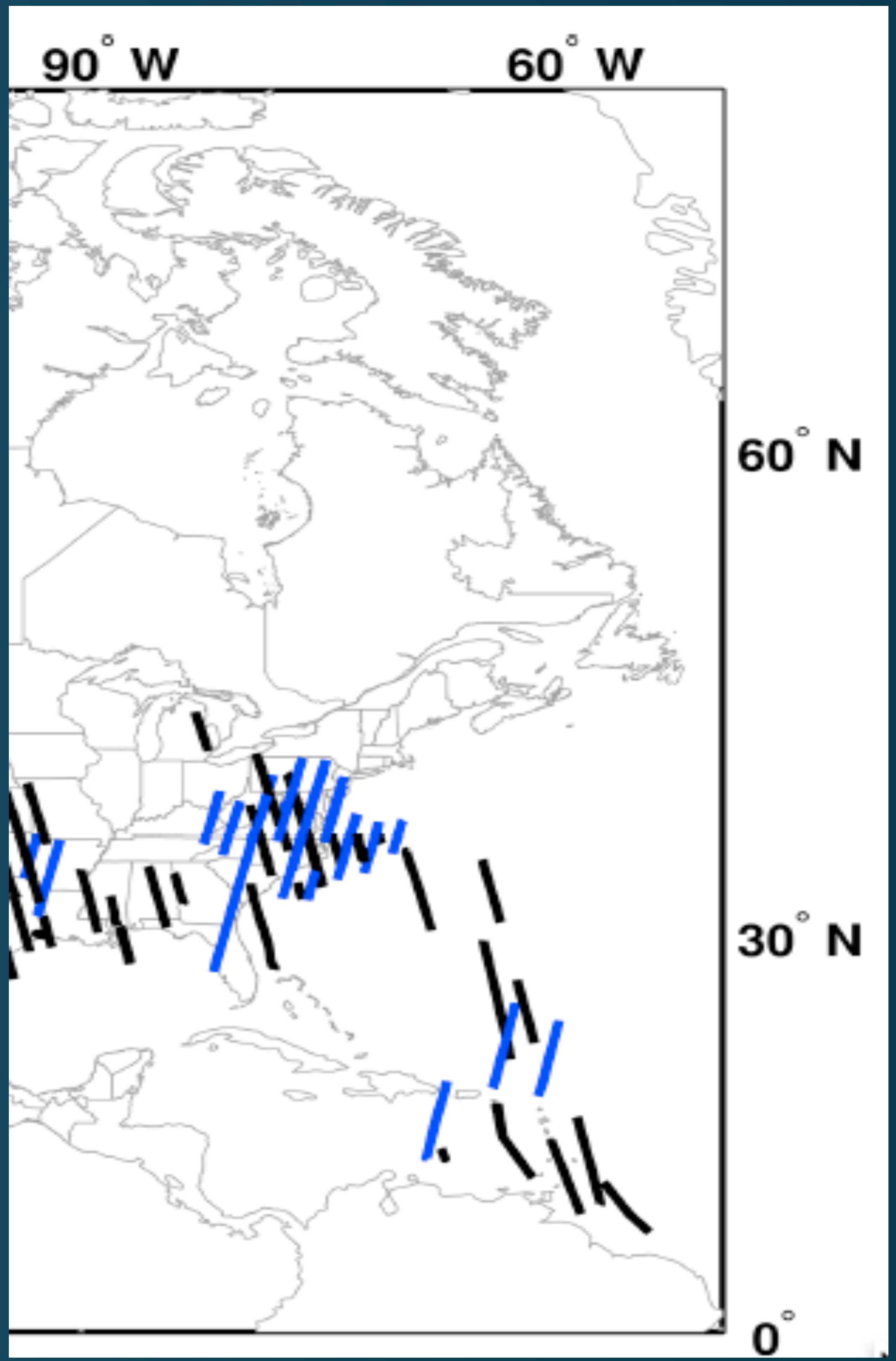

90° W
60° W
60° N
30° N
0°

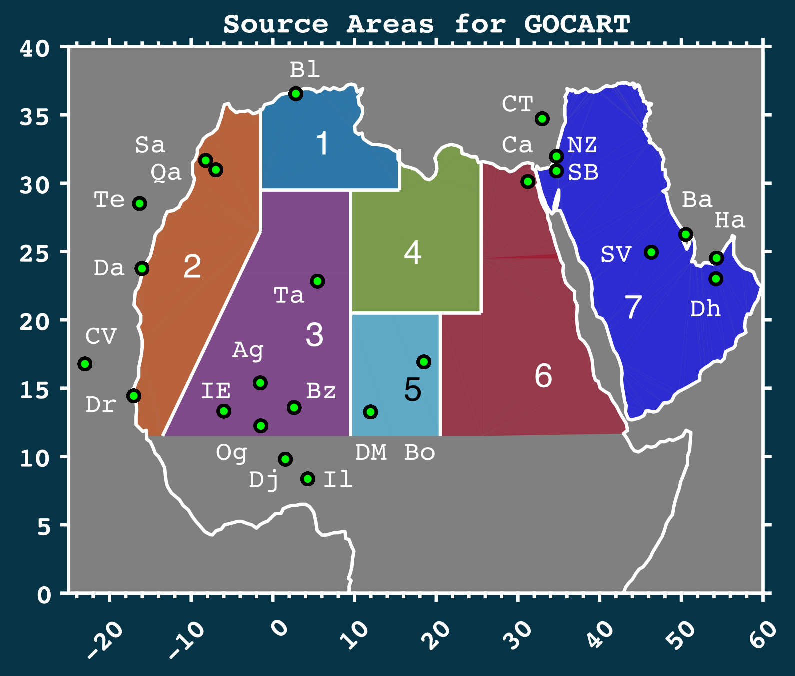

Source Areas for GOCART
Bl
CT
Sa
Qa
Ca
NZ
SB
Te
Ba
Ha
Da
SV
Ta
Dh
CV
Ag
IE
Bz
Dr
Og
DM
Bo
Dj
Il
1
2
3
4
5
6
7

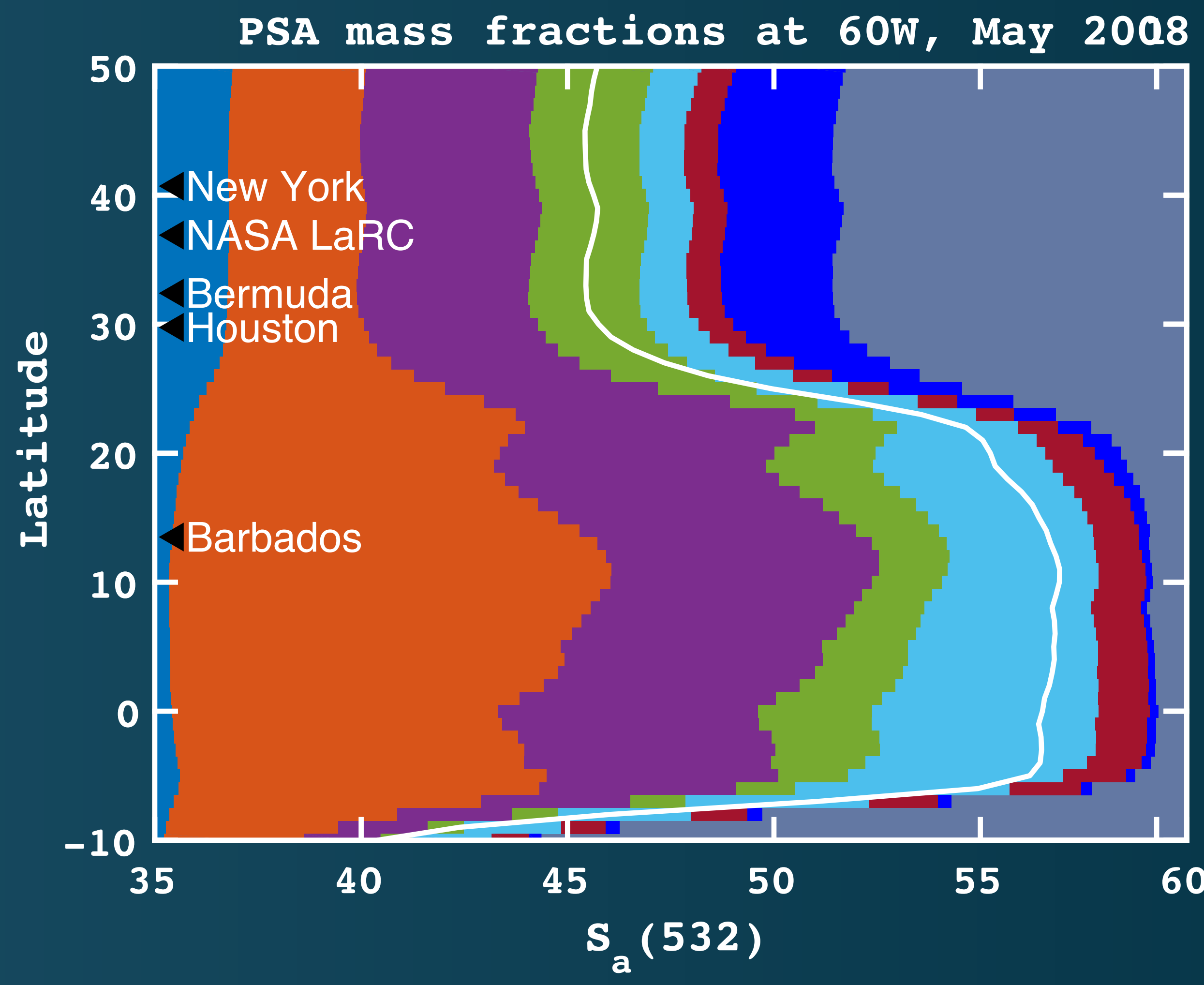

PSA mass fractions at 60W, May 2008
New York
NASA LaRC
Bermuda
Houston
Barbados
Latitude
S_a(532)

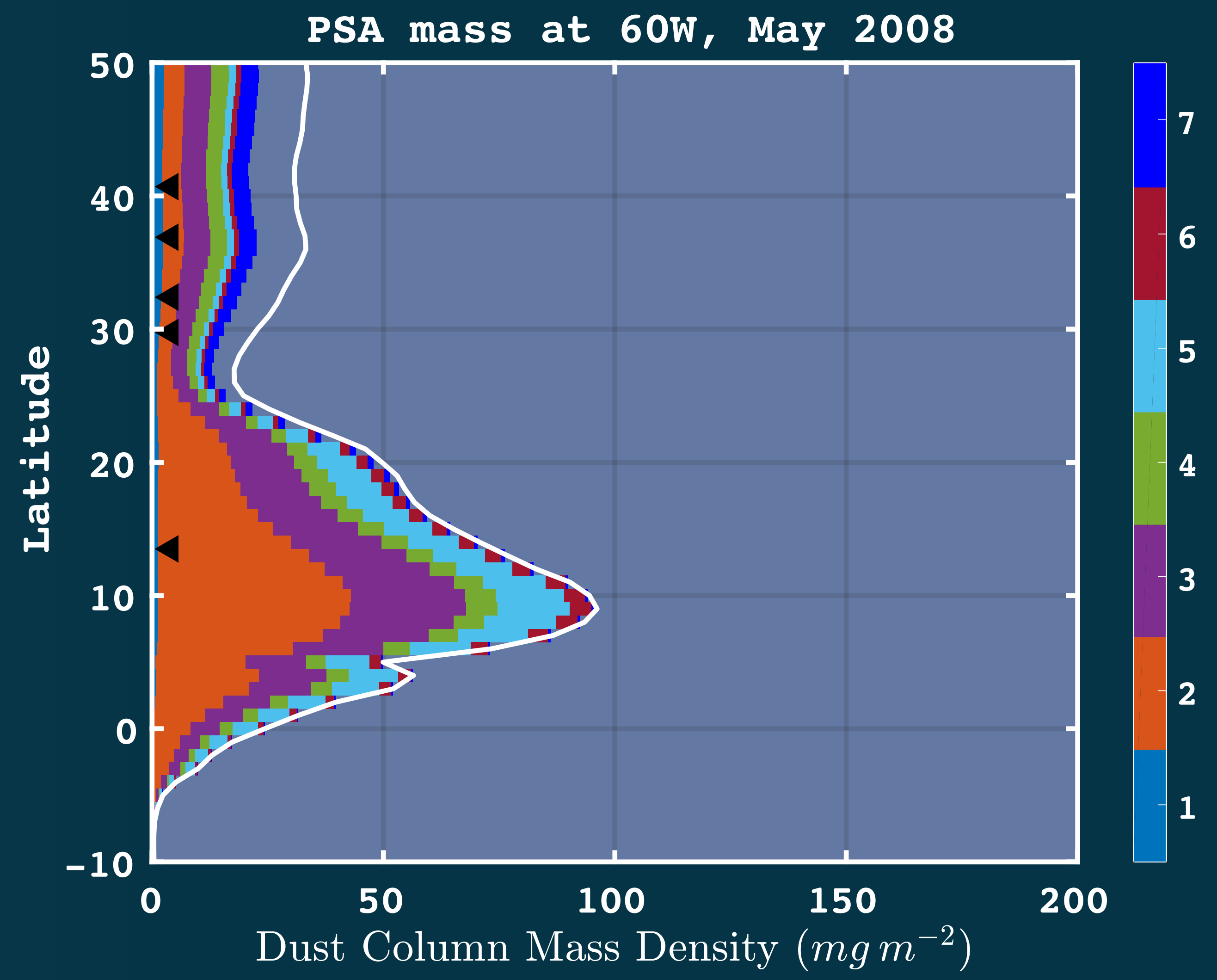

PSA mass at 60W, May 2008
Latitude
Dust Column Mass Density $(mg\,m^{-2})$

Dust originating from West Africa has highest lidar ratios

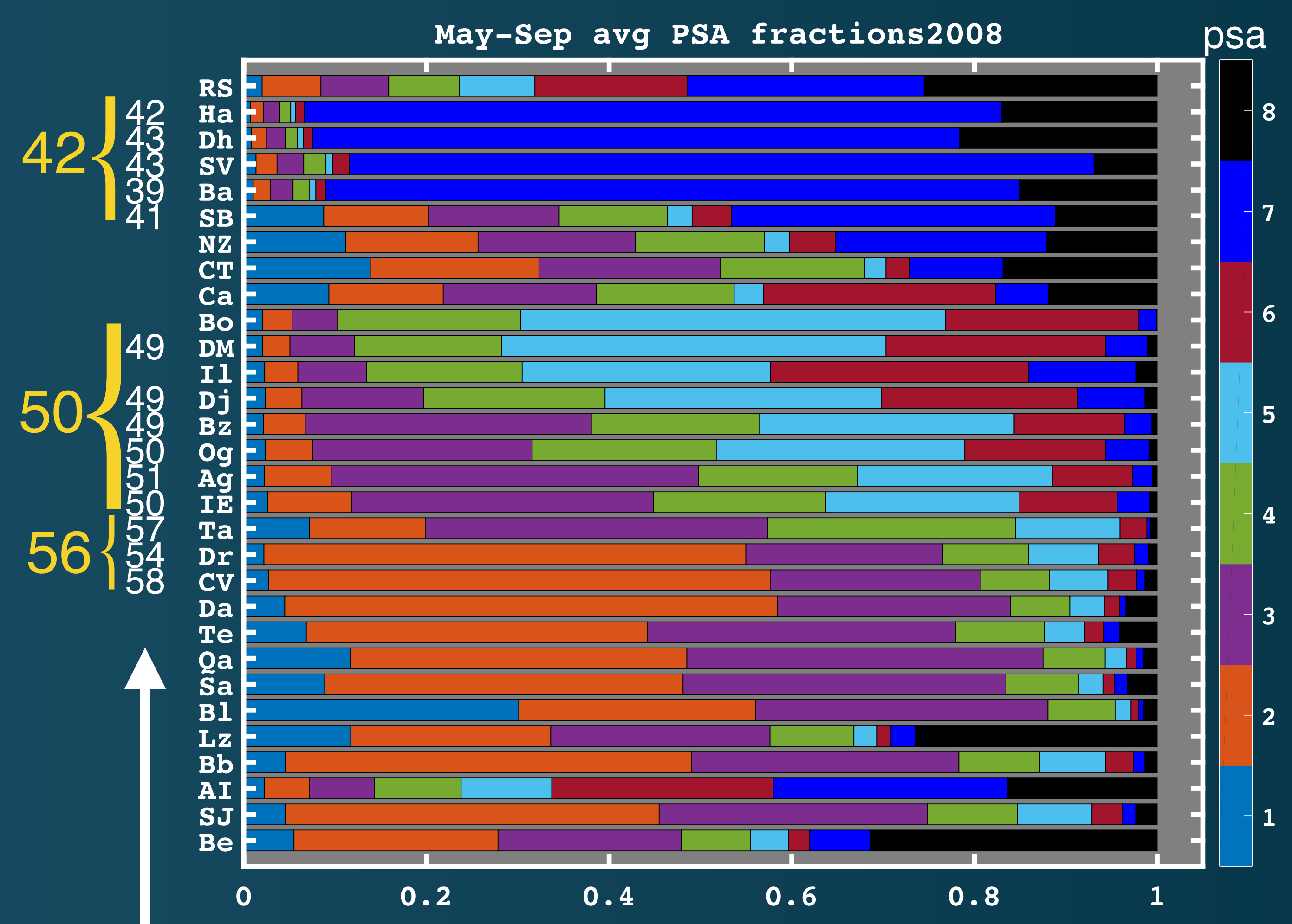

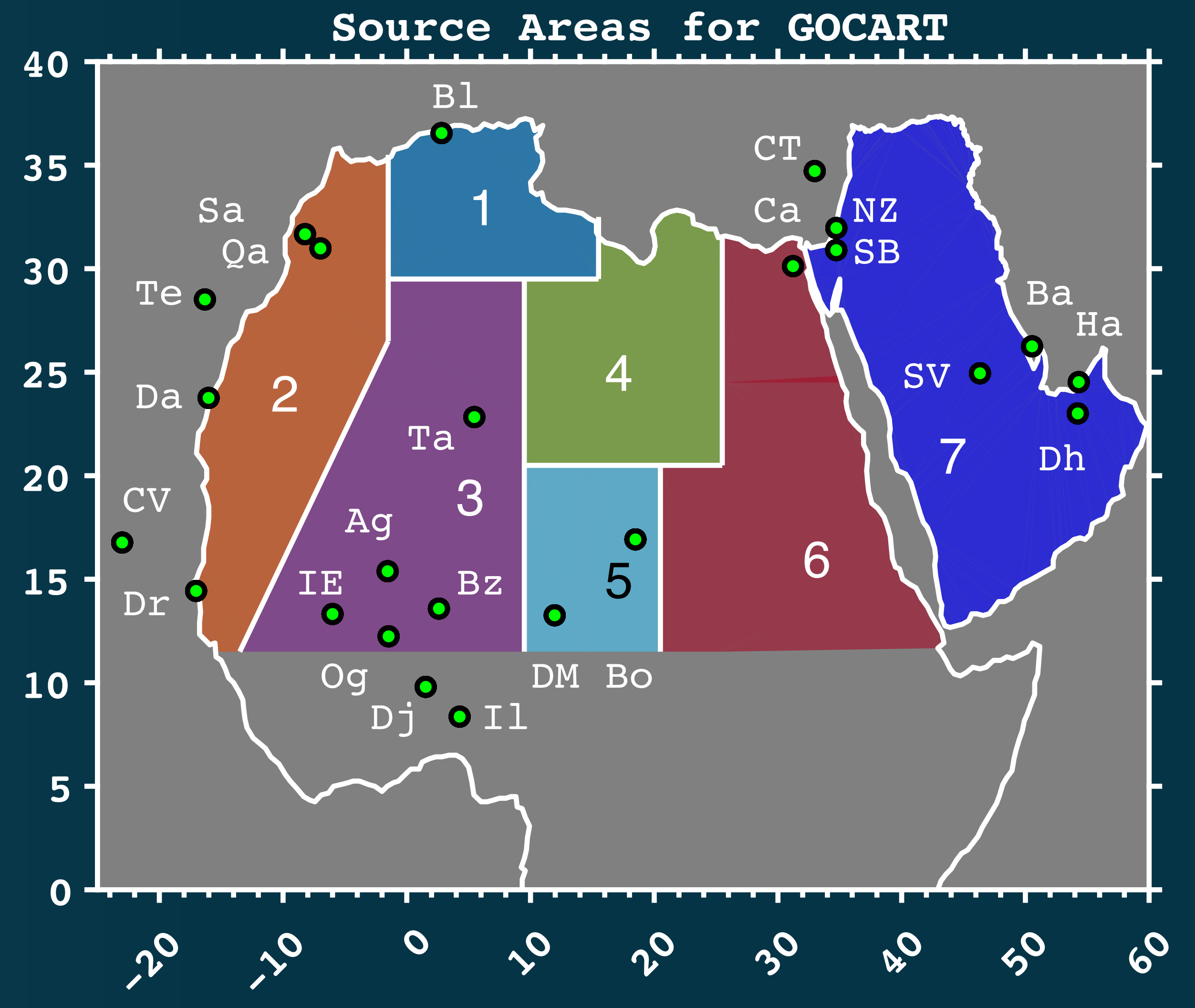

$S_a(532)$ computed from AERONET, per Schuster et al, ACP, 2012.

SAMUM 2

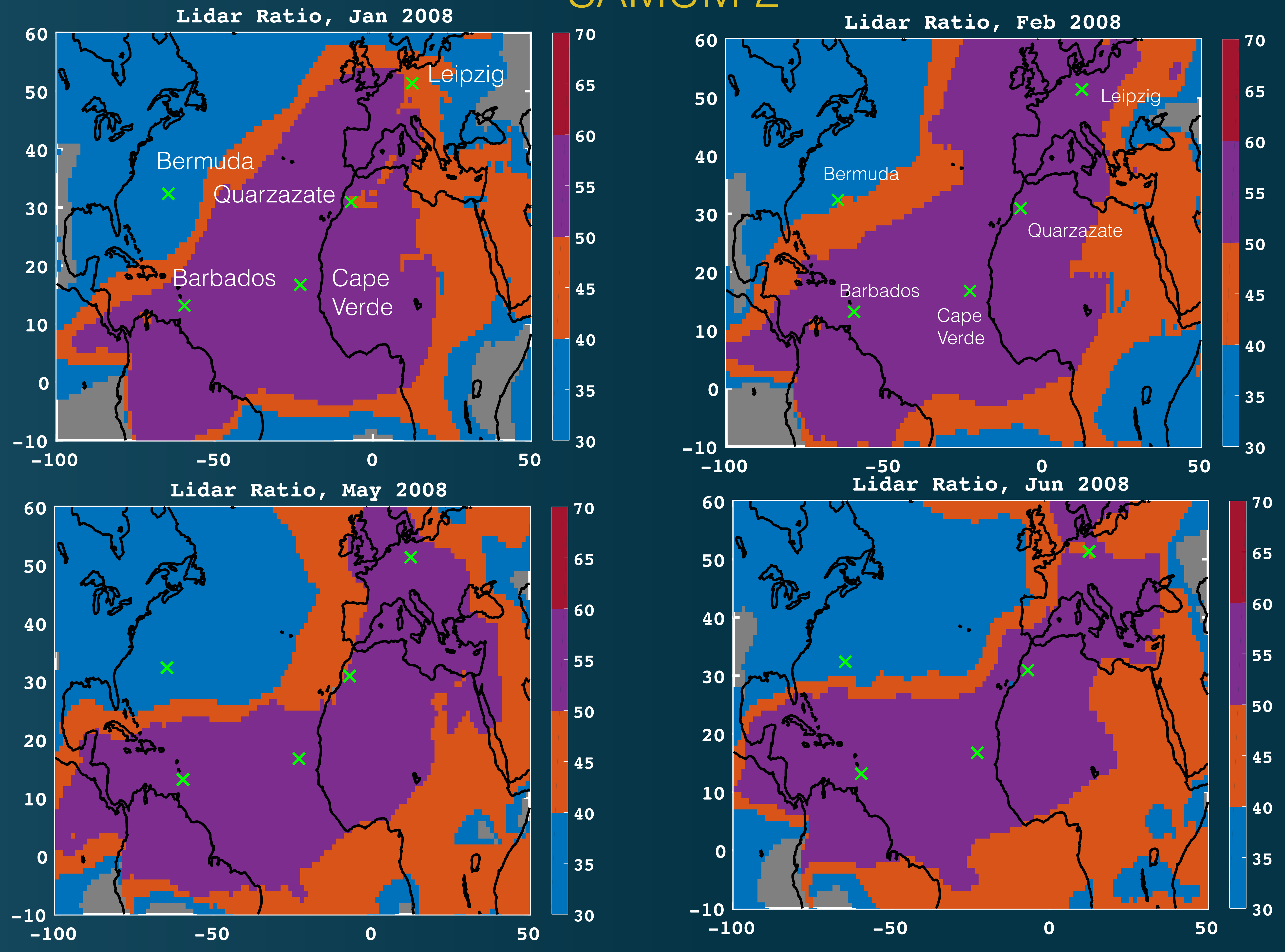

Lidar Ratio, Jan 2008
Leipzig
Bermuda
Quarzazate
Barbados
Cape Verde
Lidar Ratio, Feb 2008
Leipzig
Bermuda
Quarzazate
Barbados
Cape Verde
Lidar Ratio, May 2008
Lidar Ratio, Jun 2008
70
65
60
55
50
45
40
35
30
60
50
40
30
20
10
0
−10
−100
−50
0
50

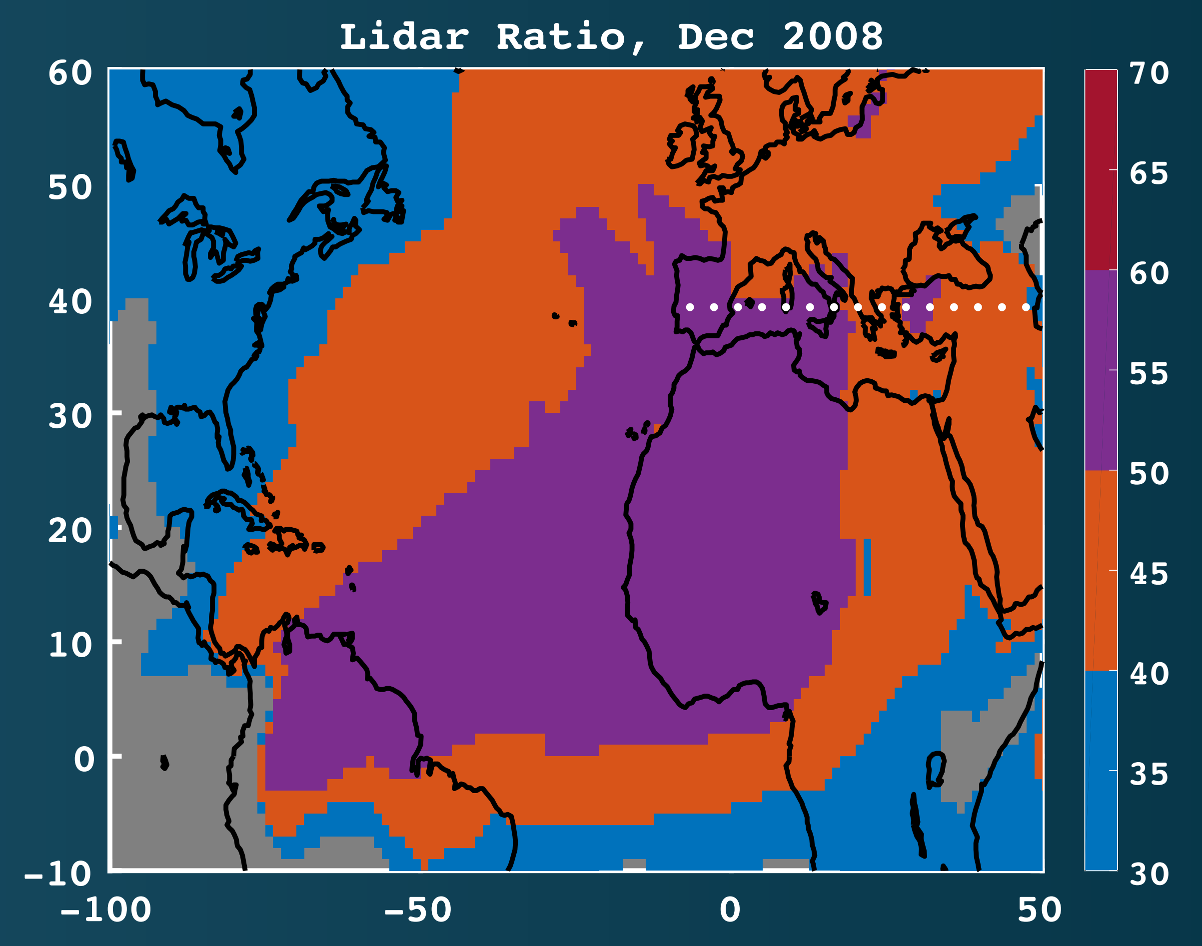
Lidar Ratio, Dec 2008
60
50
40
30
20
10
0
−10
−100
−50
0
50
70
65
60
55
50
45
40
35
30

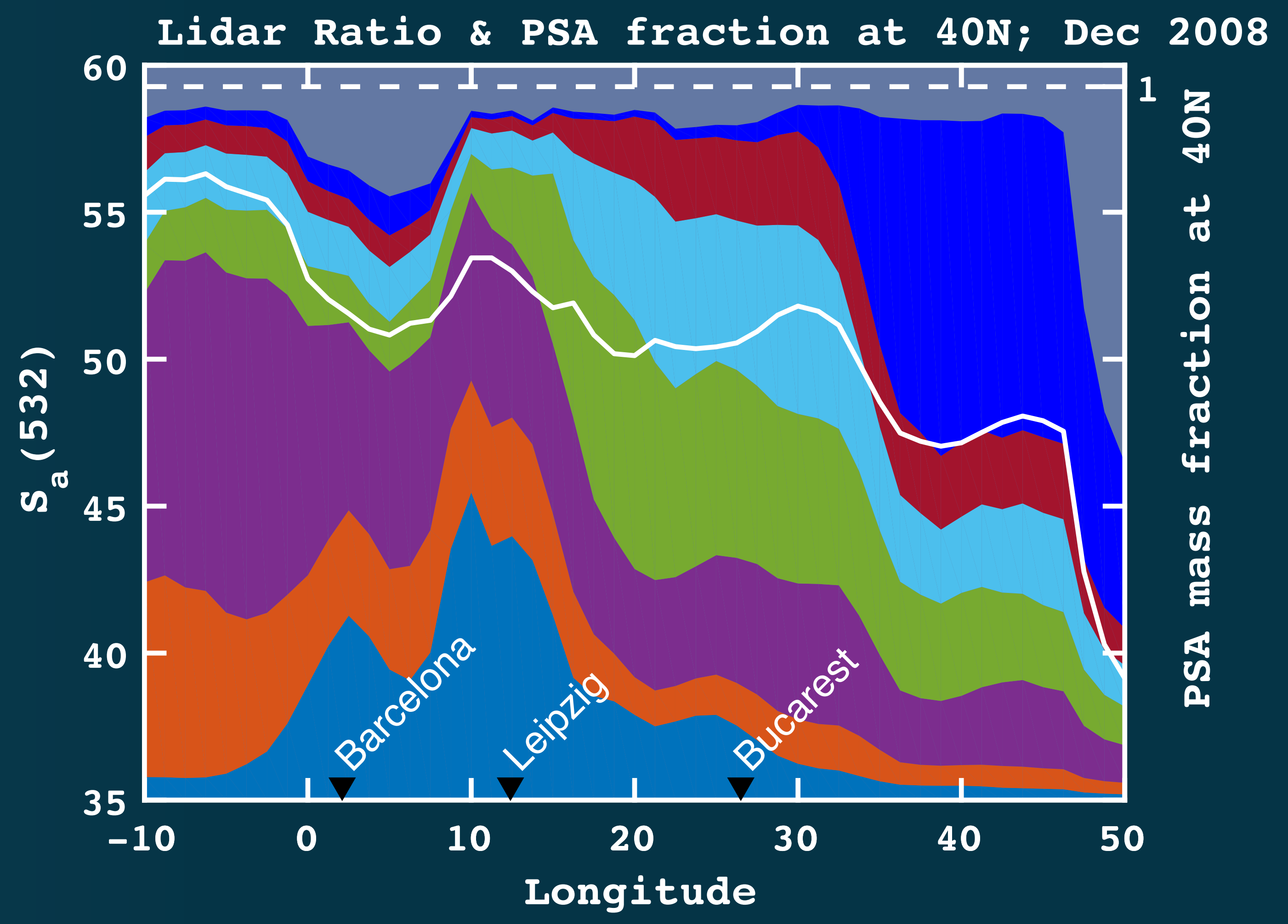
Lidar Ratio & PSA fraction at 40N; Dec 2008
S_a(532)
PSA mass fraction at 40N
Longitude
Barcelona
Leipzig
Bucarest
1
60
55
50
45
40
35
−10
0
10
20
30
40
50

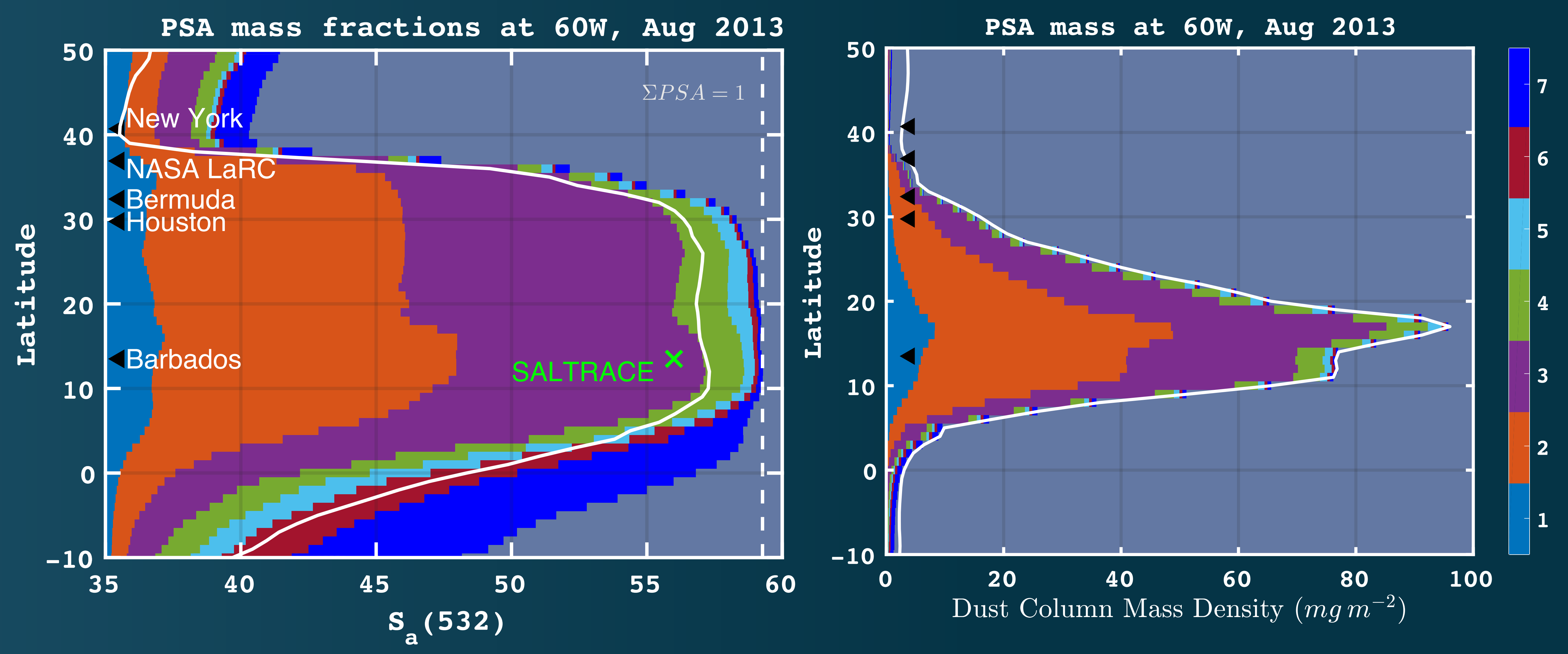

SALTRACE Lidar Ratio from Gross (ACP, 2015)

Other Field Missions with Lidar Ratio Measurements

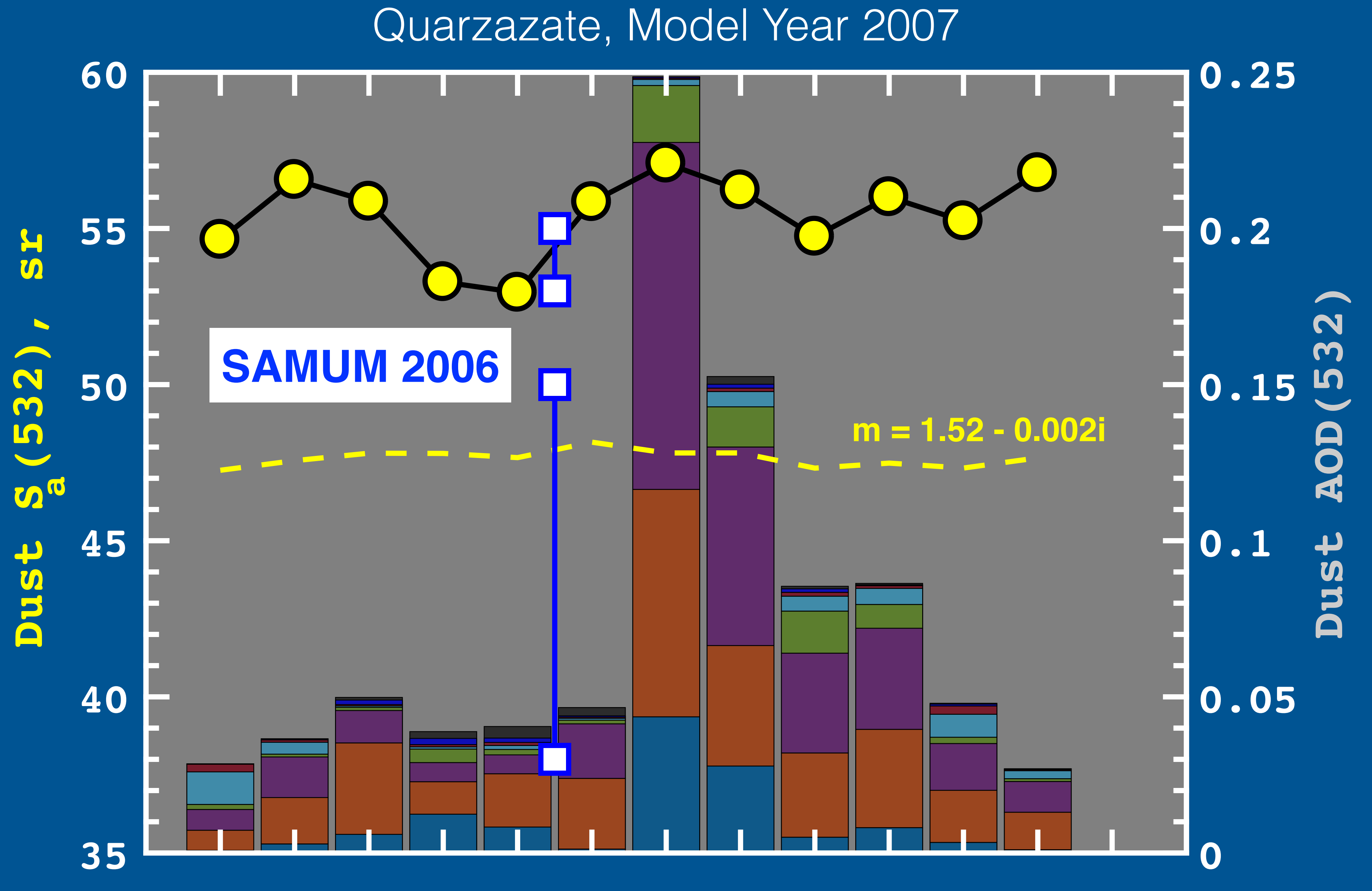

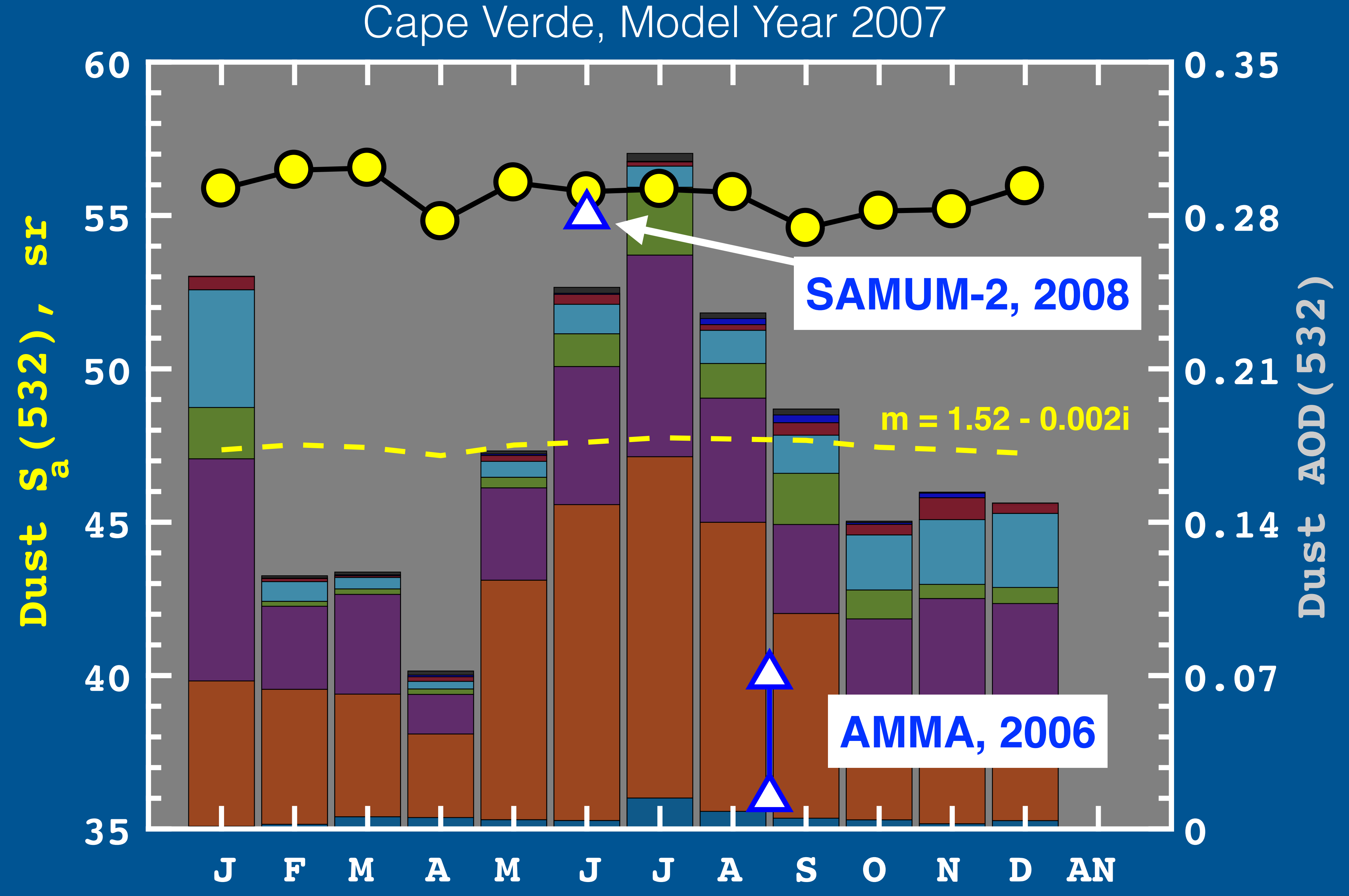

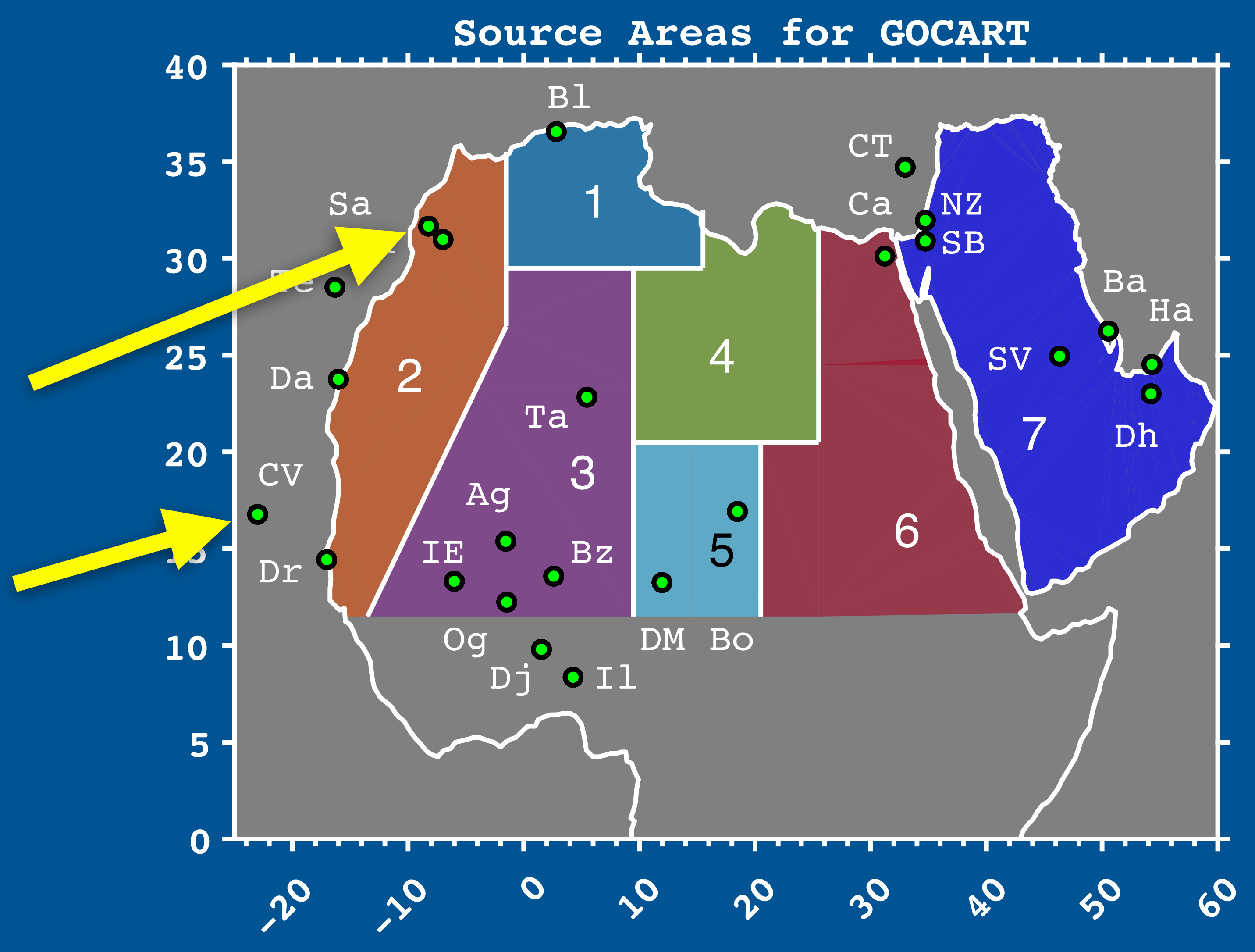

Citations:

AMMA: Omar (JGR, 2010)

SAMUM: Tesche (Tellus, 2008), Esselborn (Tellus, 2008)

SAMUM-2: Wanginger (GRL, 2010)

Quantify the Origin of Aeolian Dust Collected over the Atlantic

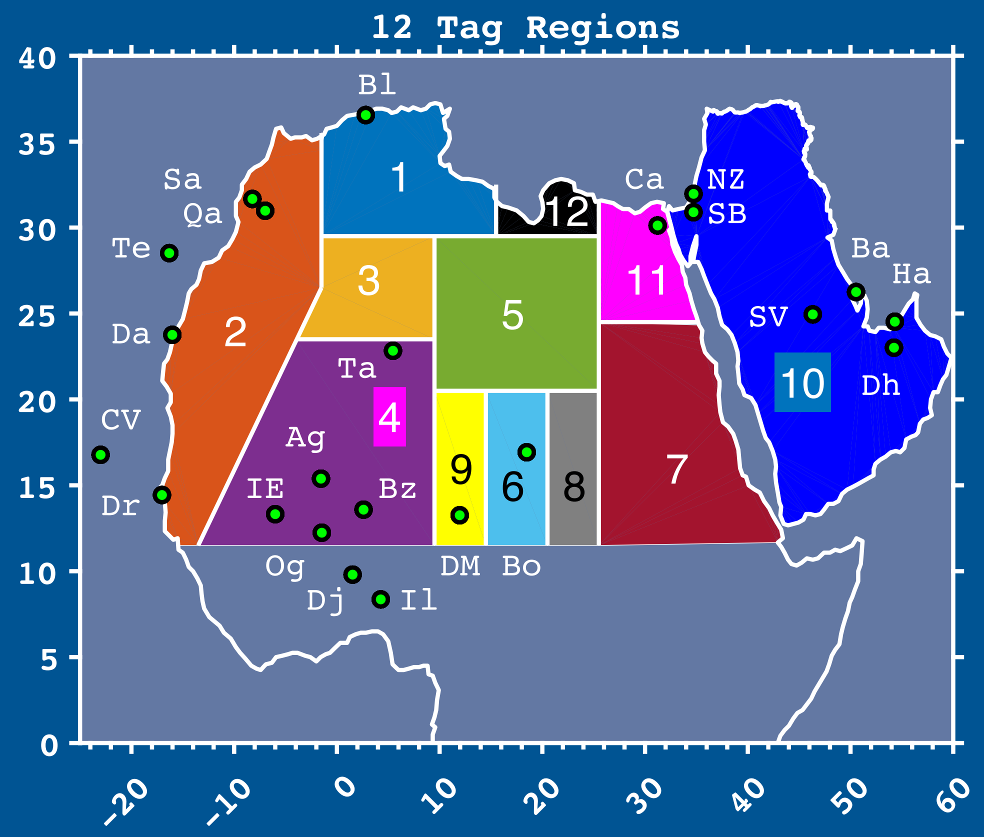

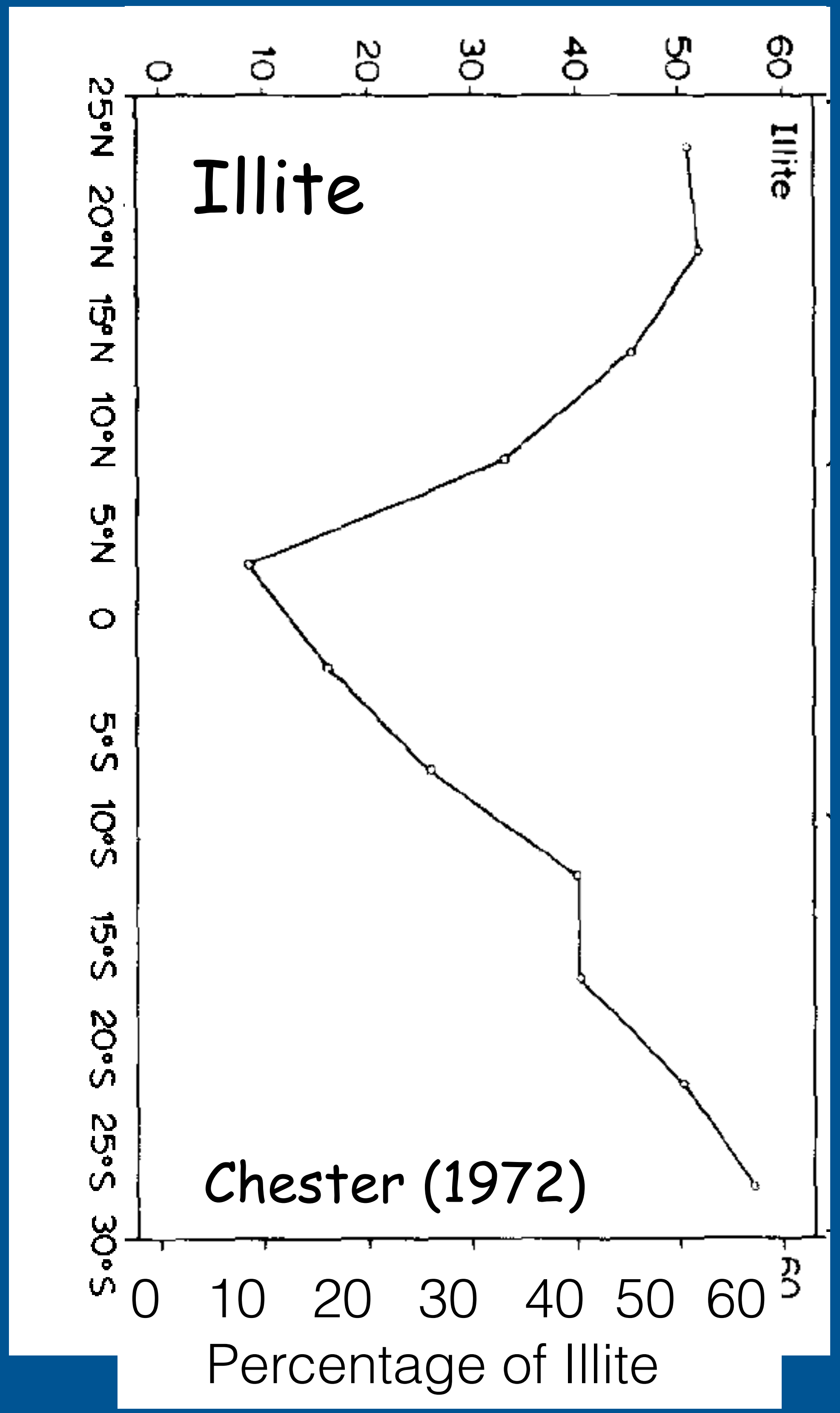

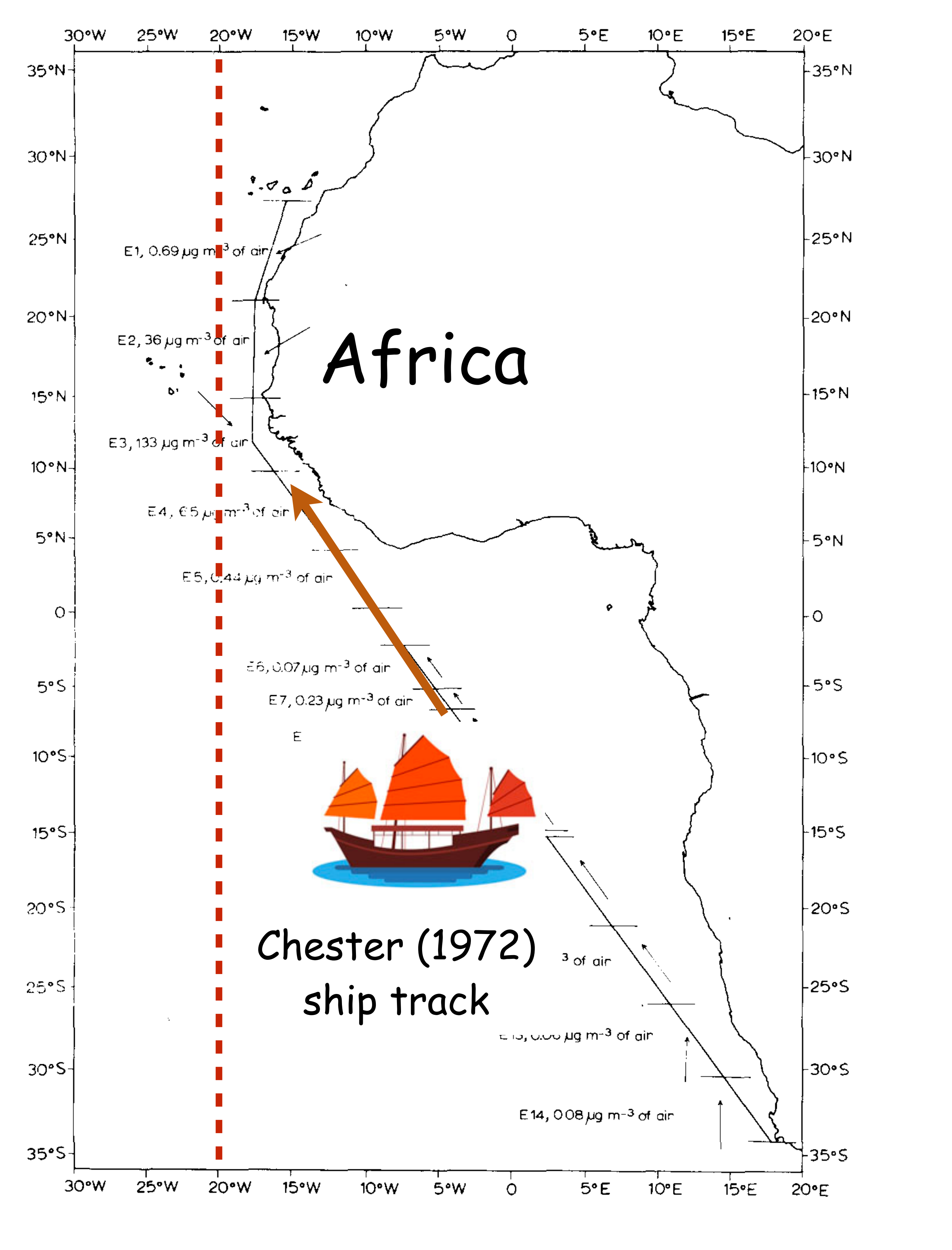

Quantify the Origin of Aeolian Dust Collected over the Atlantic

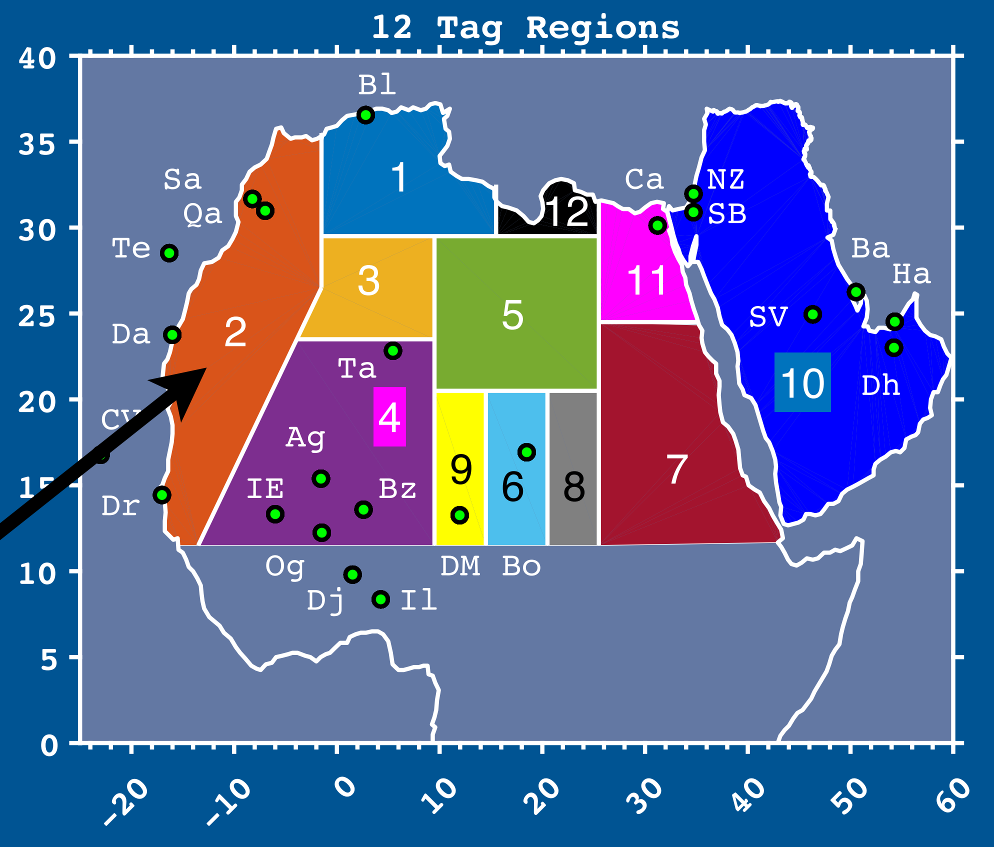

High concentrations of illite in West Africa
(Caquineau, JGR 2002)

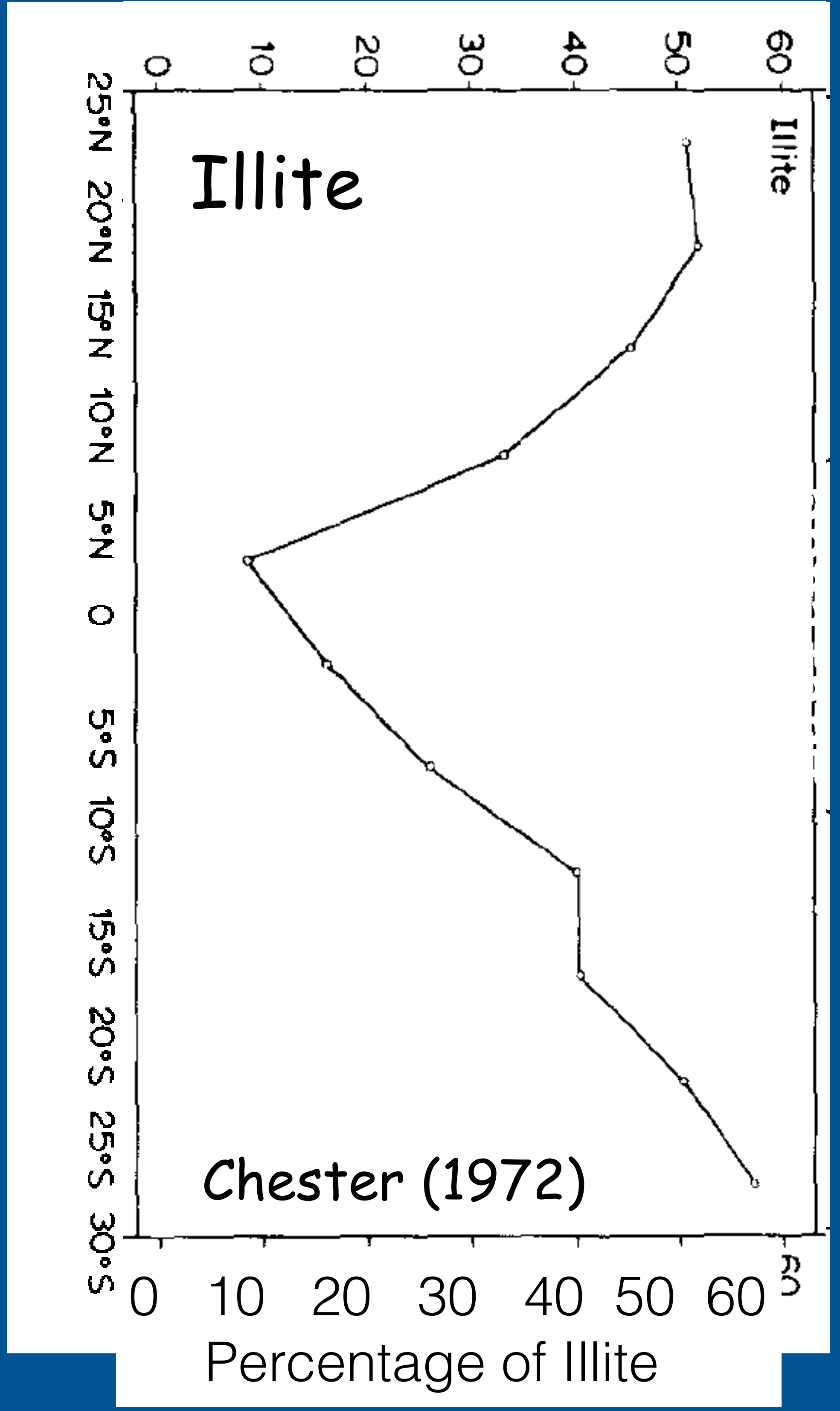

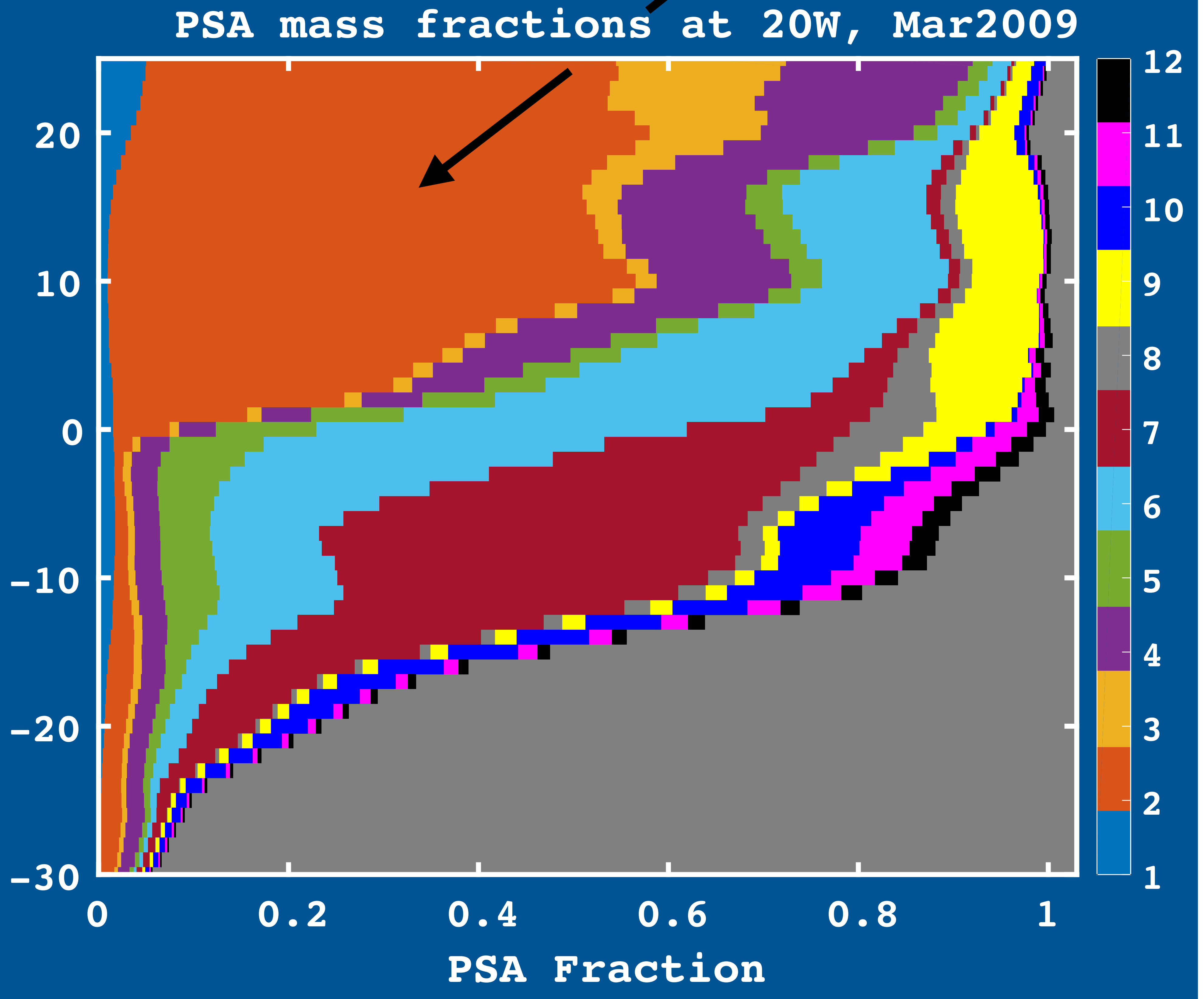

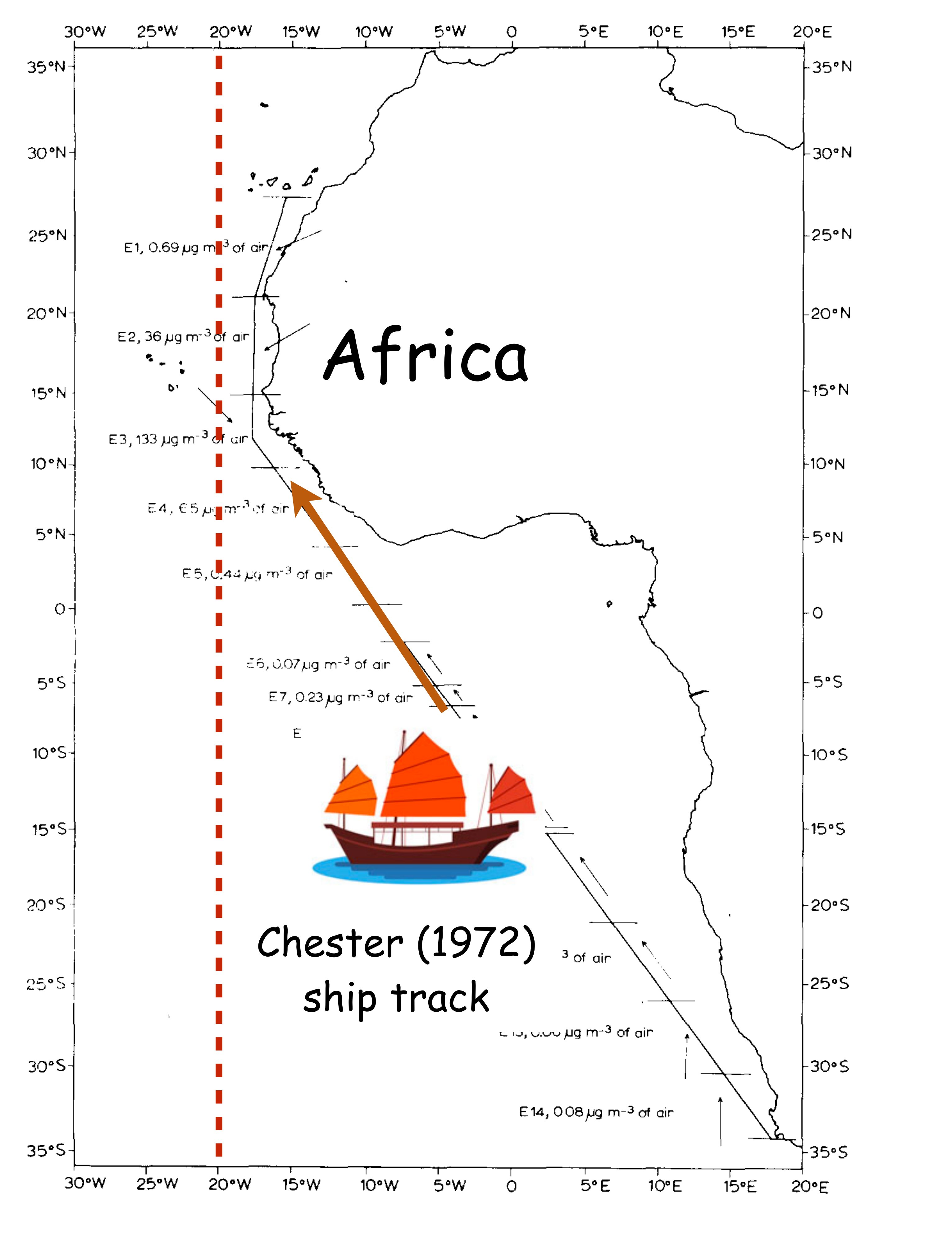

Dust originating from West Africa has highest lidar ratios

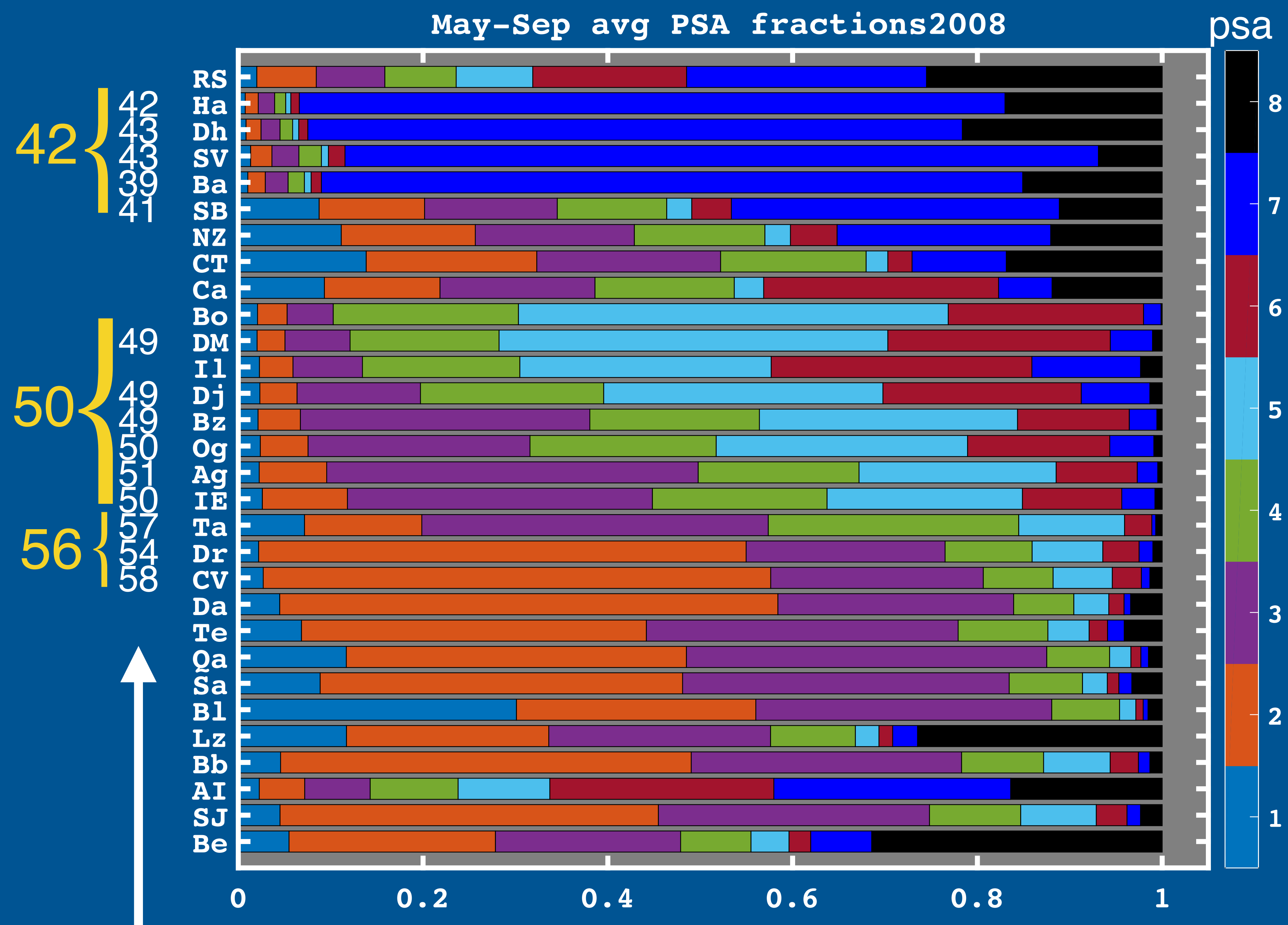

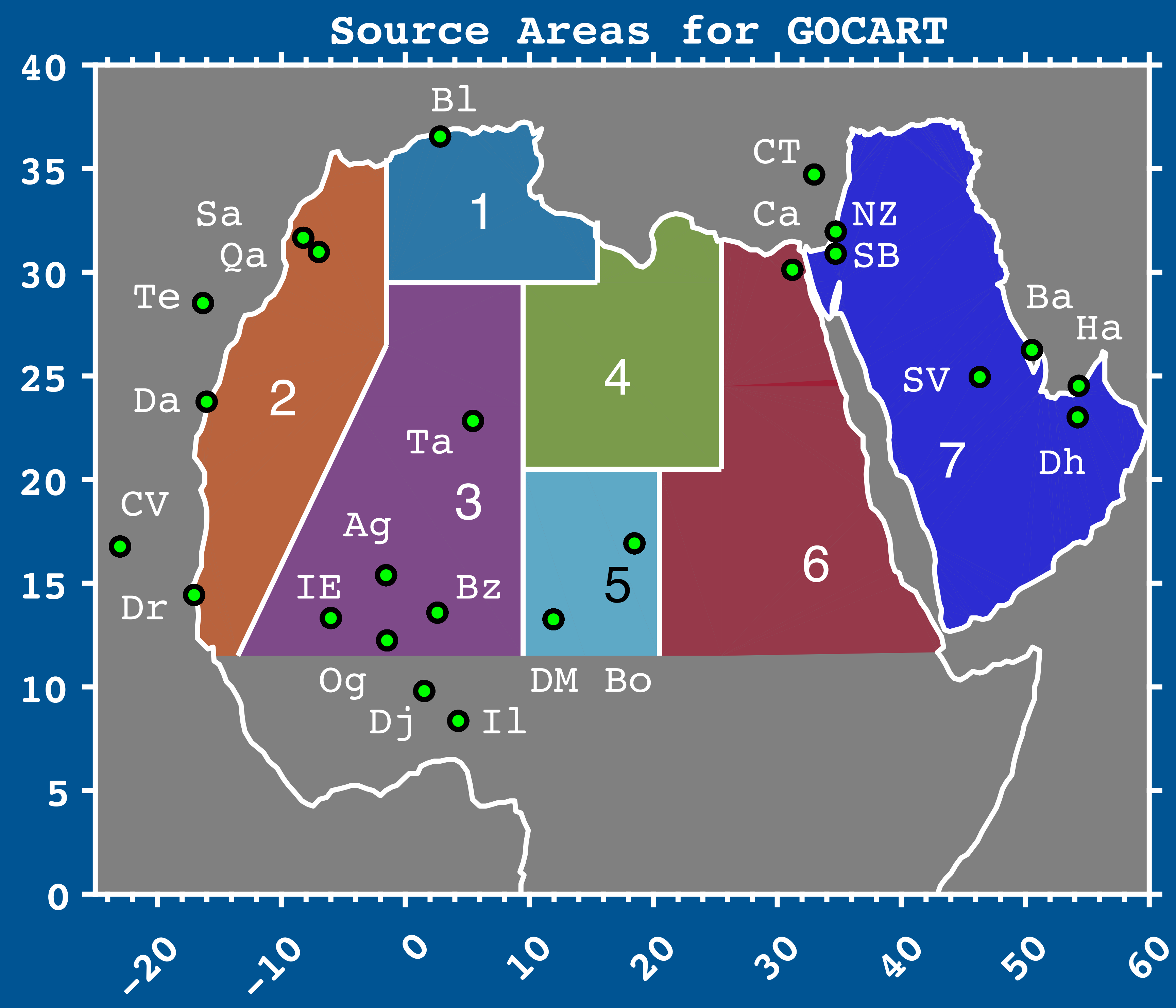

$S_a(532)$ computed from AERONET, per Schuster et al, ACP, 2012.

Highest proportion of illite is located in northwest Africa (regions 1 & 2).
However, some significant illite exists in regions 4 and 11.

Illite/Kaolinite ratios at African PSAs

CAQUINEAU ET AL.: MINERALOGY OF SAHARAN DUST OVER TROPICAL ATLANTIC AAC

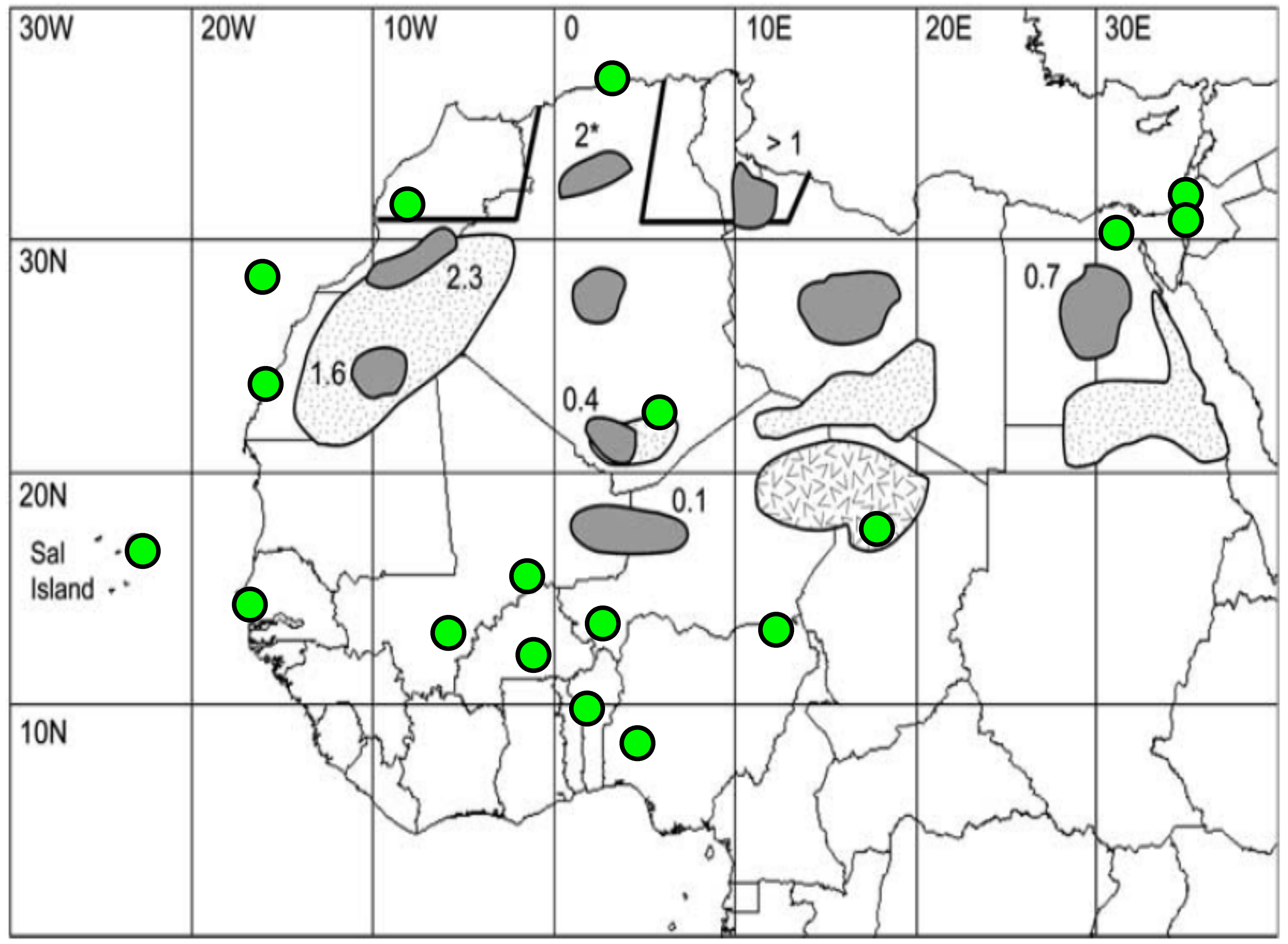

Figure 7. Location of Saharan dust sources identified by this work (shaded areas) with illite/kaolinite ratio (I/K) provided. Sources previously identified by *Bertrand et al.* [1974] (random V patterned areas), *D'Almeida* [1986] (stippled areas), and *Bergametti et al.* [1989] (solid lines) have been reported. The I/K value indicated with an asterisk is from *Gomes* [1990].

Illite/Kaolinite ratios at African PSAs

CAQUINEAU ET AL.: MINERALOGY OF SAHARAN DUST OVER TROPICAL ATLANTIC AAC

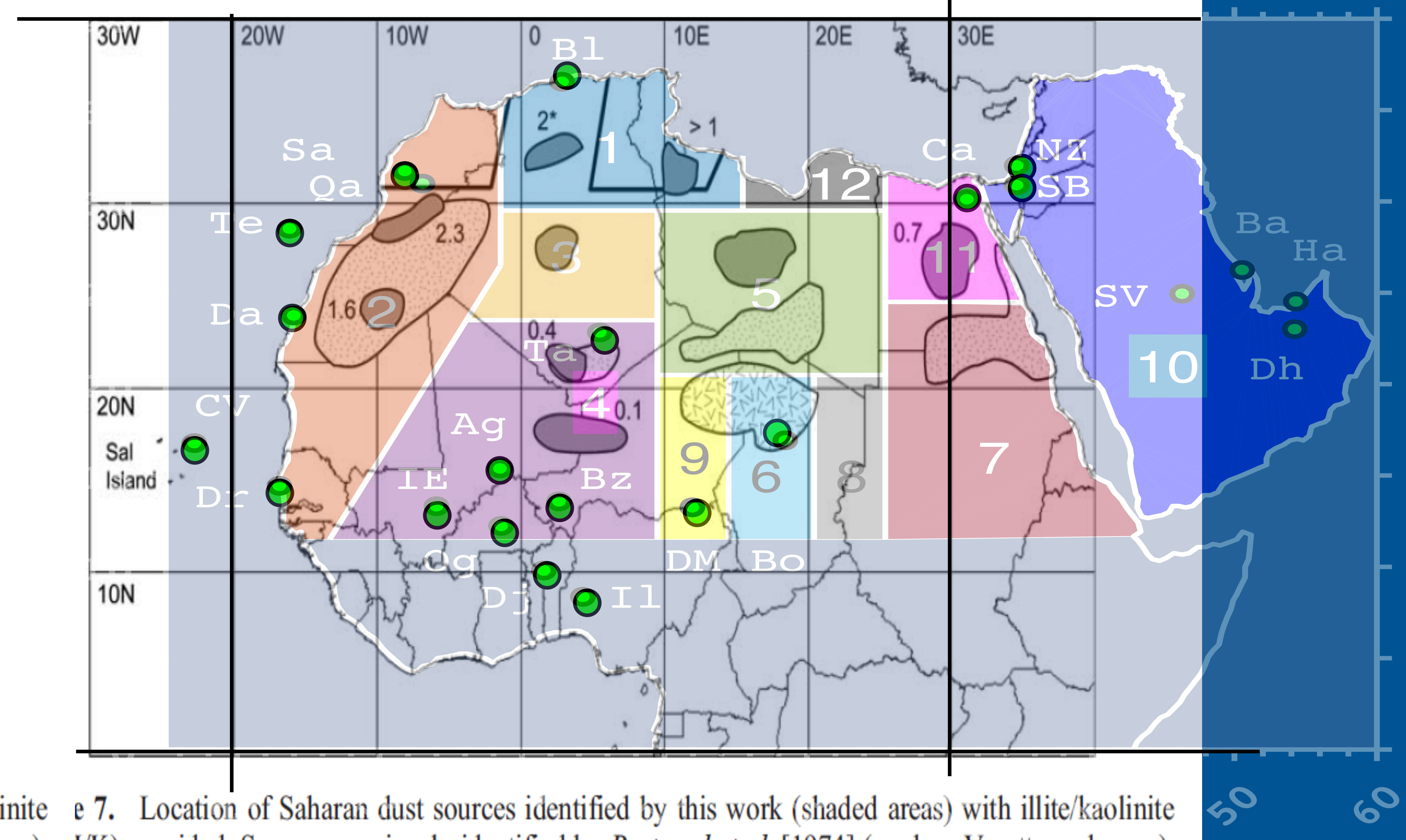

e 7. Location of Saharan dust sources identified by this work (shaded areas) with illite/kaolinite I/K) provided. Sources previously identified by *Bertrand et al.* [1974] (random V patterned areas), *ıeida* [1986] (stippled areas), and *Bergametti et al.* [1989] (solid lines) have been reported. The I/K indicated with an asterisk is from *Gomes* [1990].

Circles are AERONET sites.

Linking Optical Properties of Dust to Source Regions Over Africa and the Middle East

Greg Schuster, NASA LaRC; Dongchul Kim, NASA GSFC, JCET, UMBC, USRA; Zhaoyan Liu, NASA LaRC; Mian Chin, NASA GSFC; Kerstin Schepanski, TROPOS.

Mineral	n(532)	Reference
Hematite	3.18	Chen and Cahan (1981)
Calcite	1.58	Ghosh (1999)
Quartz	1.55	Ghosh (1999)
Gypsum	1.52	Roush (2007)
Montomorillonite	1.52	Egan and Hilgeman (1979)
Kaolinite	1.49	Egan and Hilgeman (1979)
★ Illite*	1.41	Egan and Hilgeman (1979)

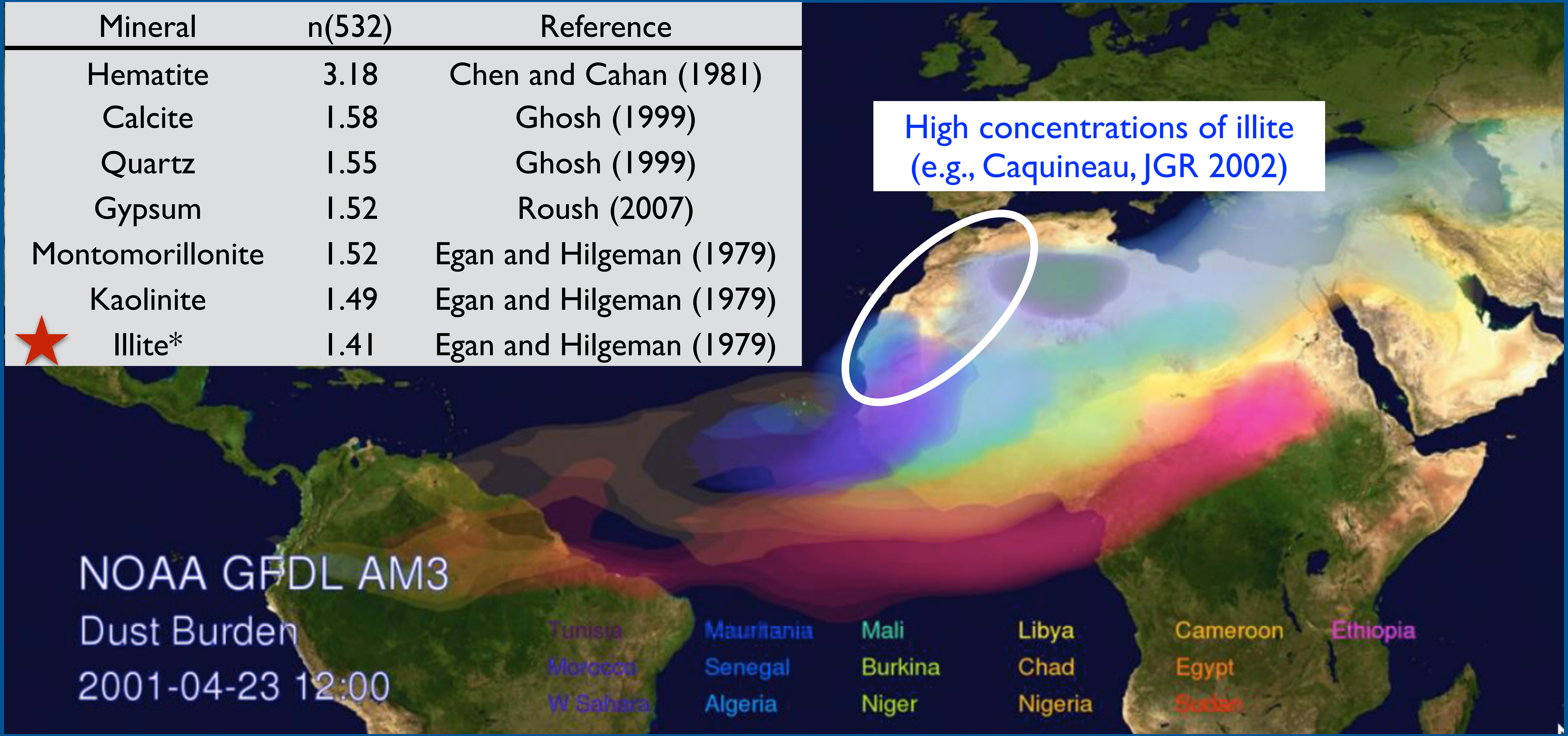

African dust sources presented by Joe Prospero at DUST 2014. Model run by Paul Ginoux

Relative Bias of CALIPSO Lidar Ratio wrt AERONET at Dust Sites

$$Bias = \frac{S_a(CALIPSO)}{S_a(AERONET)} - 1$$

	AERONET		CALIPSO		
	Lidar Ratio Climatology		Lidar Ratio Bias (S_a = 40)		
	pure dust	all dust	pure dust	all dust	
Africa	51	56	-0.21	-0.29	
Middle East	43	47	-0.06	-0.15	

	depolarization	fine volume fraction
pure dust	> 0.2	< 0.05
all dust	> 0.2	no restriction

Relative Bias of CALIPSO Lidar Ratio wrt AERONET at Dust Sites

$$Bias = \frac{S_a(CALIPSO)}{S_a(AERONET)} - 1$$

	AERONET		CALIPSO		
	Lidar Ratio Climatology		Lidar Ratio Bias (S_a = 40)		Aerosol Optical Depth Bias
	pure dust	all dust	pure dust	all dust	
Africa	51	56	-0.21	-0.29	-0.2
Middle East	43	47	-0.06	-0.15	-0.12

	depolarization	fine volume fraction
pure dust	> 0.2	< 0.05
all dust	> 0.2	no restriction

Measurements Needed to Constrain Lidar Ratios for CALIPSO Retrievals

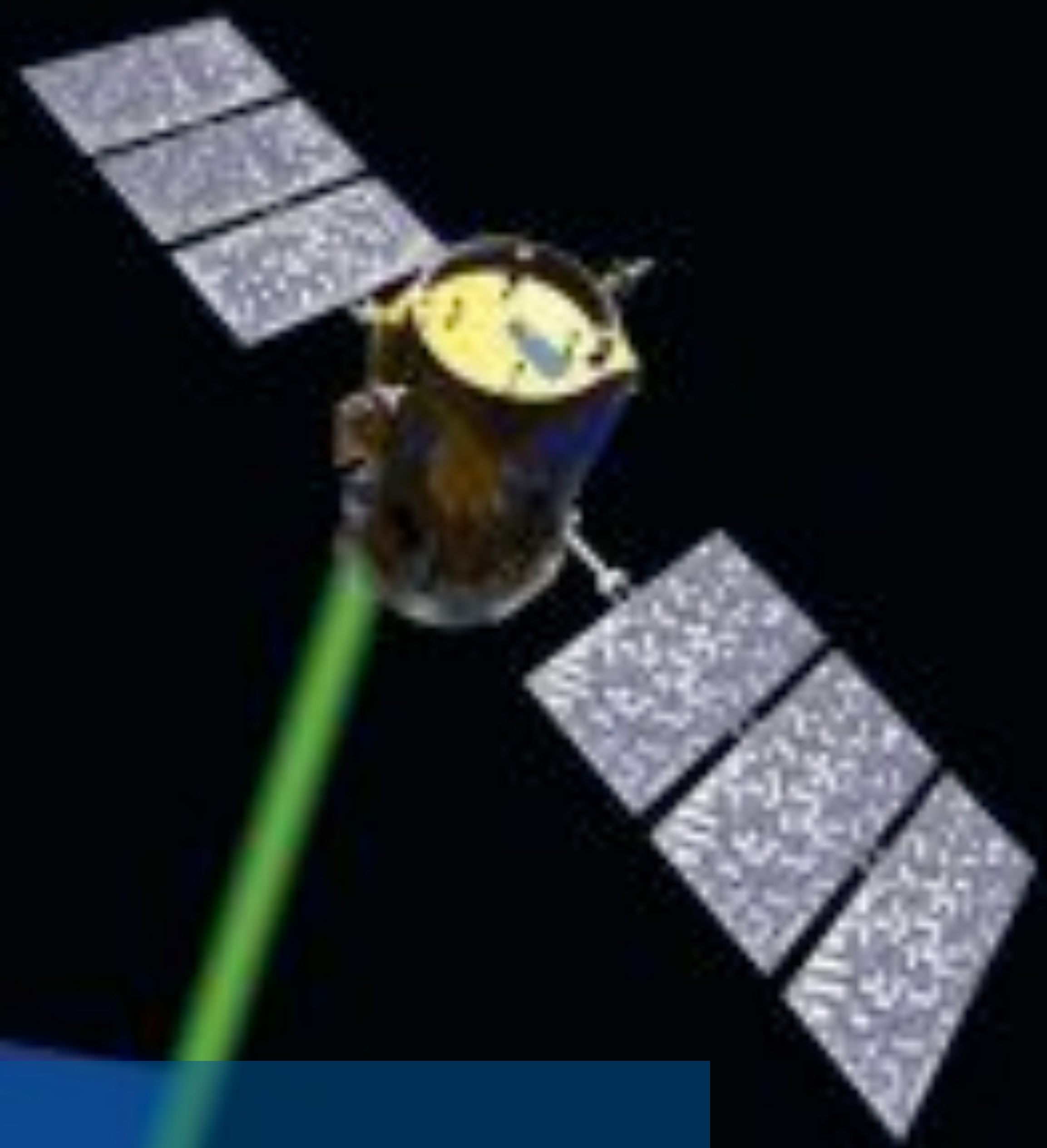

- Lidar ratio measurements are great, but we need concurrent mineralogy (or refractive index) and size distributions.
- Need these concurrent measurements near source regions in Middle East and Asia, and in transport regions over the Atlantic and Carribean.
- Refractive index measurements for “pure” African clays (illite, kaolinite, montmorillonite, and goethite).
- Studies to determine any changes in dust refractive indices during transport.

Empirical Lidar Ratios and Refr Indices at Solar Village (1/2007 to12/2016)

Empirical $S_a = \sum_{i=1}^{8} F_i (S_{psa})_i$

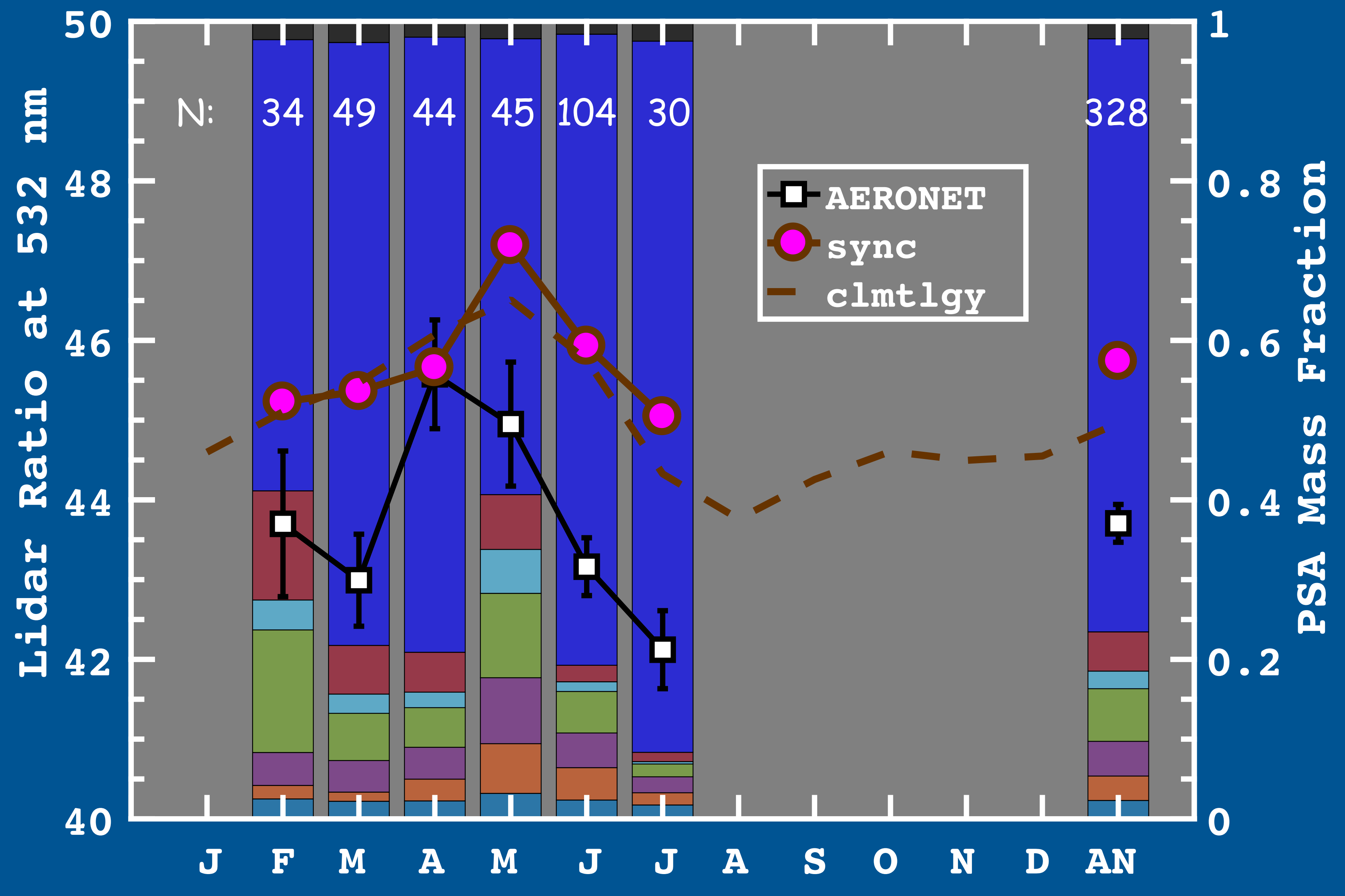

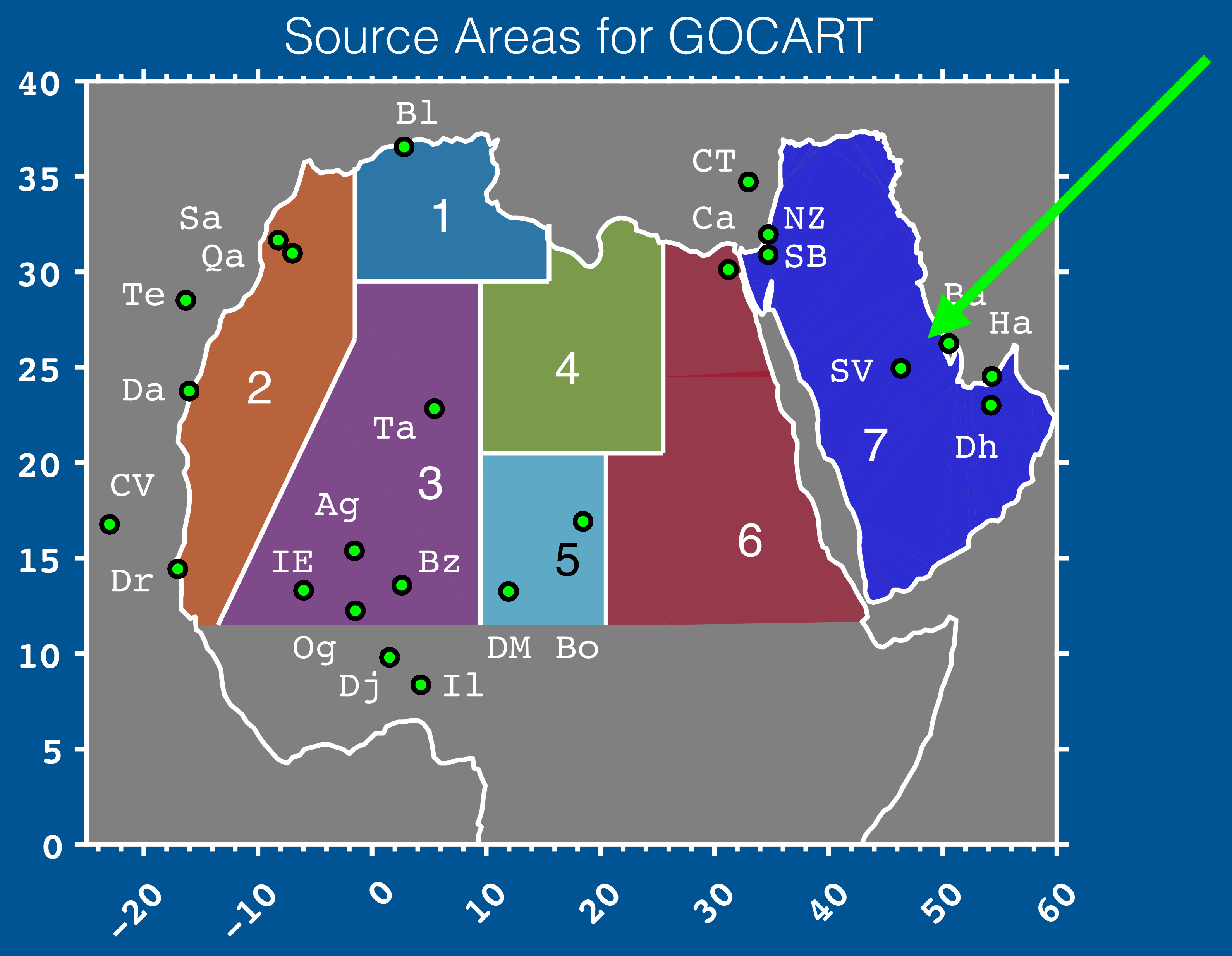

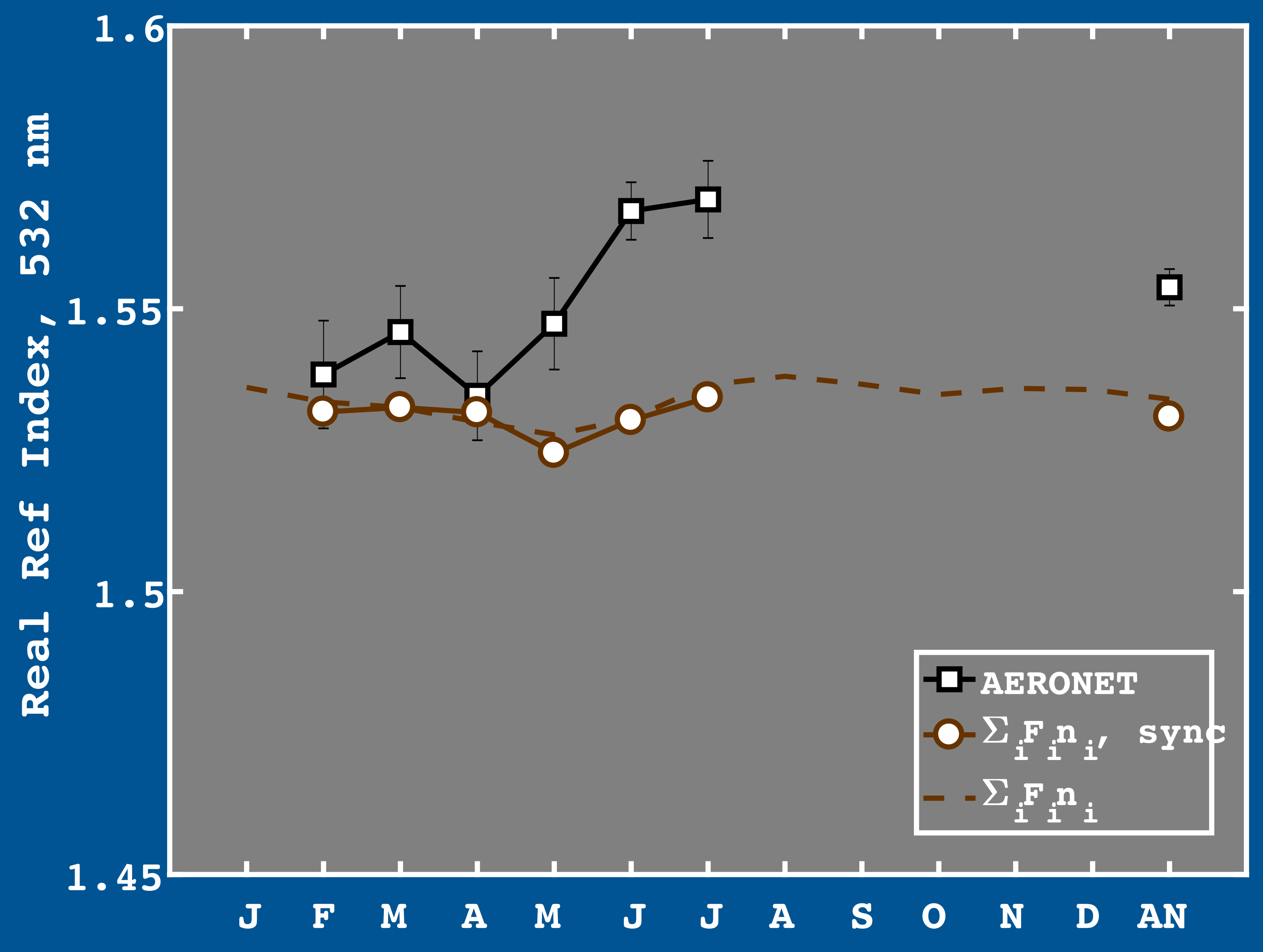

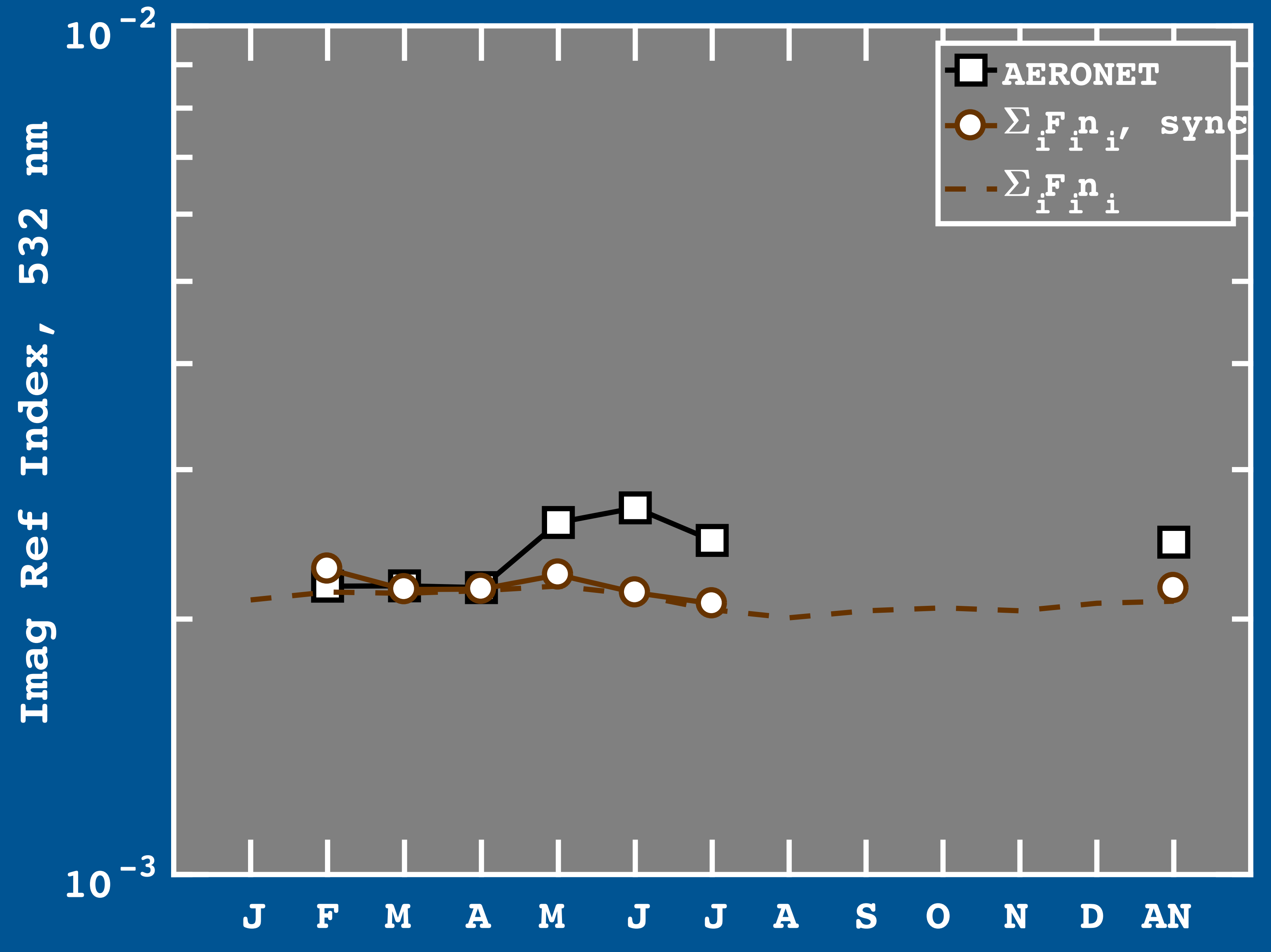

Seasonal Variability at Sede Boker

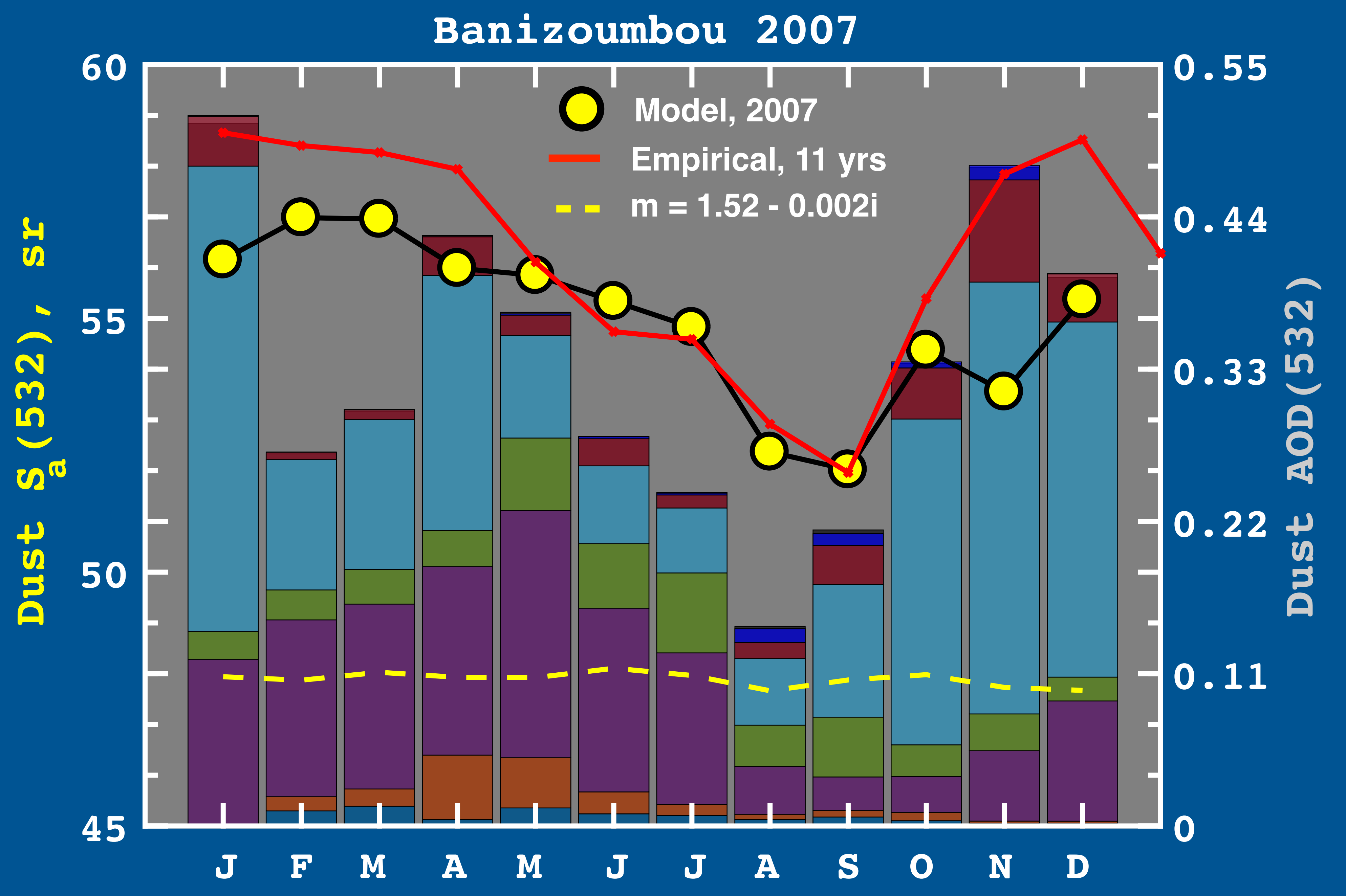

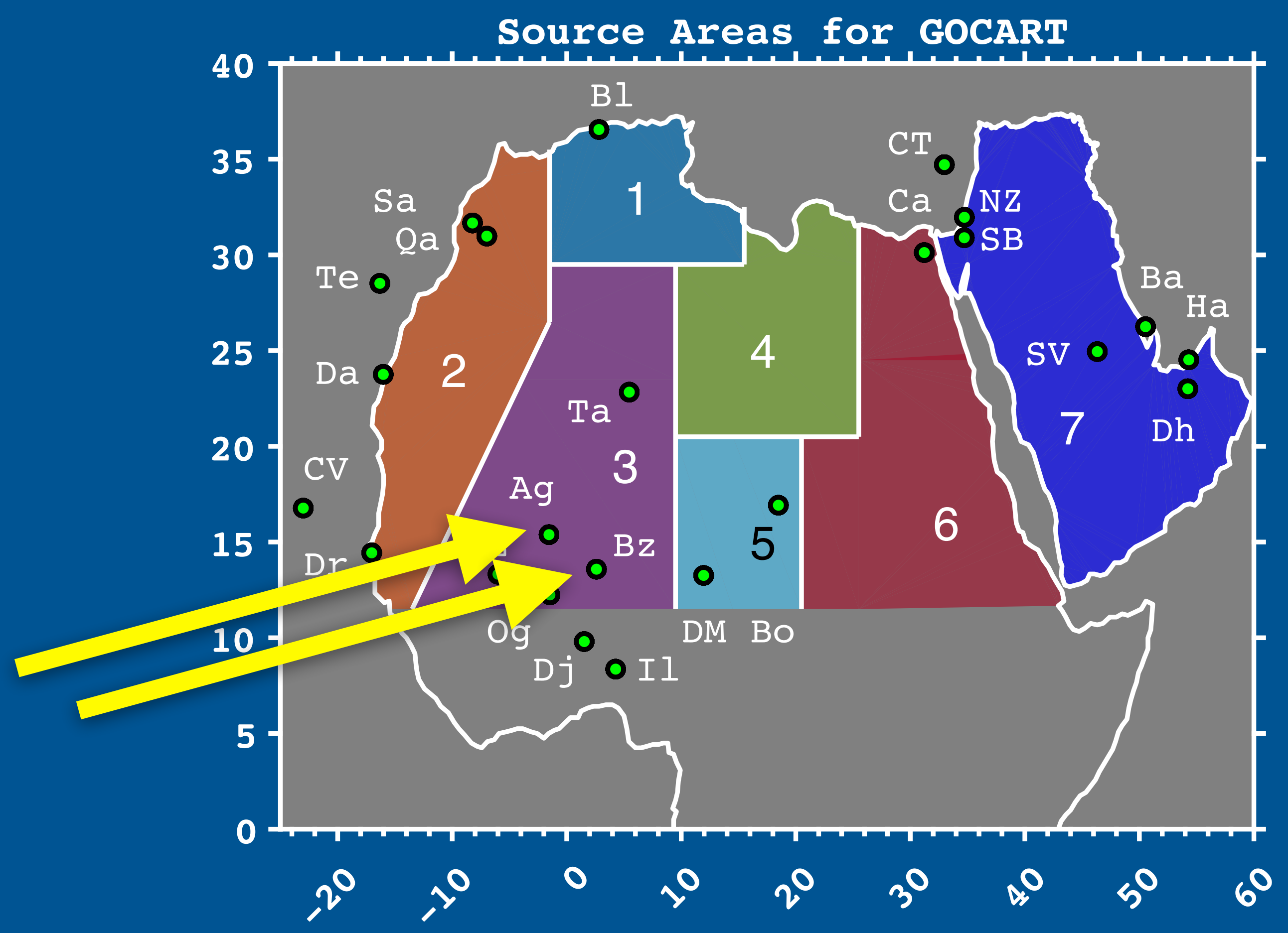

Seasonal Variability at Sede Boker

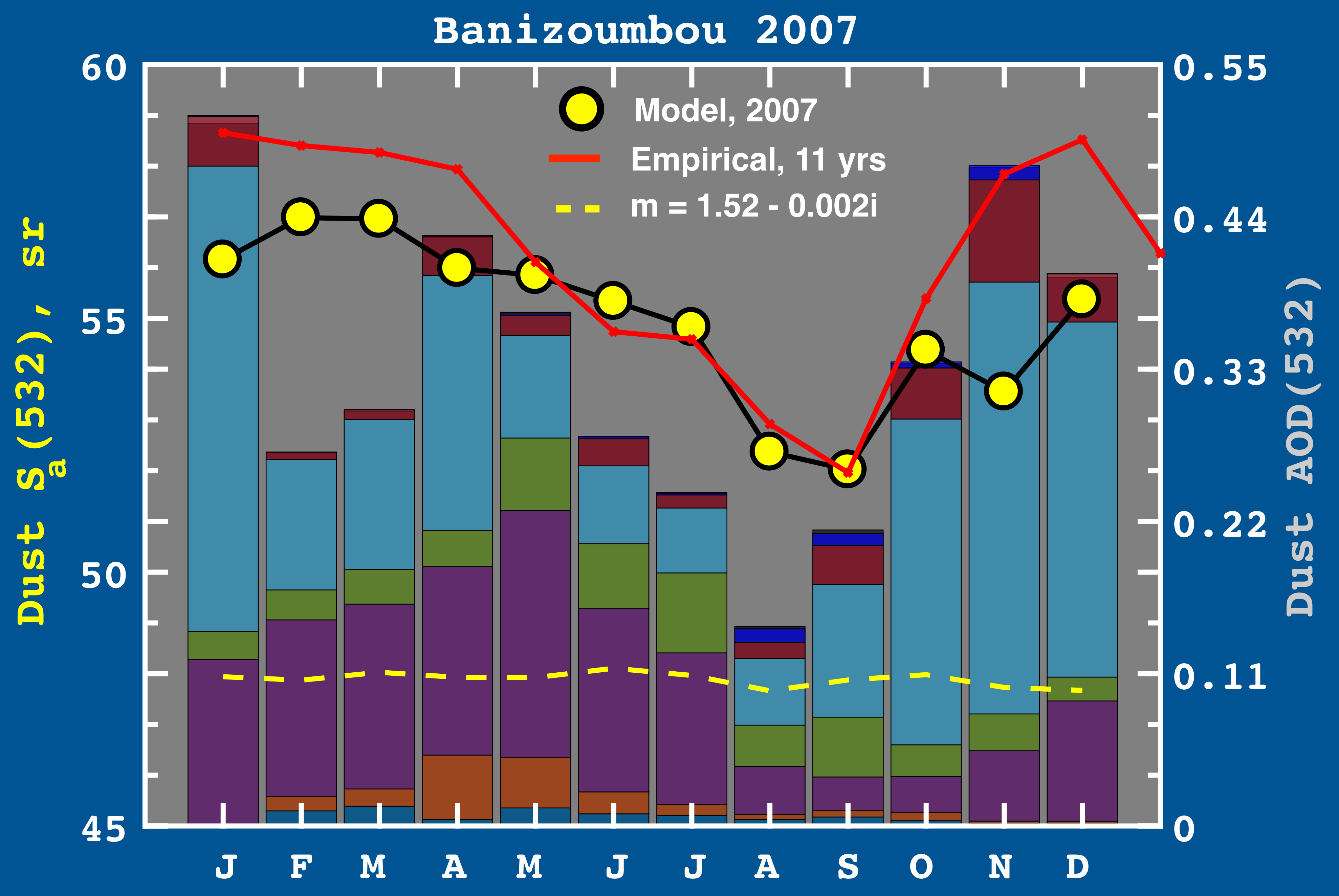

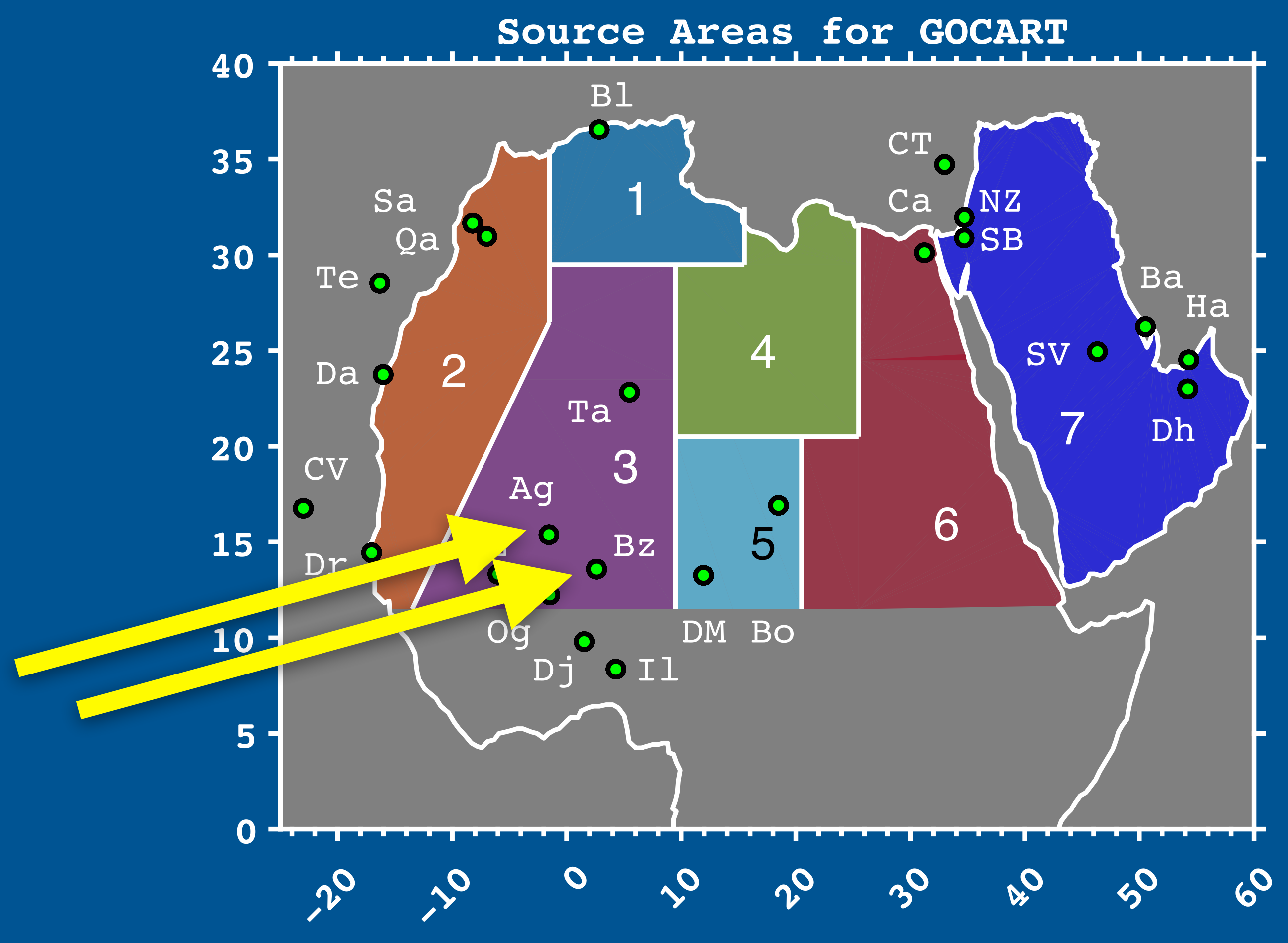

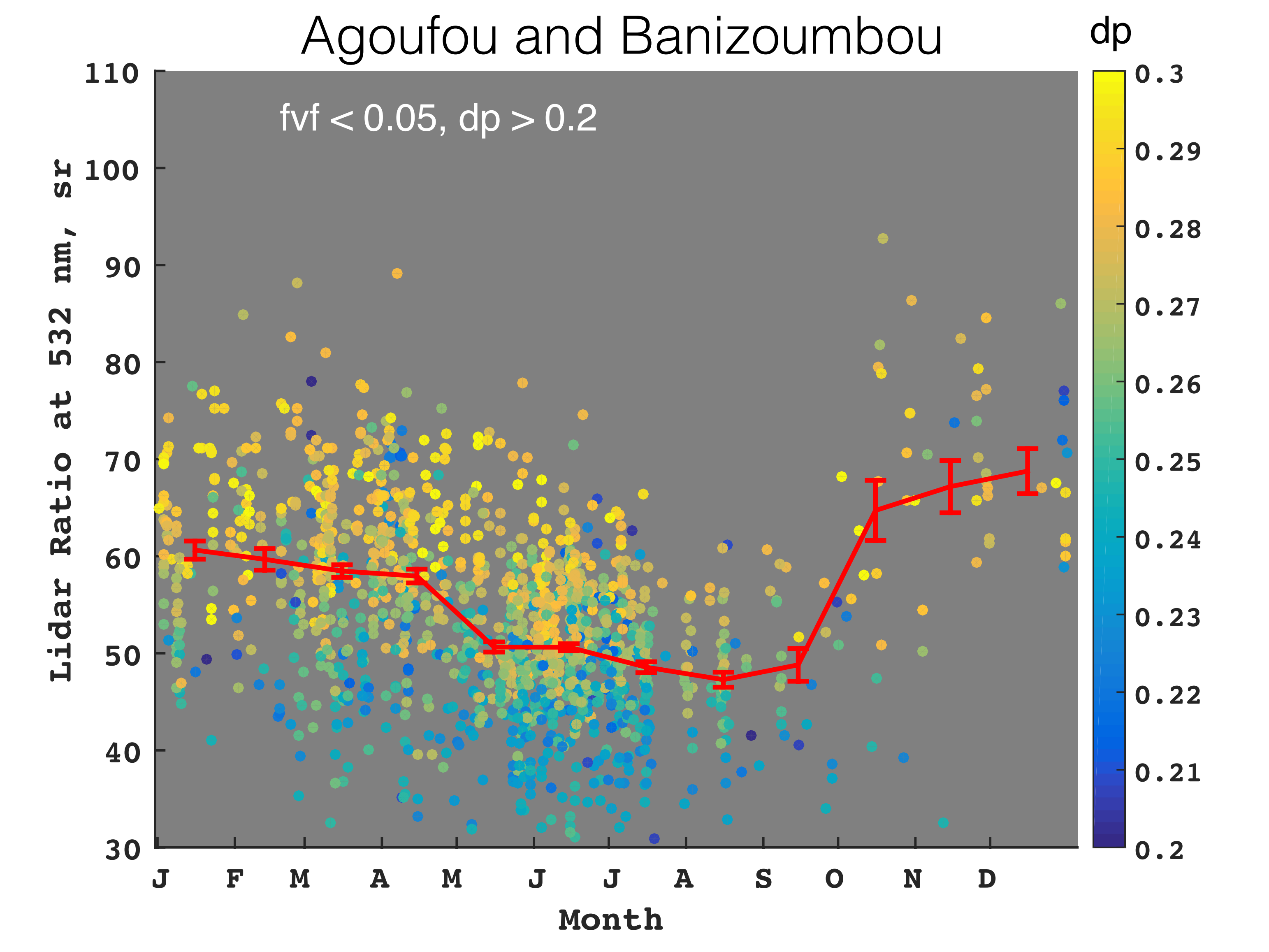

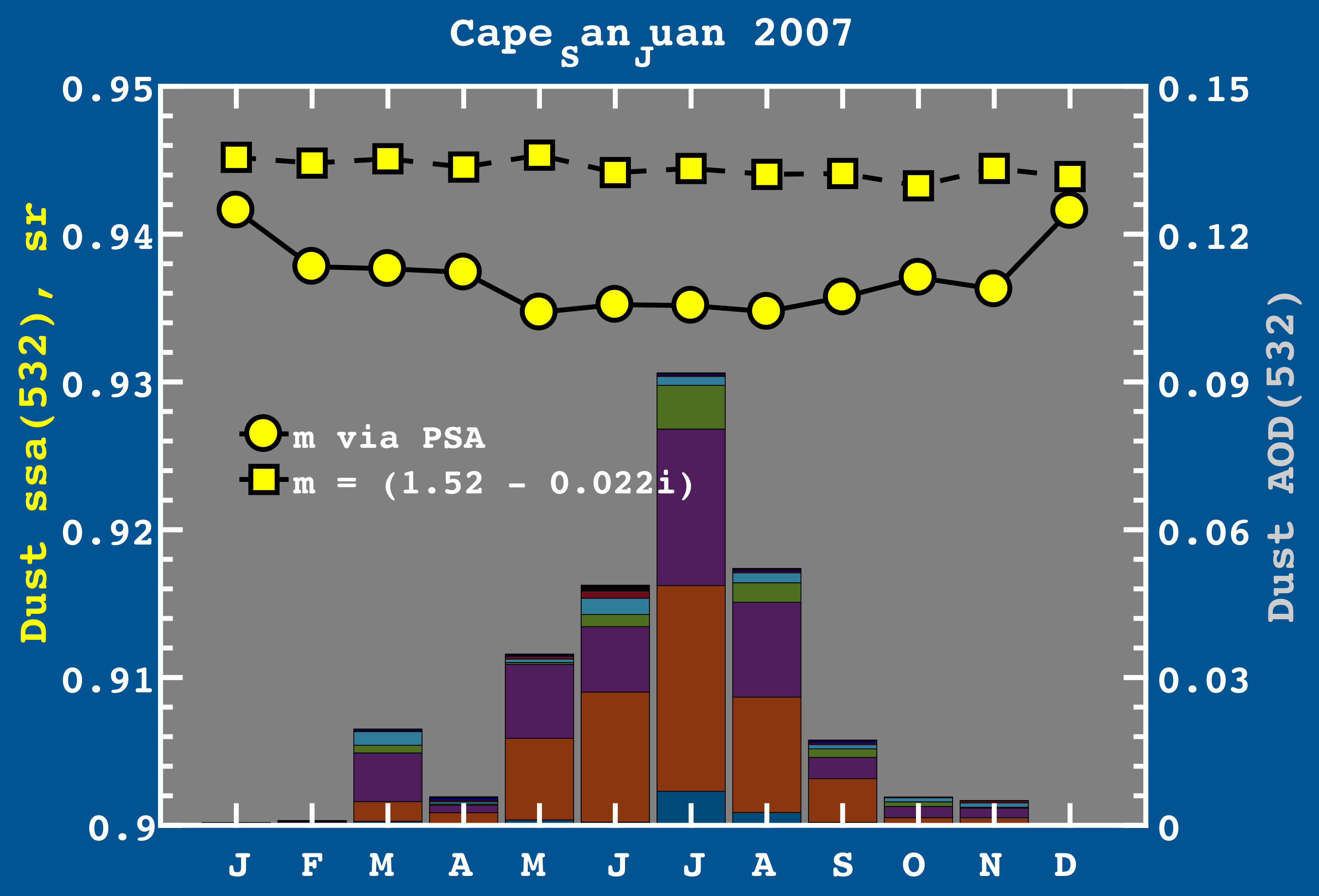
Cape San Juan 2007
Dust ssa(532), sr
Dust AOD(532)
m via PSA
m = (1.52 - 0.022i)
J F M A M J J A S O N D

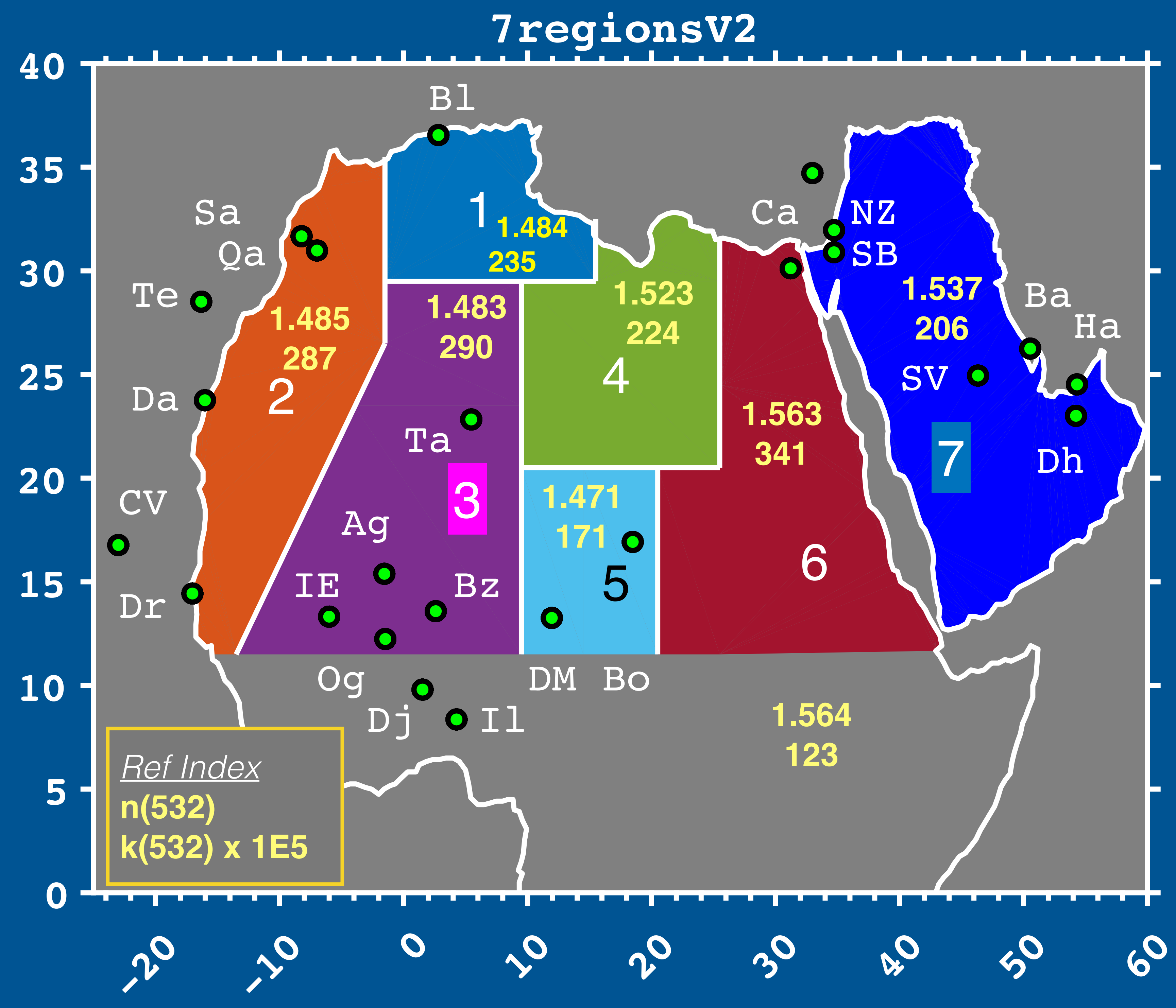
7regionsV2
Bl
Sa
Qa
Te
Da
CV
Dr
Ca
NZ
SB
Ba
Ha
SV
Dh
Ta
Ag
IE
Bz
Og
Dj
Il
DM
Bo
1 1.484 235
2 1.485 287
3 1.483 290
4 1.523 224
5 1.471 171
6 1.563 341
7 1.537 206
1.564 123
Ref Index
n(532)
k(532) x 1E5

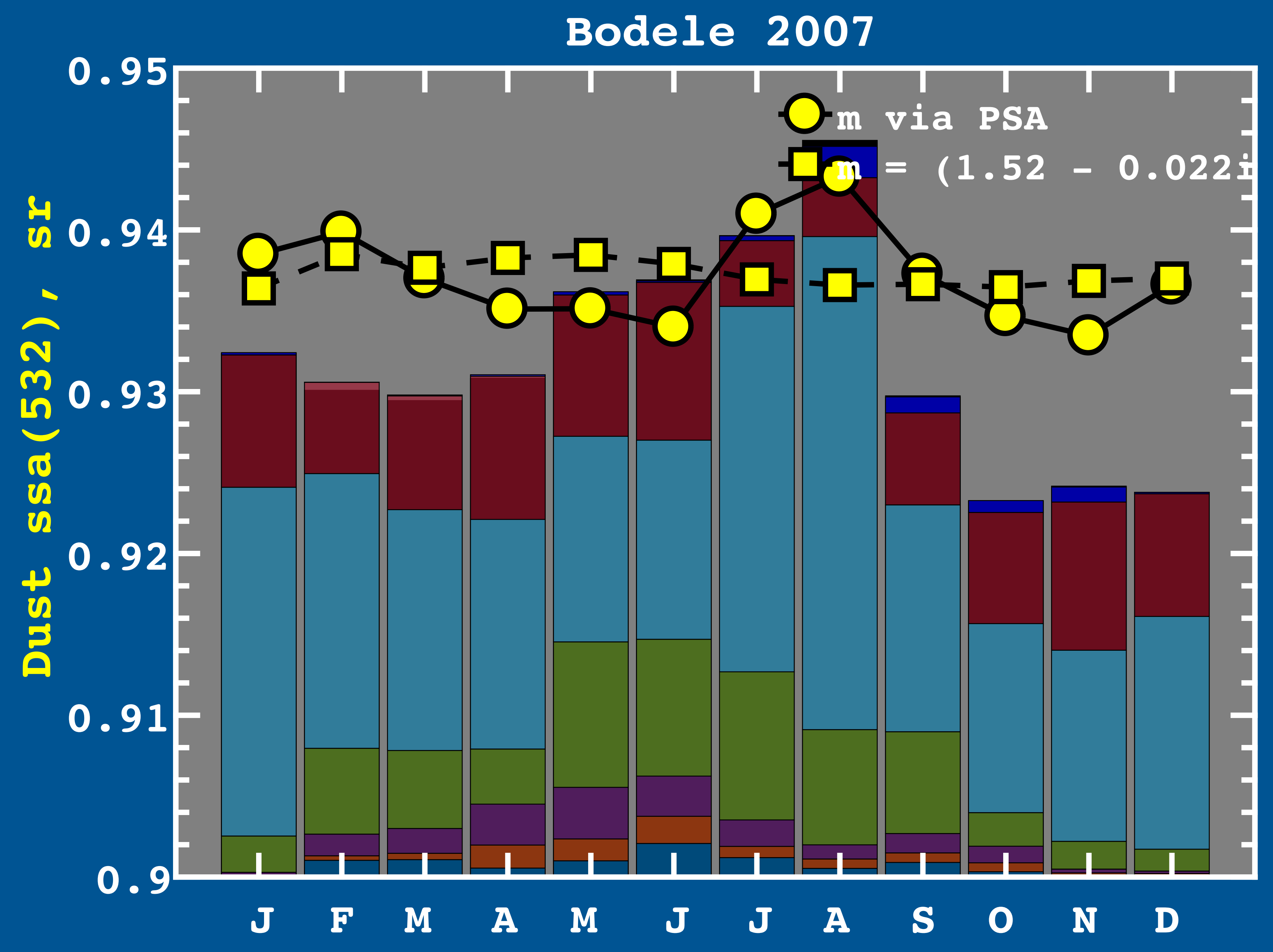
Bodele 2007
Dust ssa(532), sr
m via PSA
m = (1.52 - 0.022i)
J F M A M J J A S O N D

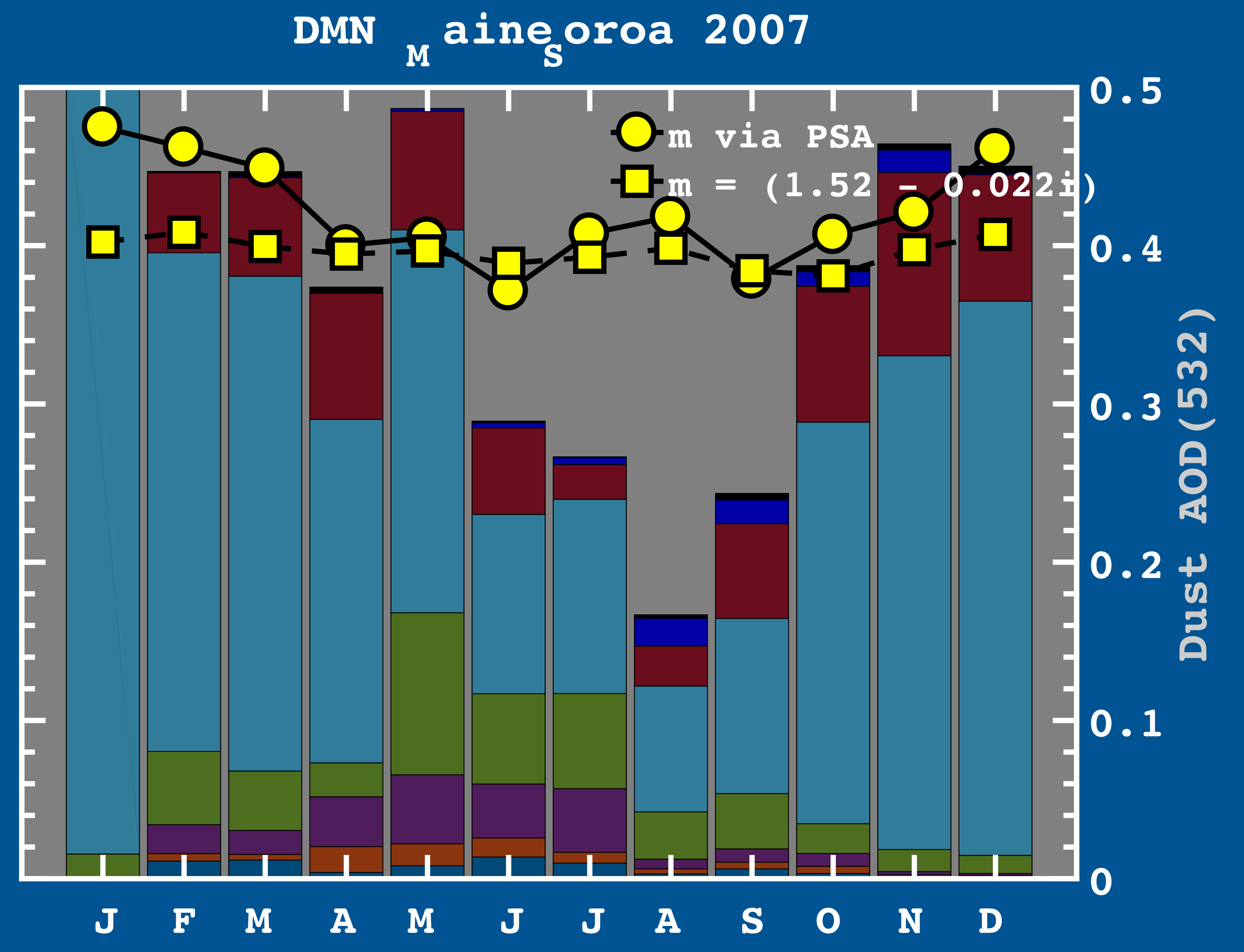
DMN Maine Soroa 2007
Dust AOD(532)
m via PSA
m = (1.52 - 0.022i)
J F M A M J J A S O N D

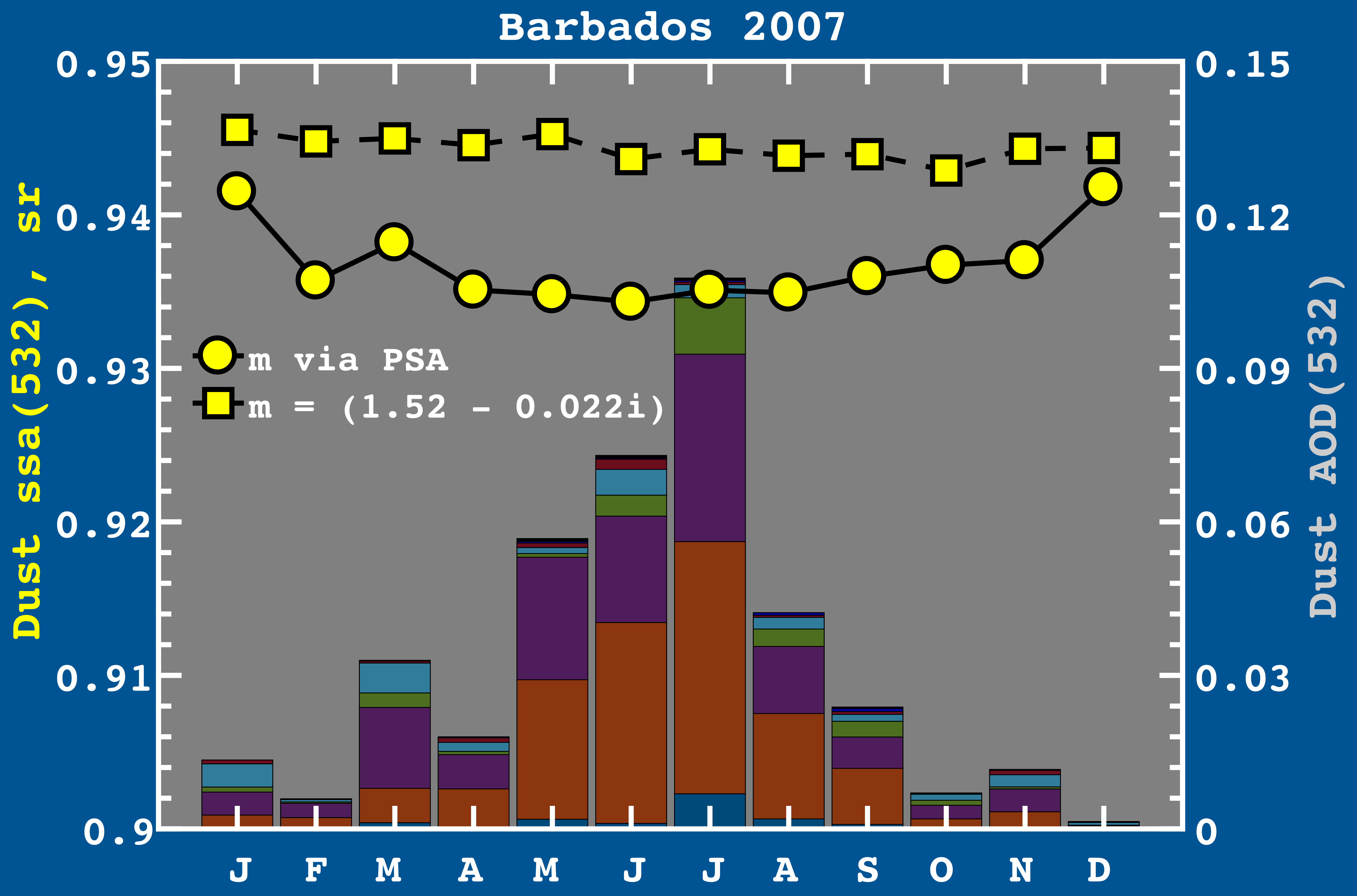

Barbados 2007
Dust ssa(532), sr
Dust AOD(532)
m via PSA
m = (1.52 - 0.022i)
0.95
0.94
0.93
0.92
0.91
0.9
0.15
0.12
0.09
0.06
0.03
0
J F M A M J J A S O N D